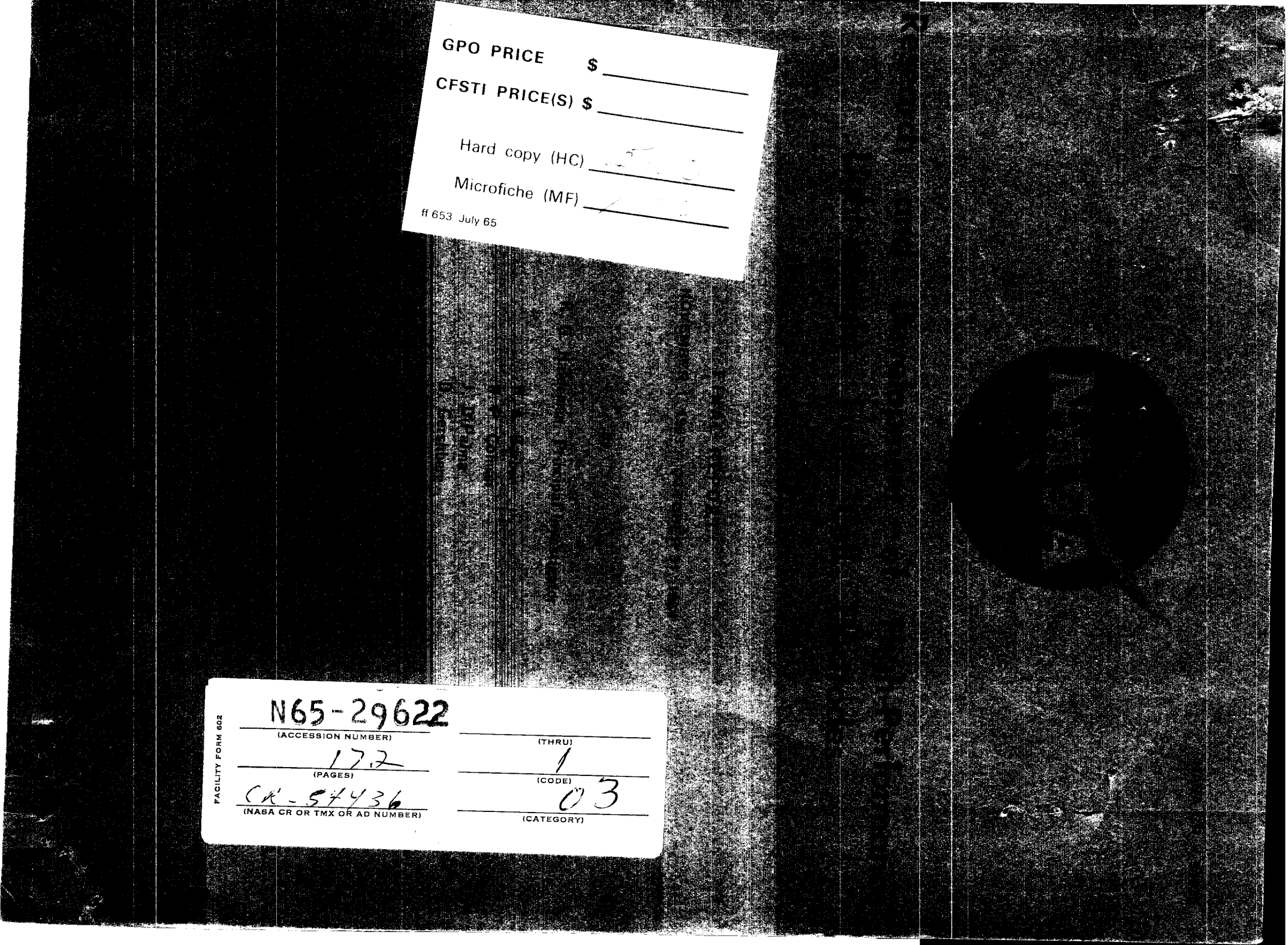

NASA CR-54436

FINAL REPORT

RESEARCH AND DEVELOPMENT OF HIGH-PERFORMANCE LIGHT-WEIGHT FUEL CELL ELECTRODES

by

R. G. Haldeman, Principal Investigator

W. A. Barber
W. P. Colman
J. DiPalma
D. Gershberg
J. P. Ward

prepared for

NATIONAL AERONAUTICS AND SPACE ADMINISTRATION

August 1, 1965

CONTRACT NAS 3-2786

Period Covered: November 1, 1963 - October 31, 1964

NASA Lewis Research Center
Cleveland, Ohio
Space Power Systems Division
Technical Manager: Mr. W. A. Robertson MS-86-1

AMERICAN CYANAMID COMPANY
STAMFORD RESEARCH LABORATORIES
1937 West Main Street
Stamford, Connecticut
(Area Code 203) 348-7331

ABSTRACT

The principle objective of the work done under this contract was to maximize performance in alkaline matrix-type fuel cells in order to reduce the weight to power ratio. Toward this objective, new catalyst materials, including high-area platinum blacks, and platinum-rhodium mixtures were prepared and evaluated. Various asbestos matrix materials, both commercial and proprietary, were investigated.

A study of modifications in electrode composition and structure led to the development of new high-performance electrodes, designated as High-Loading electrodes. The performance of these electrodes was investigated over a wide range of temperature, pressure, and electrolyte concentration.

Life tests conducted in 2" x 2" cells showed these electrodes to be capable of stable operation for 1000 hours or more at temperatures in the range 70-100°C. A scaled-up cell having a 6" x 6" active area was constructed and operated successfully.

A 2 kilowatt fuel cell battery system, incorporating the High-Loading electrodes of this study together with novel bipolar separator plates, was designed. The weight of this system (exclusive of fuel and tankage) was estimated to be approximately 50 lbs/kw. A mathematical analysis was used to predict, for two alternative cooling means, the temperature and concentration gradients within this system, and to determine the gas flow rates required to maintain these gradients within acceptable limits.

TABLE OF CONTENTS

TABLE OF CONTENTS

(Continued)

TABLE OF CONTENTS

(Continued)

LIST OF TABLES

LIST OF FIGURES

LIST OF FIGURES

(Continued)

LIST OF FIGURES

(Continued)

1. SUMMARY

Under this contract research effort was directed toward developing and evaluating electrode systems for use in matrix-type fuel cells having weight-to-power ratios substantially below 150 pounds per kilowatt. The experimental program encompassed catalyst and matrix studies, electrode development, investigation of operating parameters, and life-testing. Based on these studies a 2 kw battery system was designed, and a mathematical analysis made of its operating characteristics.

The major findings of this program are summarized below:

a. Materials Investigations

(1) Catalyst Studies

Unusually high surface area platinum blacks were prepared by reduction of chloroplatinic acid with aromatic substituted silanes. These blacks, having specific areas of 40-60 m^2/g, tended to be pyrophoric and sintered readily. Performance did not exceed that of commercial blacks.

Platinum and rhodium codeposited on carbon at low loadings had previously been shown to operate synergistically when used as an anode electrocatalyst in the base cell. However, at high loadings, no performance advantage was found over commercial platinum black.

(2) Matrix Materials

Various forms of asbestos sheet were tested as matrix materials, including a proprietary asbestos sheet and several commercial grades. The proprietary sheet, designated as "ACCO Asbestos", and the commercial material known as "Fuel Cell Asbestos" were used as standard matrix materials in life-testing and scale-up programs. ACCO Asbestos is more porous than the commercial materials. It allows a lower cell

internal resistance and higher performance, but has a relatively low "bubble pressure" (2-3 psi as compared with 10-15 psi for 20 mil Fuel Cell Asbestos).

(3) Corrosion Studies

Corrosion and electrical resistance measurements were made on a series of metals of interest for use as catalyst supports and spacer screens. On exposure to 35% KOH and oxygen at 110°C, only nickel protected by 1-2 micro inches of gold showed both negligible corrosion rate and change in resistance.

b. Electrode Development

Since the several catalyst studies indicated no significant advantages over commercial platinum black, the latter material was used exclusively in further electrode development. Variations in platinum loading, screen support, waterproofing level, and degree of porosity were investigated.

A study of platinum loadings in the range 9 to 80 mg/cm^2 indicated that 40 mg Pt/cm^2 supported on a single 40 mesh nickel screen gave optimum electrode performance. Electrodes of this type were designated "High-Loading Electrodes" and along with standard 9 mg Pt/cm^2 electrodes (Type AB-1) were used in studies of cell operating variables.

A variety of support screens and expanded metal screens were evaluated singly and in "sandwich structures". These tests indicated no advantage of expanded metal or "sandwich structures", and that a single screen selected to accommodate the desired catalyst loading should be used.

Levels of Teflon waterproofing between 8 and 50% were investigated. In our electrodes the proper level seems to be about 25%. No advantage was found for electrodes with graded waterproofing, nor did controlled variations in porosity influence electrode performance.

c. Small Scale Testing

(1) Initial Performance

In order to determine operating conditions which should result in a battery system of minimum weight per net power, the initial performance of the four electrode-matrix systems based on AB-1 and High-Loading electrodes, and ACCO Asbestos and Fuel Cell Asbestos matrices, was investigated. Cells having an active area of 5 cm^2 (one-inch diameter) or 25.8 cm^2 (2 inches x 2 inches) were used in this work.

Optimum matrix thickness, cell assembly pressures and electrolyte loadings were established. The effects of temperature in the range 70-100°C and of KOH concentration in the range 1-17N were found to be interdependent. With High-Loading electrodes, increasing concentration and temperature simultaneously from 5N and 70°C to 13N and 100°C increased cell output by 80-100 millivolts. High-Loading electrodes with ACCO Asbestos performed stably at 1000 ma/cm^2 and 0.7 volt in short-term tests, whereas with standard AB-1 electrodes, limiting current densities were reached at about 300-400 ma/cm^2. Thus, the performance advantage of High-Loading electrodes was clearly indicated.

In exploratory studies, operating temperature was extended to 200°C and electrolyte concentrations to as high as 75% KOH. It appears that operation at temperatures of 140-150°C and electrolyte concentrations of 17-19N is possible and may lead to performance as high as 0.9 volt at 400 ma/cm^2.

The general effect of increasing reactant gas pressure to 15-45 psig was to increase cell performance by 20-100 mv at current densities up to 400 ma/cm^2.

(2) Life-Testing

Using the several components described above, a total of 68 life tests were run at temperatures of 70-100°C, current densities of 100-400 ma/cm^2, and with dry and presaturated reactant gases. In most tests downward trends in performance of 50-100 mv/1000 hours were observed. This decline was usually accompanied by a gradual increase in cell internal resistance, which was found to be due primarily to gradual oxidation of the cathode support screen. Much improved life performance was achieved in tests performed with platinum or with gold or rhodium plated nickel support screens, declines were observed amounting to 0-15 mv/1000 hours in test run at 100 ma/cm^2 and 70°C.

Reasonably stable performance was obtained at 200 and 300 ma/cm^2 although further investigations are required to determine conditions for optimum performance at these high current densities.

A limited study of life operation under pressures up to 25 psig was made. In general, the initial level of performance was higher than observed at atmospheric pressure, but performance declined at a rate of 25-50 mv/1000 hours. Again, further investigations are required to determine optimum conditions of operation.

It was shown that build up of carbonate in the electrolyte can become significant in tests run at high current densities for prolonged periods, e.g., 100 ma/cm^2 for 5000 hours. For cells with an initial KOH concentration of 30-35%, conversion of about half the KOH to carbonate causes a loss of performance of 40-50 mv. Greater conversion can result in a major loss of performance.

Used electrodes from the life-testing program were examined for evidence of change of physical or electrochemical properties. It was noticed that the anode developed a grey appearance on the matrix side. There is some evidence that a loss of surface area can occur also. The effect of these changes on performance has not been firmly established, but does not, in general, appear to be serious for tests up to several thousand hours duration in the temperature range 70-100°C.

d. Battery-Sized Single Cell

Based on the study of operating variables and a preliminary analysis of battery system weights, conditions were chosen for scale-up to battery-sized (6" x 6") cells. Temperature was selected to be 100°C and pressure 45 psig. Two electrolyte concentrations, 5N and 13N, were chosen.

A 6" x 6" single cell was designed and constructed employing a gas distribution system based on controlled flow through a series of orifices in the face plates. This design was first proven satisfactory by plastic models. Polarization curves obtained in this cell using High-Loading electrodes and ACCO Asbestos matrix at 100°C, atmospheric pressure, and 13N KOH showed good agreement with data obtained in one-inch diameter cells.

The 6" x 6" cell was operated under the above conditions for a total period of 420 hours at current densities of 100, 200, 300, and 400 ma/cm^2. At all but the latter current density, performance was relatively steady. At 400 ma/cm^2 operational difficulties were encountered.

Measurements made in the 6" x 6" cell indicate that in battery operation, pressure drop in the recirculating hydrogen stream should not exceed 0.1 psi.

e. Battery Systems

A 2 kilowatt battery system incorporating the thin, light-weight electrodes of this study, and based on dynamic removal of product heat and water from the battery into a recycle hydrogen stream was designed. The system features bipolar separators based on the design of the face plates of the laboratory 6" x 6" cells, and on the mathematical analysis described below. Essentially, they consist of thin parallel plates with gas distributi and coolant channels between them, and gas distribution orifices in the faces With this design the critical pressure drop in the circulating gas stream occurs at the orifices. Two system modifications were developed, one in whic cooling is accomplished entirely by the recirculating gas stream, and the other in which an auxiliary liquid coolant is passed through the bipolar separator.

A mathematical analysis was made to determine theoretically the magnitude of gradients in electrolyte concentration, electrolyte loading, and temperature which would occur in a given cell in a battery stack. General differential mass and energy balances were set up and solved for the system employing dynamic heat and water removal from the battery both with and without auxiliary cooling. Based on this analysis, feasible region of cell operation were established in terms of required gas circulation

rates to maintain specified minimum matrix concentration gradients. It was shown that gas circulation rate can be reduced by a factor of 3 or 4 if auxiliary cooling is provided.

A comparison of the two cooling systems was made on the basis of estimated weight per net power for the 2 kilowatt battery. For both systems the estimated weight (including all auxiliaries except fuel and tankage) was approximately 50 lbs/kw. The weight and parasitic power requirements of hydrogen blower and liquid coolant pump essentially compensate for one another in the two designs. Auxiliary cooling appears to be preferable, however, because it permits operation at higher electrolyte concentrations and smaller concentration gradients and, therefore, offers a greater degree of operational control and flexibility.

2. INTRODUCTION

2.1 Prior Work

Prior to the inception of the National Aeronautics and Space Administration Contract NAS 3-2786 (this contract) American Cyanamid Company had conducted a research and development program on thin, high-performance gas diffusion electrodes suitable for matrix cells. This work included polarization and endurance studies on several types of electrodes as well as investigations of practical methods for their manufacture. It included also development of promising matrix materials. Based on the demonstrated performance in five square centimeter cells of 80-100 watts/ft^2 at 0.8 volt, it was possible to predict that a substantial improvement in battery weight-to-net power could be achieved over the existing state-of-art.

2.2 Objectives

The chief objective of fuel cell research for space flight applications is the reduction of the weight-to-power ratio. A fuel cell utilizing hydrogen and oxygen reactants is of considerable interest to NASA because of its high electrical work output per unit weight of reactants. The efficiency of hydrogen-oxygen fuel cells is 60% or better in practical cells. These cells have a power plant weight of approximately 150 pounds per kilowatt neglecting reactants and tankage.

An important factor in determining the fuel cell weight is the weight of the electrode and its supporting structure. The intent is to support research and development efforts directed towards obtaining electrode systems which will produce a higher electrochemical reaction rate per unit weight of electrode and assembly while maintaining a satisfactory fuel consumption efficiency.

While this program suggests that high-performance, light weight electrodes are the basic interest, it should be understood that the weight and efficiency of the entire power plant must be included to, in fact, achieve the purpose of this effort; namely, the reduction of the fuel cell weight-to-power ratio.

2.3. Scope

The scope of work to be done by American Cyanamid Company is shown in the following description which is a condensation of the Schedule of Work for Contract NAS 3-2786.

Available materials shall be evaluated and new or modified materials developed as required to permit incorporation into components of high-performance hydrogen-oxygen fuel cells of improved power-to-weight ratio. Such components shall include catalysts, supports, and matrices.

Catalyst investigations shall include studies of degree of uniformity and despersion of platinum either as platinum black or as supported on a carbonaceous or fiber substrate. Synergistic effects of catalytic materials, effect of substrates, and physical characterization of promising catalysts shall be included.

Wire and expanded metal screens of various deminsions shall be evaluated as catalyst supports and electrode matrix materials.

Matrix investigations shall be devoted to improvement of the characteristics of asbestos matrix material by modification of asbestos type or physical properties or by admixture of other fibers in the asbestos paper.

American Cyanamid Company Type A, B and C electrodes shall be evaluated, and modified electrodes fabricated and tested to the extent necessary to permit selection of candidates for extended testing. Type A electrodes consist of a porous layer of platinum black and waterproofing agent spread uniformly on a suitable screen. Type B electrodes consist of carbon extended catalysts and waterproofing agent spread uniformly on a suitable screen. Type C electrodes consist of fiber extended catalysts and waterproofing agent formed into a sheet by paper-making techniques.

Selected electrodes shall be tested for performance in suitable laboratory matrix type cells to provide service experience and design data for single cell prototypes and battery modules. Initial performance testing shall be conducted in cells having an active area of five square centimeters. Cell structure and operating variables shall be studied. Extended evaluation of promising electrodes shall be made in cells of 2" x 2" active area. A minimum of five cells shall be operated at battery design loads for 1000 hours to study component stability and operating variables.

Single cells of approximate battery dimensions shall be developed and tested as prototypes of ultimate battery structure. For a single preferred design, as agreed upon by the NASA technical representative and the American Cyanamid Company, experiments will be conducted and data developed to determine heat transfer, mass transfer, and pressure drop of the fuel cell. A configuration and operating condition will be proposed which will maximize power-to-weight ratio for the system. A preliminary control system analysis will be made.

Based on the above developments a fuel cell will be designed having a weight-to-power ratio substantially lower than those presently available.

2.4 Significance

The experimental investigations and theoretical analyses described herein indicate clearly that weight-to-power ratio for a 2 kilowatt fuel cell battery system (excluse of fuel and tankage) can be reduced to approximately 50 lbs. per kilowatt net power.

3. MATERIALS

3.1 High Area Platinum Catalysts

In attempts to prepare a more active platinum for use as a fuel cell catalyst, platinum blacks with surface areas up to 60 m^2/g were prepared by silane reduction in alcohol[1A]. These high area blacks had crystallite sizes estimated by X-ray measurement as low as 40 Å (corresponding values for commercial platinum black are about 30 m^2/g surface area and 100 Å crystallite size).

Higher performance in a fuel cell electrode was not achieved, however, with these samples probably for several reasons. It was found that the process for making electrodes on screen caused a relatively larger decrease in effective surface area with high area platinum than with commercial platinum black[2A]. Also, the high area platinum samples were more sensitive to sintering on alternate exposure to hydrogen or oxygen even at room temperature and below[1B]. The conclusion was reached that while high area platinum blacks can be made, so far we have been unable to take advantage of this property in an operating fuel cell.

3.2 Platinum-Rhodium Electrodes

It had been found in previous work that at very low total catalyst concentrations, mixtures of platinum and rhodium were more effective at the hydrogen electrode than either metal alone. A series of experiments was performed to try to retain this synergistic advantage at higher catalyst loadings and thus improve the total cell performance[1C]. The data are shown in Table 3-1 and Figure 3-1. At high loadings of the mixed catalyst performance no better than that obtainable at an equivalent loading of platinum black was observed. It was concluded that, using the

present system for making electrodes, an increase in the amount of platinum and rhodium in the electrodes did not produce any significant performance increase on the hydrogen side of a base cell.

3.3 Matrix Materials

Various forms of asbestos were tested as matrix materials, including a proprietary asbestos sheet as well as several commercial grades[1D]. These materials are listed in Table 3-2.

Mineralogical examination shows that the Johns-Manville asbestos samples are both of the mineral form chrysotile, ($Mg_6(OH)_8Si_4O_{10}$), but differ in the type and amount of impurities present. The Fuel Cell Asbestos Board is an Arizona chrysotile, and contains an estimated 2-4% of carbonate minerals such as calcite ($CaCO_3$) and dolomite [$CaMg(CO_3)_2$]. The Quinterra asbestos is a "de-ironed" Canadian chrysotile, containing very low carbonate impurity (probably less than 0.5%), but with traces of chromite ($FeCr_2O_4$). Analysis of the Quinterra paper showed 1.97% Fe, as compared with 0.34% Fe for the Fuel Cell Asbestos Board.

The "ACCO" asbestos sheet is an experimental material made from a caustic-leached tremolite [$Ca_2Mg_5Si_8O_{22}(OH)_2$] asbestos, with 10% polyvinyl alcohol fiber as a binder. It is more porous than the commercial materials, as shown by the data in Table 3-2.

Preliminary evaluation of these materials showed that 30-mil Fuel Cell Asbestos Board used as a matrix had a relatively high internal resistance, and gave poor performance at high current densities. In the life-testing program, some difficulties were experienced with the thinner asbestos sheets (Quinterra and 10-mil Fuel Cell Asbestos) in atmospheric pressure cells. These matrices exhibited a tendency to permit cross-leakage of gas[2B].

The ACCO Asbestos and the 20-mil Fuel Cell Asbestos were evaluated in more detail. Cell internal resistance and performance were determined over a wide range of cell assembly and operating variables. The results of these studies are summarized in Section 5.2 of this report. In general, the ACCO Asbestos, because of its greater porosity, gave a lower cell resistance and higher level of performance (about 30-40 mv higher at 200 ma/cm^2) than did the 20-mil Fuel Cell Asbestos.

Some preliminary data have been obtained on the maximum pressure differential that asbestos matrix materials will withstand before allowing gas to pass through. Tests were conducted at 70°C in an assembled fuel cell, using 8N KOH in the matrix. Gas pressure was applied to one side of the cell while monitoring the other side for leakage. In preliminary tests, 20-mil Fuel Cell Asbestos withstood differential pressures in the range 10-15 psi. whereas 25-mil ACCO Asbestos permitted gas leakage at about 2-3 psi. Thus, the more open structure of ACCO Asbestos may be a disadvantage in cells operating above atmospheric pressure, in which differential pressures of as much as 2-3 psi may be difficult to avoid. It may be possible to modify the structure of the ACCO Asbestos to reach a better compromise between performance and gas permeability. This will be a subject for future investigation.

3.4 Corrosion Studies

In the life-testing program carried out under this contract, a considerable increase in performance stability has been observed when platinum rather than nickel screens are used as electrode support and spacers. It appears that formation of surface oxides on nickel screens leads to a gradual increase in cell internal resistance and decrease in cell voltage.

Several approaches toward finding a practical substitute for nickel cell parts were investigated:

(a) Plating of nickel parts with precious metals.

(b) Substitution of more corrosion-resistant non-precious metals.

(c) The use of Teflon electrode support screens.

(d) Development of conductive oxide films by lithiation.

To evaluate various possible materials, a corrosion-testing program was set up, in which metal coupons were partially submerged in a 35% KOH solution at 110°C, with oxygen bubbling through. Twelve metals, mostly chromium-nickel alloys, were selected for testing after a survey of the literature. These metals, and their nominal composition, are listed in Table 3-3. Since it was felt that the problem probably involved the formation of surface oxide films, the metals listed in Table 3-3 were exposed for short periods of time and then examined qualitatively for tarnishing. All of the samples showed some degree of tarnishing within ten days of exposure. Some of the metals which showed least tarnishing, together with a gold-plated nickel specimen and a lithiated nickel coupon, were exposed for longer periods of time. For these samples, weight loss determinations, and electrical resistance measurements were made. The gold-plated sample was prepared by an "electroless" process in which a very thin layer of gold, on the order of 1-2 micro-inches, was deposited on a nickel coupon. The lithiated nickel specimen was prepared by sintering a low-carbon nickel coupon coated with lithium hydroxide at 800°C for 15 minutes.

Corrosion rate and resistance measurements on the above samples are summarized in Table 3-4. The weight loss data indicate a negligible corrosion rate (< 1 mil per year) for all specimens tested. Actually, tests for shorter periods indicate that, in general, the corrosion rate is essentially zero, within experimental error, after the first 100 hours or so of exposure.

The electrical resistance measurements were made through the thickness of the 2" x 1" x 1/16" coupons, thus including the resistance of the bulk metal plus two surface oxide layers. The data in Table 3-4 show that, except for the gold-plated and lithiated coupons, the resistance of the exposed coupons was at least two orders of magnitude greater than that of the clean specimens. For the gold-plated specimen, there was virtually no loss in weight during the test exposure, and no increase in electrical resistance. Similarly, the lithiated nickel showed no significant weight loss or resistance increase. In this case, however, because of the heavy oxide layer built up during the lithiation treatment, the resistance of the "clean" specimen was very high compared to that of bare metal. The apparent decrease in resistance for the lithiated coupon during exposure is well within experimental error, and should not be considered significant.

TABLE 3-1

PERFORMANCE OF PLATINUM/RHODIUM ELECTRODES; H_2 SIDE OF BASE CELL[1],[2]

AMBIENT TEMPERATURE

Rhodium mg/cm²	Platinum mg/cm²	Carbon mg/cm²	Total Load mg/cm²	Teflon %	Voltage at 40 ma/cm²	Voltage at 180 ma/cm²
0.0	9.0	0.0	9.0	20	.88	.80
2.5	7.5	0.0	10.0	20	.87	.77
5.0	5.0	10.0	20.0	20	.88	.80
5.0	5.0	10.0	20.0	10	.88	.77
2.5	2.5	15.0	20.0	20	.90	.80
2.5	2.5	15.0	20.0	10	.88	.80
2.5	2.5	5.0	10.0	20	.89	.80
-	5.0	15.0	20.0	20	.86	.75
2.0	2.0	36.0	40.0	10	.90	.77
1.0	1.0	18.0	20.0	10	.90	.80
1.0	1.0	18.0	20.0	20	.88	.78
1.0	1.0	8.0	10.0	10	.87	.77
-	2.0	18.0	20.0	20	.85	.68
0.5	0.5	19.0	20.0	10	.90	.79
1.0	0.0	19.0	20.0	10	.85	.73
0.0	1.0	19.0	20.0	10	.83	.68

(1) Oxygen electrode: Type AB-1

(2) Fil er paper matrix, 5N KOH

TABLE 3-2

DENSITY AND VOID VOLUMES, ASBESTOS MATRICES

Material	Skeletal Density g/cc	Bulk Density g/cc	Calculated Void Volume %	Calculated Void Volume cc/g
"ACCO" Asbestos(A)	3.0	0.37	88	2.4
#10 Quinterra(B)	2.5	0.54	78	1.4
Fuel-Cell Asbestos(B)				
10-mil	2.5	0.78	69	0.88
20-mil	2.5	0.85	66	0.78
30-mil	2.5	0.81	68	0.83

(A) American Cyanamid Co.

(B) Johns-Manville Co.

TABLE 3-3

METALS IN CORROSION TESTING

Alloy	Major Constituents, Wt. %									
	Cr	Ni	Mo	Cu	Fe	Ti	Co	W	Al	Cb
Monel	-	67	-	31	-	-	-	-	-	-
Hastelloy R-235	15	65	5	-	9.5	2.5	-	-	2	-
Hastelloy B	-	66	27	-	5	-	-	-	-	-
Hastelloy C	15	56	16	-	6	-	1	4	-	-
Carpenter 20 Cb	20	27	2.5	3.5	44	-	-	-	-	1
Nimonic 75	20	77	-	-	1	-	-	-	-	-
Incoloy 804	30	44	-		24	-	-	-	-	-
Inconel	15	77	-	-	7	-	-	-	-	-
Alloy 25	19	9	-	-	3	-	51	15	-	-
Nickel A										
Nickel L (Low Carbon)										
Zirconium										

TABLE 3-4

CORROSION TEST DATA

	Exposure Time[a] (hrs.)	Corrosion Rate (mils/year)	Electrical Resistance[b] (ohms) Clean Specimen	Electrical Resistance[b] (ohms) After Test Exposure
Nickel A	1004	0.2	0.0002	.015
Low-Carbon Nickel	1004	0.2	0.0002	.014
Monel	209	0.5	-	-
Carpenter 20 Cb	336	0.5	.0001	20.[c]
Nimonic 75	1003	0.1	0.0023	0.120
Incoloy 804	1003	0.2	0.0022	0.180
Zirconium	1025	0.6	0.0048	> 1000
Gold-Plated Nickel[d]	308	< 0.1	0.0003	0.0003
Lithiated Nickel	1148	< 0.1	300	160

(a) Exposure (partially immersed) to 35% KOH and oxygen at 110°C.

(b) Measured through the thickness of 2" x 1" x 1/16" thick specimens. Clean specimens measured at 30°C, test specimens at 100°C.

(c) Measured at 30°C

(d) Totally immersed.

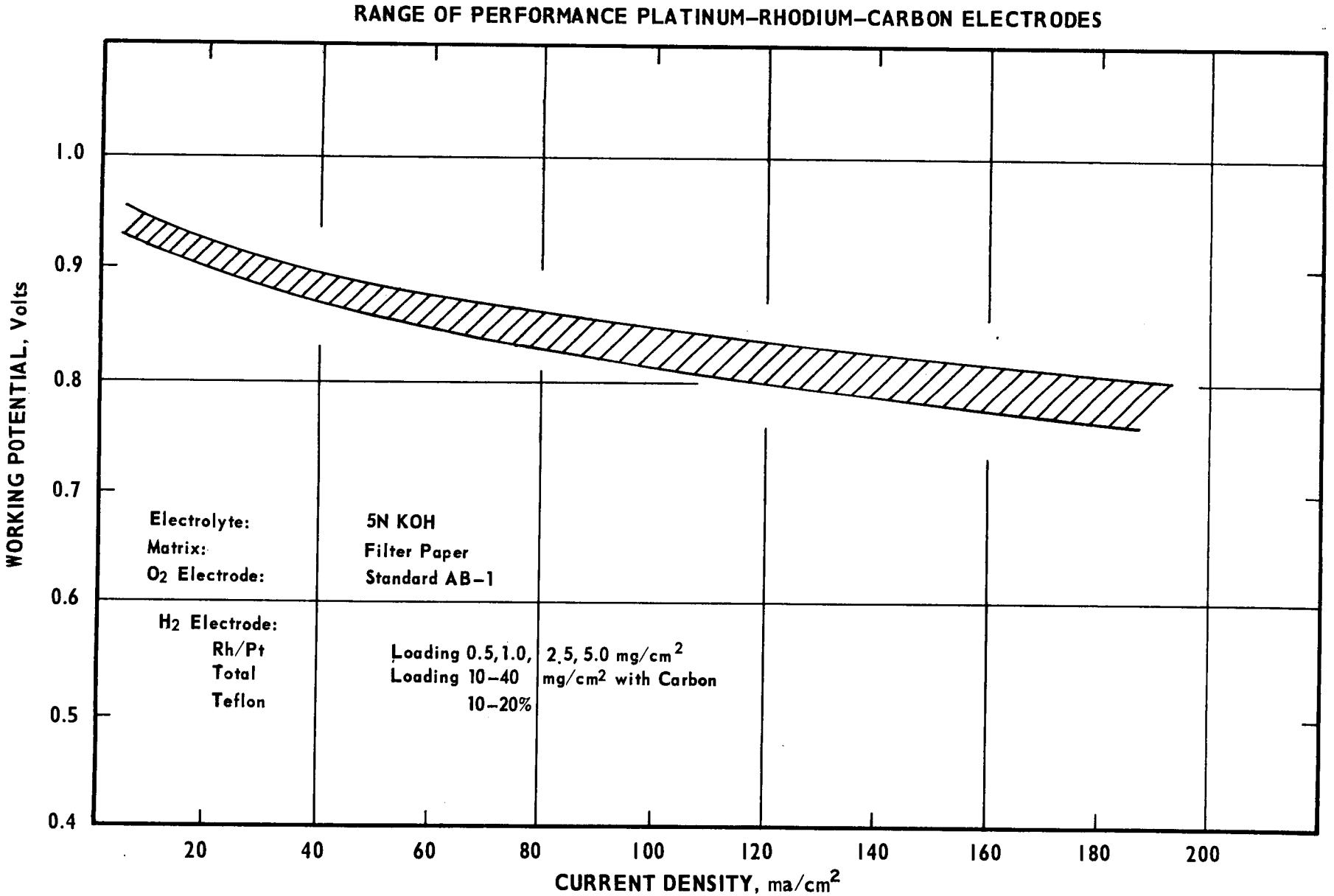
RANGE OF PERFORMANCE PLATINUM–RHODIUM–CARBON ELECTRODES
WORKING POTENTIAL, Volts
1.0
0.9
0.8
0.7
0.6
0.5
0.4
20
40
60
80
100
120
140
160
180
200
CURRENT DENSITY, ma/cm2
Electrolyte: 5N KOH
Matrix: Filter Paper
O2 Electrode: Standard AB–1
H2 Electrode:
Rh/Pt
Total
Teflon
Loading 0.5, 1.0, 2.5, 5.0 mg/cm2
Loading 10–40 mg/cm2 with Carbon
10–20%

FIGURE 3–1

4. ELECTRODE DEVELOPMENT

The principal objective of the work done under this contract has been to maximize performance in the alkaline fuel cell system. Toward this objective, modifications in electrode composition and structure were studied. Inasmuch as the investigations reported in Section 3 did not lead to more promising catalytic materials, commercial platinum black (obtained from Engelhard Industries, Inc.) was used in this work. Typical properties for this platinum black are: surface area, 27-32 m^2/g; crystallite size, 95-110 Å; bulk density (settled), < 1 g/cc.

4.1 American Cyanamid Type AB-1 Electrodes

American Cyanamid Type AB-1 electrodes were taken as a standard for comparison of modified electrode structures. These electrodes are formulated to contain 9 mg Pt/cm^2 of superficial electrode area, and use 100 mesh 2 mil wire nickel screen as a catalyst support. Teflon, at a nominal level of 25% (1 part Teflon, 3 parts platinum), is used as a binder-waterproofing agent. The waterproofing allows optimum contact between gas, catalyst, and electrolyte. A high degree of porosity in the electrodes provides a large exposed catalyst area and aids in gas-liquid contacting.

4.2 Electrode Modifications

For the electrode development program, variations in platinum loading, in screen support, in waterproofing level, and in degree of porosity were investigated(IE). Not all of these variables are independent. For example, wide variations in catalyst loading cannot be achieved without changing the screen support.

Electrodes prepared for this program were evaluated by running polarization curves at 70°C using a filter paper matrix saturated with 5N KOH. In most cases the test electrodes were used at both anode and cathode. Preliminary evaluation data are given in Table 4-1.

4.2.1 Platinum Loading

Platinum loadings were increased to 20 and 40 mg/cm^2 on a variety of nickel support structures, and to 80 mg/cm^2 using several layers of expanded metal. The data given in Table 4-1 show an increase in performance with increasing loading up to 40 mg/cm^2, for electrodes prepared with single-layer support structures. The performance obtained with 40 mg Pt/cm^2 on a single 40-mesh nickel screen support was the best observed for any of the electrodes evaluated in this program. Additional electrode samples of this type were prepared with varying waterproofing levels[2C]. Performance of these samples, as compared with standard AB-1 electrodes, is shown in Table 4-2. Electrodes containing 40 mg Pt/cm^2 were designated as High-Loading electrodes, and were used extensively in the life-testing and scale-up programs. A more comprehensive evaluation of High-Loading electrodes, with asbestos matrices, and over a range of temperature, pressure, and electrolyte concentration, is reported in Section 5.2.

To determine whether the improvement in performance noted for High-Loading electrodes was associated with the hydrogen or the oxygen electrode (or both), a series of tests was run in which High-Loading

electrodes were tested against Standard AB-1 counter-electrodes[2D]. These tests (see Table 4-3) indicated that at low current densities, improvement in performance is associated with the oxygen electrode, and at high current densities, with the hydrogen electrode. Thus it would appear that while the reaction mechanism at the oxygen electrode may be performance-limiting at low current densities, the ability of the hydrogen electrode to handle a high rate of water production may be critical at high current densities.

4.2.2 Nickel Support Screens

In preparing electrodes with varying catalyst loadings, nickel woven wire screens in the following sizes were utilized:

100 mesh, 2 mil wire
70 mesh, 4.5 mil wire
40 mesh, 10 mil wire

These were used both singly and, in some cases, as a "sandwich" structure in which the catalyst was held between two layers of screen[1E]. In addition to the woven wire, a variety of expanded nickel screens were evaluated as catalyst supports[1E,2E].

Because of the interdependence of screen-support and catalyst loading, it was not possible to make direct comparisons between different single screens at a given platinum level. In general, however, it appeared that single screen structures were significantly better than sandwich structures (see Table 4-1).

Expanded nickel sheets with from 25 to 625 openings/in^2 and thicknesses from 5-23 mils were evaluated. Electrode sheets were prepared with single or multiple thicknesses of expanded metal (sandwich structures),

with total platinum loadings from 10 to 80 mg/cm^2, and Teflon levels from 10-40%. These electrodes were tested at ambient temperature as oxygen electrodes versus a Standard AB-1 hydrogen electrode. The data are shown in Table 4-4. In no case was performance superior to that for an AB-1 oxygen electrode. Thus, from the standpoint of initial performance, expanded metal supports appear to offer no advantage over woven-wire screens.

4.2.3 Alternate Support Screen Materials

In view of the apparent need for an electrode support material more stable than nickel in the base system, the use of (1) gold-plated nickel screens, and (2) Teflon screens was investigated.

Gold-plating was applied to the nickel screens by an electroless process, to a thickness of approximately 1.5 micro inches. At this thickness, the nickel substrate is not completely covered, as can be demonstrated, for example, by immersing the plated screen in concentrated HCl. Coverage should be adequate, however, to eliminate or minimize the increase in cell resistance which, with unplated nickel screens, has been attributed to build-up of oxide-films at points of electrical contact. Screens plated in the above manner have been used successfully in the life-testing program (See Section 5.3).

Electrodes utilizing a woven Teflon support screen have also been used in the life-testing program with some success. Although the Teflon support screen is not electrically conductive, good performance can be achieved by using a close-meshed current collector. As shown in Table 4-5, performance very close to that of AB-1 electrodes was obtained

with an electrode containing approximately 12 mg Pt/cm^2 on a 100 mesh Teflon screen. While this performance was very encouraging, further development of these electrodes (toward higher catalyst loadings) was not undertaken in view of the more attractive alternative afforded by gold-plating.

4.2.4 Waterproofing Level

A number of electrode sheets were prepared with high catalyst loading (40 mg Pt/cm^2), but with the waterproofing reduced from the standard level of 25% to 14% and 8% Teflon. Preliminary testing indicated that at the 8% level, performance was erratic, and poorer than with Standard AB-1 electrodes. More extensive data (Table 4-2) obtained on electrodes containing 14% Teflon showed these to be comparable to electrodes with 25% Teflon at low current densities. At high current densities (200 ma/cm^2 and higher) however, performance was lower and less reproducible for the 14% Teflon electrodes. Thus, there appears to be no advantage to lowering the Teflon level from the standard 25%.

Electrodes with a 10 mg Pt/cm^2 catalyst loading, but with a high Teflon level (50%) were evaluated in the life-testing program (Test 2-38, Tables 5-3, 5-4). After several hundred hours on test, the voltage began to decline and resistance to rise at an accelerated rate. After gas reversal, the cell ran stably for approximately another 250 hours, but then started another period of accelerated decline.

The accelerated trends in this test are believed to be associated with "over-waterproofing" in the electrode. Thus, increasing the waterproofing level to as high as 50% Teflon does not appear to be desirable.

Several electrodes having a graded waterproofing structure were also prepared and evaluated[2D]. In these electrodes, the Teflon level was 35% on one face and 8% on the other. They were tested with the low-waterproofing face toward the matrix. The data are shown in Table 4-6. Performance of these electrodes was equivalent to that for electrodes having similar support structure but with uniform waterproofing.

4.2.5 Porosity

By proper adjustment of the electrode formulation and processing conditions, some variations in "porosity" can be achieved. For this program, two electrodes having a relatively less dense or more open structure were prepared and evaluated (see Table 4-1). In both cases, polarization performance was equivalent to similar electrodes having standard "porosity".

TABLE 4-1

PERFORMANCE OF MODIFICATIONS OF TYPE AB-1 ELECTRODES

Electrode	S-6609-2-1	LD-213-358-1	S-6501-47-1	S-6609-1-2	S-6609-1-1	S-6609-3-1	S-6609-3-2	S-6609-3-3	S-6609-5-1	S-6609-4-1
Platinum Loading mg/cm^2	9	9	9	20	20	20	20	20	40	40
Formulation	Std	Std	Increased Porosity	Std	Std	Std	Increased Porosity	Decreased Waterproofing	Std	Std
Support Screen	100 Mesh	100 Mesh	70 Mesh	100 Mesh "Sandwich"	70 Mesh	5 Ni 7-4/0 Expanded Nickel	70, 40 Mesh "Sandwich"	70,100 Mesh "Sandwich"	40 Mesh	70 Mesh "Sandwich"
				Working Voltage at 70°C (Average of Three Tests)						
Current Density ma/cm^2										
0	1.036	1.036	1.036	1.036	1.043	1.036	1.040	1.040	1.047	1.046
40	0.923	0.918	0.913	0.934	0.946	0.929	0.927	0.938	0.944	0.934
100	0.884	0.882	0.875	0.899	0.908	0.895	0.892	0.902	0.907	0.900
200	0.844	0.836	0.840	0.848	0.866	0.847	0.848	0.859	0.870	0.859
300	0.812	0.790	0.808	0.799	0.832	0.820	0.813	0.823	0.846	0.825
400	0.769	0.593	0.767	0.771	0.788	0.750	0.749	0.787	0.799	0.793

TABLE 4-2

Performance of High-Loading Electrodes

1" Diameter Cell; 70°C; 5N KOH; Filter Paper Matrix; Test Electrodes Both Sides

Electrode No.	Pt Loading mg/cm²	Teflon Level %	No. of Tests	Ave. Cell Working Potential (Volts) at Indicated Current Density (ma/cm²) 40	100	200	300	400
6609-5-1	40	25	3	.945	.908	.870	.847	.800
6609-9-1	40	25	4	.952	.913	.873	.842	.805
6609-9-2	40	25	3	.951	.913	.872	.839	.802
	Grand Average:		10	.950	.911	.872	.843	.802
	Standard Deviation:		10	.008	---	.007	---	.012
6609-8-1	40	14	3	.963	.921	.874	.832	.781
6609-9-3	40	14	4	.950	.906	.857	.817	.776
6609-9-4	40	14	3	.956	.914	.864	.819	.775
	Grand Average:		10	.955	.913	.864	.822	.777
	Standard Deviation:		10	.007	---	.017	---	.045
LD 213-365-16(1)	9	25	6	.930	.894	.855	.820	.781
6609-75-1(1)	9	25	3	.935	.897	.856	.819	.767
	Grand Average:		9	.931	.895	.855	.821	.777
	Standard Deviation:		9	.010	---	.008	---	.019

(1) Standard Type AB-1 Electrodes

TABLE 4-3

Evaluation of High-Loading Electrodes vs. Standard Counter Electrodes

1" Diameter Cell; 70°C, 5N KOH; Filter Paper Matrix

Oxygen Electrode:	40 mg Pt/cm² 25% Teflon		40 mg Pt/cm² 14% Teflon		Standard AB-1(1)		Standard AB-1(1)	
Hydrogen Electrode	Standard AB-1(1)		Standard AB-1(1)		40 mg Pt/cm² 25% Teflon		40 mg Pt/cm² 14% Teflon	
Total Data Points	4		4		5		3	
Current Density, ma/cm²	Cell Working Potential, Volts							
	Ave.	Std. Dev.	Ave.	Std. Dev.	Ave.	Std. Dev.	Ave.	Std. Dev.
40	.960	.002	.960	.006	.938	.001	.935	.001
100	.918	-	.922	-	.901	-	.898	-
200	.870	.003	.873	.020	.864	.002	.858	.004
300	.826	-	.832	-	.835	-	.826	-
400	.775	.009	.779	.050	.808	.004	.794	.012

(1) Electrode Sheet LD 213-365-16

TABLE 4-4

Evaluation of Expanded Nickel as Electrode Support

As Oxygen Electrode vs. Standard Hydrogen Electrode

1" Diameter Cell; Ambient Temperature; 5N KOH; Filter Paper Matrix

Expanded Ni(1)			Total Platinum, mg/cm^2	Teflon %	Cell Potential, Volts at		Run No.
Mesh, Openings/in^2	Single Layer Thickness, mils	No. of Layers in Sandwich			40 ma/cm^2	180 ma/cm^2	S-6792
	Standard AB-1 Expanded Nickel		9	25	0.925	0.835	
25	21	3	40	40	0.93	0.76	75-1
65	14	3	40	40	0.945	0.82	74-1
65	14	6	80	40	0.945	0.73	75-2
120	13	2	10	30	0.92	0.81	61-1
120	13	1	20	30	0.95	0.835	54-1
120	13	2	20	30	0.93	0.785	62-1
120	13	1	40	10	0.92	0.78	53-1
120	13	1	40	30	0.95	0.82	47-2
120	13	2	40	50	0.94	0.80	56-1
120	13	2	80	10	0.95	0.79	50-1
120	13	2	80	30	0.95	0.79	31-1
120	23	1	40	30	0.94	0.82	54-2
120	23	1	40	40	0.93	0.81	55-1
300	10	1	40	30	0.93	0.80	48-2
300	10	2	80	10	0.94	0.79	29-2
300	23	1	20	30	0.92	0.795	48-1
300	23	1	40	20	0.94	0.795	45-1
300	23	2	40	30	0.92	0.79	50-2
300	23	2	80	10	0.90	0.68	29-1
300	23	2	80	20	0.95	0.775	34-1
300	23	2	80	30	0.95	0.79	43-1
625	5	3	40	14	0.94	0.81	195-1
625	5	6	80	14	0.92	0.75	192-1

(1) Obtained from Exmet Corporation, Bridgeport, Connecticut

TABLE 4-5

Polarization Data - Teflon Screen Electrodes

Electrolyte: 7N KOH

Temperature: 70°C

Matrix	#42 Filter Paper		20 Mil Fuel Cell Asbestos	
Electrode:	AB-1	Teflon(a)	AB-1	Teflon(a)
Current Density ma/cm^2	Working Potential, volts			
5	1.01	1.00	0.99	1.00
20	0.97	0.97	0.96	0.96
40	0.94	0.94	0.93	0.93
100	0.90	0.90	0.88	0.86
200	0.84	0.85	0.80	0.77
400	0.66	0.76	0.65	0.55

(a) Approximately 12 mg Pt/cm^2 on 100 mesh Teflon screen.

TABLE 4-6

Evaluation of Electrodes with Dual Waterproofing Structure(1)

1" Diameter Cell; 70°C; 5N KOH; Filter Paper Matrix; Test Electrodes Both Sides

Electrode	S6609-1-2	S6609-7-2	S6609-7-3	S6609-4-1	S6609-8-2
Pt Loading, mg/cm^2	20	20	20	40	40
Teflon Level, %	**Standard:** 25	**Dual:** 8, 35	**Dual:** 8, 35	**Standard:** 25	**Dual** 8, 35
Support Screen	2 x 100 mesh "Sandwich"	2 x 70 mesh "Sandwich"	70 mesh Single Screen	2 x 70 mesh "Sandwich"	2 x 70 mesh "Sandwich"
Current Density, ma/cm^2			Working Voltage		
0	1.036	1.047	1.034	1.046	1.050
40	0.934	0.929	0.921	0.934	0.955
100	0.899	0.888	0.884	0.900	0.910
200	0.848	0.844	0.839	0.859	0.855
300	0.799	0.806	0.801	0.825	0.807
400	0.771	0.770	0.762	0.793	0.750

(1) Consisting of 8% and 35% Teflon on opposite sides, evaluated with 8% Teflon side toward electrolyte

5. SMALL SCALE TESTING

5.1 Test Cell Development

Small-scale fuel cells have been designed and built in two sizes for the evaluation of electrodes and matrices. Cells having a one-inch circle active area (5 cm^2) were used for obtaining polarization data. For life-testing, cells having a 2" x 2" active area (25.8 cm^2) were constructed in two types, one for testing at atmospheric pressure, and another for pressures up to about 50 psig.

5.1.1 2" x 2" Cell - Atmospheric Pressure Design

5.1.1.1 General Configuration

Figure 5-1 shows schematically the general relationship of parts in 2" x 2" matrix-type fuel cells utilizing two different gasketing arrangements. The face plates serve as housing, gas distributors, and current collectors. The matrix, sandwiched between the electrodes and saturated with electrolyte, permits ion transport between electrodes and prevents gas mixing. The spacer screens carry current from the electrodes to the face plates and also insure adequate contact between the electrodes and the matrix. The gaskets define the gas space, and prevent liquid or gas leakage out of the cell.

The cells are heated by flat heating elements cemented to the outside of the face plates. The cell temperature is regulated to within $\pm$ 0.5°C by an on-off thermistor-type controller and is measured by an iron-constantan thermocouple. Probes for the controller and thermocouple are inserted into the face plates.

Figure 5-1 shows two different gasketing arrangements which have been used in this program. The Type I arrangement, used in the early phases of the life-testing program, utilizes silicone rubber gaskets covered with Teflon tape, flat spacer screens, and a polyethylene film seal around the edges of the matrix[1F]. An exploded view of a test cell with the Type I gasketing arrangement is shown in Figure 5-2. The Type II arrangement, using solid Teflon gaskets, represents a modification designed to eliminate the possibility of contamination from degradation of silicone rubber or plastic film[2F]. The use of corrugated screens in this design eliminates the close thickness tolerance required for the spacer screens in the earlier design.

5.1.1.2 Face Plate Design

The face plate design finally adopted for the 2" x 2" cells to be used for life-testing at atmospheric pressure is shown in Figure 5-3. The general configuration is similar to that shown in Figure 5-2, but the outside dimensions have been increased, and the number of bolts increased from four to six to prevent bowing of the plates during assembly. The gas distribution pattern remains the same, the gas entering from holes in a manifold at one end of the cell active area, flowing through the spacer screens across the back of the electrode, and out through the exit manifold. The spacing between the inlet and exit gas manifolds was reduced from 2" to 1-3/4", however, to eliminate difficulties associated with having the gas enter at the very edge of the electrode.

5.1.2 2" x 2" Pressure Cell

A cell was designed and constructed for operation at pressures up to 50 psig, and with differential pressures between H_2 and O_2 of at least 5 psig. Figure 5-4 shows the basic design features. The active area, as with the standard cell, is 2" x 2". Gas distribution within the active area (not shown in the figure) is also the same as in the standard cell. Sealing against cross-leakage of gas is accomplished by compression of the matrix between the lands in the grooved area surrounding the active area of the cell. The grooves permit electrolyte to be squeezed out during cell assembly, thus preventing hydraulic rupture of the matrix. Leakage of gas or electrolyte out of the cell is prevented by an O-ring seal.

5.1.3 One-Inch Cell

The one-inch cell is similar in general design to the 2" x 2" cell described in section 5.1.1, except that the gasket opening is a 1-1/16" circle to accommodate 1" circular electrodes and spacer screens. In using the one-inch cell, the matrix is usually cut as a 1-1/2" circle. A Type I gasketing arrangement is used, but since this cell is used only for tests of short duration, the silicone rubber gaskets are not usually protected with Teflon tape, nor are the edges of the matrix sealed with polyethylene film.

5.2 Performance vs. Operating Conditions

In order to determine the electrode-matrix system and the operating conditions which should result in a battery system of minimum weight per net power, the initial performance of four electrode-matrix systems was investigated in one-inch and two-inch cells. These systems are as follows:

Electrodes	Matrix
Standard AB-1	ACCO Asbestos
Standard AB-1	Fuel Cell Asbestos
High-Loading	ACCO Asbestos
High-Loading	Fuel Cell Asbestos

The effect of the following important variables on initial performance was determined.

(1) Matrix thickness

(2) Cell assembly pressure

(3) Electrolyte (KOH) loading

(4) KOH concentration

(5) Temperature

(6) Gas Pressure

This report summarizes the principal observations and conclusions of this study.

5.2.1 Polarization Curves

Polarization curves were determined at increasing current densities up to the maximum obtainable. All voltages reported are working voltages. At each current density, the voltages were considered initially stable if they remained constant within 3 mv for two minutes. Constant electrolyte concentration was maintained by setting the gas flow rates at each current density to remove product water as fast as it was formed. After reaching the maximum current density, the first polarization curve was checked by running a second curve, again at increasing current density.

With Standard AB-1 electrodes, the second polarization curve was nearly always the same as the first. In a very few runs, the voltages of the second curve were 20-40 mv greater than those of the first. In these runs, the maximum current density of the first polarization curve was 500-600 ma/cm^2, compared with the usual value of 300-400 ma/cm^2.

With High-Loading electrodes, maximum current densities of 1000-1400 ma/cm^2 were attained. In nearly all runs at 70 and 100°C, the second polarization curve voltages ranged from 20-40 mv above the first out to about 500-600 ma/cm^2, but this difference tended to disappear at still higher current densities. Running a third polarization curve produced no further voltage change. These voltage increases occurred at all electrolyte concentrations and so probably were not the result of electrolyte concentration changes during a measurement. The voltage increases probably arise from some activation of the electrode at high current densities or relatively low voltages. While the long-term permanence of this effect was not established, stable performance for at least four hours at the increased voltage level was demonstrated. Since no further changes occurred during third polarization curves, the performance reported for High-Loading electrodes in Sections 5.2.2 to 5.2.9 is that of the second polarization curve.

5.2.2 Matrix Thickness

The influence of matrix thickness on cell internal resistance and performance was investigated[3A]. Figure 5-5 shows the effect of thickness on cell resistance for ACCO and Fuel Cell Asbestos matrices, using High-Loading electrodes and 13N KOH at 100°C. With both matrix

materials, the cell internal resistance is proportional to the uncompressed matrix thickness and extrapolates to zero resistance at zero thickness. The resistivity of ACCO Asbestos (1.49 ohm-cm) is substantially below that of Fuel Cell Asbestos (3.86 ohm-cm), probably a result of the greater porosity of the former (Section 3.3).

Figures 5-6 and 5-7 show the effect of matrix thickness on performance. At equal matrix thickness and (total) electrolyte loading the two matrix materials yield comparable voltages at current densities up to 200 ma/cm^2 at least for matrix thickness less than 20 mils. Above this current density, ACCO Asbestos gives increasingly higher voltages than Fuel Cell Asbestos. This is also true at a matrix thickness greater than 20 mils even at low current density. This is partly due to the lower internal resistance of cells using ACCO Asbestos matrix. In studies of other operating variables, a 20 mil matrix was used.

5.2.3 Cell Assembly Pressure

With either matrix material, and over wide ranges of electrolyte loading, the electrolyte distribution throughout the cell, the cell internal resistance, and the cell performance, are all generally independent of cell assembly pressure(a) in the range 60-180 psi[3B]. Below 60 psi, cell resistance is high and cell performance poor, probably because of insufficient contact among cell components.

5.2.4 Electrolyte Loading

The effect of initial electrolyte loading (g KOH solution per gram of dry matrix) on the distribution of electrolyte throughout the cell after assembly is similar for the two matrix materials[3B]. The amount of

(a) Assembly pressure is calculated from torque applied in tightening bolts when cell is assembled.

electrolyte remaining in the matrix after assembly is nearly proportional to the initial loading; 12-33% of the initial electrolyte loaded is pressed out of the matrix into the electrodes and spacer screens. The amount retained in the electrodes increases relatively little with loading and amounts to 14-28% of the dry electrode weight (compared with a saturation level of about 40%).

The lowest cell resistance and the highest performance are obtained at initial electrolyte loadings of 1.5-3.0 g/g and 1.0-1.5 g/g with ACCO Asbestos and Fuel Cell Asbestos, respectively. Since ACCO Asbestos is about one-half as dense as Fuel Cell Asbestos, these ranges correspond to approximately the same total quantity of electrolyte solution loaded into the matrix. At lower loadings, cell resistance is high and cell performance is poorer because of dry areas in the matrix. These results are the same for both electrode types.

In all studies of other operating variables, the cell was assembled at 150 psi, with electrolyte loadings within the optimum ranges given above.

5.2.5 KOH Concentration

The dependence of cell resistance on KOH concentration is generally similar for all four electrode-matrix systems. Figures 5-8 and 5-9 show the data obtained at 70°C and 100°C, respectively[2G,3C]. Cell resistance decreases sharply in the concentration range 1-3N but is little affected by concentration in the range 3-13N. The resistance-concentration curves have essentially the same shape as that of free electrolyte, computed from conductivity data[4], which indicates a broad minimum between 7 and 11N (see Figure 5-9). Cell resistance is generally the same for the two electrode types but, at all concentrations, is approximately one-half as great with ACCO Asbestos as with Fuel Cell Asbestos. As stated in Section 5.2.2 this is probably due to the greater porosity of ACCO Asbestos.

The dependence of performance on KOH concentration was investigated in detail for the four electrode-matrix systems at 70°C and 100°, and at KOH concentrations up to 13N[2G,3C]. The data are shown in Figures 5-10 through 5-17. Highest performance in this range of temperature and concentration was obtained with High-Loading electrodes and ACCO Asbestos. Using High-Loading electrodes some exploratory studies were also made at higher temperatures (to 200°C) and concentrations (to approximately 75%[3D]). Performance data for these conditions are given in Table 5-1.

The general conclusions drawn from these studies are summarized below:

(1) Open circuit voltage increases by 20-90 mv with increasing KOH concentration in the range 1-13N, exceeding in some instances the theoretical increase of 30 mv in the reversible emf for the same concentration change[5].

(2) Performance increases markedly with increasing concentration in the range 1-3N or 1-5N, depending on the matrix material. At 1N, the maximum current density does not exceed 100-200 ma/cm^2. This poor performance is probably the result of gas concentration polarization resulting from the high vapor pressure of water.

(3) In the concentration range 5-13N, cell voltage generally increases continuously by 20-90 mv with increasing concentration except at very high current densities. At very high current densities highest performance occurs at concentrations (5-9N) which correspond to the condition of maximum electrolyte conductivity.

(4) At 100°C, increased concentration in the range of 13-17N generally results in small increases in performance at current densities up to 300-400 ma/cm^2, but results in substantial decreases in the performance at current densities of 400-1000 ma/cm^2.

(5) At 140°C, performance generally increases with increasing concentration over a somewhat higher concentration range (up to 17-19N) and up to much higher current densities (500-1200 ma/cm^2) than at 100-120°C. From KOH solubility-temperature data[6] it was calculated that the maximum concentrations employed at 140°C were 5-17% below the solubility limit (72%).

The varying effects on cell performance of changes in KOH concentration at different levels of concentration, temperature, and current density described in results (1) to (5) arise from the combined effects of concentration and temperature on the reversible emf, the internal cell resistance, and on various polarization phenomena. Based on these concepts, qualitative explanations of the observed effects can be derived. However, this analysis will be deferred until additional experimental data can be obtained.

5.2.6 Temperature

Cell resistance decreases with increasing temperature, more rapidly at higher KOH concentration (13N) than at lower concentration (5N), as shown in Figure 5-18. At both KOH concentrations, the resistance-temperature curves parallel the equivalent curves for free electrolyte, which indicates that changes in cell resistance depend primarily on changes in electrolyte conductivity.

Figures 5-19 and 5-20 illustrate the dependence of cell performance on temperature in the range 50-100°C for High-Loading electrodes - ACCO Asbestos matrix system. With 13N KOH, (Figure 5-19) performance increases with increasing temperature at all current densities. The increase in performance is especially marked at high current densities and represents a substantial improvement in electrode efficiency, since the resistance factor can account for only 5-25% of the voltage increase at all densities. At 50°C, the polarizations operating in the cell are severe enough to limit the maximum current density to 600 ma/cm^2 compared to 1000-1400 ma/cm^2 at 70-100°C. With 5N KOH, (Figure 5-20) performance also increases as the temperature increases, although less strongly than with 13N KOH. This is due in part to a smaller dependence of cell resistance on temperature at the lower concentration.

Performance at temperatures in the range 100-140°C of High-Loading electrodes in combination with the two matrix types can be seen from the exploratory data in Table 5-1. At 100-140°C, performance increases with increasing temperature at KOH concentrations (17-19N) which approach the solubility limit at 100°C, whereas performance is unaffected at a lower concentration (13N). As at 50-100°C, the increase in performance is due in part to a decrease in cell resistance, and in part to an improvement in electrode efficiency. This is indicated in Run 137 in which simultaneous increases in temperature (100-140°C) and KOH concentration (13-18N) increased cell performance at current densities up to 300 ma/cm^2; cell voltage increased by 20 mv despite a resistance increase equivalent to a voltage loss of 42 mv.

At higher current densities, the resistance factor apparently predominates and performance decreases. A similar effect is evident from Run 140 in which the temperature was increased from 100-200°C simultaneously with a concentration increase from 50% (13N) to approximately 75% KOH while the current density was maintained at 100 ma/cm^2. It can be seen that cell voltage is the same at 180°C as at 100°C despite an increase in resistance equivalent to a voltage loss of 33 mv.

5.2.7 Gas Pressure

The effect of total gas pressure on performance is shown in Table 5-2 for various electrode-matrix systems. Some difficulties with sudden cell failure at 30-45 psig were encountered with the ACCO matrix. While some variation in cell performance was encountered from run to run, the general effect of increasing pressure in the range 0-45 psig is to increase cell performance by 20-140 mv at current densities up to 400 ma/cm^2 and by 100-260 mv at 500-1200 ma/cm^2. For the most part, these gains in performance are considerably greater than the theoretical increase in reversible emf (30 mv) with increased pressure, which shows that increased pressure from 0-45 psig substantially decreases polarization effects.

As indicated in section 5.2.5, the low performance of the High-Loading electrodes-ACCO Asbestos matrix system at 100°C and 3N KOH (Figure 5-17) is probably the result of gas concentration polarization caused by the high water vapor pressure and correspondingly low partial pressure of reactant gases (ca. 100 mm Hg). This view is supported by the marked gain in cell voltage (60 mv at 100 ma/cm^2 and 130 mv at 200 ma/cm^2) and by the marked increase in maximum current density (from 200 ma/cm^2 to 1200 ma/cm^2)

caused by a relatively modest increase in pressure from 0-15 psig (Runs 13, 16, 24 in Table 5-2). These voltage increments are substantially above those obtained for the same pressure increase at 100°C and 13N KOH (10-30 mv at 100 ma/cm^2 and 0-40 mv at 200 ma/cm^2). In the latter case (Run 93) the partial pressure of reactant gases at 0 psig is much greater (580 mm Hg).

5.2.8 Electrode and Matrix Type

The performance data discussed in sections 5.2.2 - 5.2.7 show that High-Loading electrodes (40 mg Pt/cm^2) give substantially higher initial performance at all current densities than do Standard AB-1 electrodes (9 mg Pt/cm^2), with either ACCO Asbestos or Fuel Cell Asbestos as the matrix, and at all combinations of matrix thickness, cell assembly pressure, electrolyte loading, electrolyte concentration, temperature, and gas pressure which were studied. (This is true even if the increase in performance caused by running the first polarization curve out to high current densities (section 5.2.1) is neglected.) The range of current densities over which only small variations of voltage with KOH concentration are observed is considerably greater for High-Loading electrodes (up to 1200 ma/cm^2) than for Standard AB-1 electrodes (up to 300 ma/cm^2). Thus, High-Loading electrodes should be capable of operating at higher current densities with smaller voltage changes caused by KOH concentration fluctuations.

The ACCO Asbestos matrix generally gives higher initial performance than does an equal thickness of Fuel Cell Asbestos, with either High-Loading or Standard AB-1 electrodes at nearly all combinations of the operating variables mentioned above.

Consequently, on the basis of initial performance, the High-Loading electrodes - ACCO Asbestos matrix system appears to be the best of the four.

5.2.9 Maximum Performance Obtained

The work done under this contract has shown that increased performance can be obtained with light-weight fuel cell electrodes by judicious choice of components and operating conditions, as discussed in the previous pages of this section.

The best performance test (also reported in Table 5-2) is shown in Figure 5-21) for operation at 140°C and 15 psig pressure. For comparison the polarization curve for AB-1 electrodes at 100°C and 15 psig is also shown. Results close to this highest performance were obtained under other combinations of conditions. The best obtained at 100°C and 45 psig is also shown in Figure 5-21.

It should be emphasized that these very high results are for initial polarization only and sustained performance for more than several hours has not yet been investigated.

5.3 Life-Testing

During the course of this investigation, test cells were developed, life-testing procedures established, and a total of sixty-eight life tests run. Test conditions and performance data for these tests are summarized in Tables 5-3 and 5-4.

Most of the early tests were run with Standard AB-1 electrodes, at 70°C and 100 ma/cm^2, using dry gases$^{(1G,2H)}$. Various asbestos matrix materials, both proprietary and commercial, were evaluated. Both Johns-Manville Fuel Cell Asbestos and ACCO Asbestos in 20-25 mil thickness gave satisfactory performance in tests at 70°C, the ACCO Asbestos, because of its more open structure, giving a slightly higher level of performance.

In all of the early tests, downward trends in performance were noted. In most cases, upward trends in cell resistance with time were also observed. Losses in voltage of 50-100 millivolts in 1000 hours at 100 ma/cm^2 were typical, with approximately half of this loss being directly attributable to the increase in cell resistance. These same trends were observed in tests with High-Loading electrodes, in tests utilizing partially saturated inlet gases, and in tests run in cells in which the silicone rubber gaskets and polyethylene matrix-seals were replaced with Teflon.

It was observed in Tests 2-71, 19 and 24 that reversing the gases (hydrogen on the oxygen side and vice-versa) had a beneficial effect on both voltage and cell resistance[2I]. Following gas reversals, stable operation for several hundred hours or more would typically be observed before the usual trends again became evident. This pattern suggested the possibility that oxidation of nickel cell parts might be responsible for the observed trends. Therefore tests were run in which platinum was substituted for nickel in electrode support and spacer screens. In these tests (2-39, 46) operating at 70°C and 100 ma/cm^2, very little decrease in voltage (< 2 mv/100 hours) was observed[3E].

Two life tests (2-10, 22) were run with experimental silver oxygen electrodes, and one (1-1) with a nickel black hydrogen electrode[2J]. While these electrodes run successfully for several hundred hours or more, performance was not as high as can be obtained with platinum, and no further tests were scheduled as part of this program.

Using both Standard AB-1 and High-Loading electrodes, some exploratory tests were run at higher temperatures and current densities. One test (2-33) using AB-1 electrodes ran well at 100°C and 100 ma/cm^2 dropping only about 30 millivolts in 1000 hours. Other tests (2-45, 51, 59) at this temperature exhibited a more rapid decline in performance, however, and were terminated after only a few hundred hours. Several tests were run at 70°C and 400 ma/cm^2 (2-29, 32, 34 and 40). In all of these latter tests, there was a relatively rapid downward trend in voltage, as well as wide fluctuations within the overall trend.

During the final phase of the life-testing program, attention was focused on evaluation of various practical means for overcoming the increase in cell resistance apparently associated with oxidation of nickel cell parts. Electrodes prepared on gold-plated or on Teflon screens were used extensively. Continued emphasis was placed on testing at higher temperatures and current densities, and some exploratory testing at pressures above atmospheric was initiated.

5.3.1 Electrodes With Corrosion Resistant Support Screens

5.3.1.1 Tests at 100 ma/cm^2

As indicated above, very stable performance at 70°C and 100 ma/cm^2 was achieved in tests with platinum electrode support and spacer screens. Life test 2-46, in which the electrode screens were platinum but the spacer screens were nickel, was continued for 1056 hours with a total drop of only about 15 millivolts, and very little if any increase in cell resistance.

This suggests that the major problem is in the electrode screen rather than the spacer screens under these test conditions. To further pin point the problem, life test 2-72 was set up with a platinum electrode support screen on the oxygen side, but with all other cell parts of nickel. Again, very stable performance was obtained with virtually no loss in voltage or increase in resistance in 1000 hours.

In view of these excellent results with platinum screens, other more practical corrosion-resistant materials were sought. Life tests were run using electrodes made on nickel screens plated with gold, rhodium, or tin-nickel alloy, and on Teflon screens.

The gold-plated screens, as discussed in Section (4.2.3), had a very thin layer of gold (about 1.5 micro inches) deposited by an "electroless" procedure. Rhodium-plated screens were prepared by J. Bishop and Company. Rhodium thickness was approximately 15-20 micro inches. Electrodes made from gold-plated screens were tested at 70°C and 100 ma/cm^2 in life tests 2-73 and 2-89. Life test 2-73 utilized Fuel Cell Asbestos, High-Loading electrodes on gold-plated screens, and gold-plated spacer screens on both sides. Life test 2-89 was run with ACCO Asbestos; gold-plated electrode and spacer screens were used only on the oxygen side. As with the tests using platinum screens, very stable performance was obtained, although in the test 2-89 there was a slight downward performance trend amounting to about 1.5 mv/100 hours. Figure 5-22 illustrates the excellent performance obtained in these tests.

Several tests were run with electrodes containing approximately 10 mg Pt/cm^2 supported on a 100 mesh Teflon screen. Test 2-53 (70°C, 100 ma/cm^2), ran stably at .83-.84 volts for about 300 hours but then began to decline and was terminated after 528 hours. A second test under the same conditions (2-74) showed a similar but more gradual decline after 300 hours, and a resistance rise similar to that observed in tests with nickel support screens. Following gas reversal at 460 hours, performance improved, but a gradual drop in voltage and increase in resistance was noted as the test was continued to 2014 hours. In life test 2-76, electrodes with Teflon support screens performed very poorly at 100°C. Thus, the use of Teflon screen to replace nickel screen as a catalyst support does not appear promising in this application.

In life test 2-70, the face plates as well as the electrode and current collector screens were plated with 0.2 mils of a tin-nickel alloy. This test ran poorly, declining at an average rate of about 16 mv/100 hours.

5.3.1.2 Tests at 200 and 300 ma/cm^2

Using electrodes with both gold-plated and platinum support screens, a number of tests were run at 200 and 300 ma/cm^2. Cell temperature, matrix material, inlet gas humidity, and ratio of hydrogen to oxygen were varied. In none of these tests was performance as stable as that obtained at 100 ma/cm^2. Downward voltage trends occurred in all tests, gradual and relatively uniform in some cases, and others rapid at the beginning and then more slowly. In most of these tests, cell internal resistance remained relatively constant, although a slight upward trend was noted occasionally, for example, in tests 2-79 and 2-94.

Best performance (with respect to stability) at 200 ma/cm^2 was obtained in test 2-60, with 10 mg/cm^2 platinum loading on platinum support screens. In this test the voltage declined at an average rate

of about 2.2 mv/100 hours over the 1000-hour period, while the cell resistance remained essentially constant (Figure 5-23). Test 2-93, in which virtually all product water was removed on the hydrogen side, declined from .835 volts to .808 volts in the first 100 hours, and then remained essentially constant for the next 400 hours. After 500 hours total time, however, performance began to decline more rapidly, although there was no corresponding increase in internal resistance.

At 300 ma/cm^2, two tests were run for 1000 hours. Initial and final voltages were about the same for the two tests, but whereas in test 2-94 there was a gradual decline in performance over the whole period, test 2-75 ran stably at .74-.755 volts after the first 150 hours. The best level of performance at 300 ma/cm^2 was demonstrated in test 2-95 (Figure 5-24). This test was run at 100°C with ACCO Asbestos, 11.5N KOH, and rhodium-plated electrode support and spacer screens on the oxygen side. Performance declined from .83 to .79 volts during the first 160 hours, and then was maintained at .79 - .80 volts for approximately 300 hours until the test was terminated because of internal gas leakage. Cell resistance remained essentially constant during this test.

These tests show that reasonably stable performance can be maintained at current densities as high as 300 ma/cm^2. Further investigation would be required, however, to determine conditions for obtaining optimum performance at these high current densities.

5.3.2 Pressures Above Atmospheric

Using the pressure cell described in Section 5.1, a number of tests were run at 100 ma/cm^2 and at gas pressures of 15 and 25 psig. In all tests hydrogen and oxygen pressures were maintained equal (within 0.5 psi.). Teflon supported electrodes were used in test 2-68. Difficulty in controlling the hydrogen flow was experienced in this test. Performance declined rapidly and the test was terminated after 335 hours. In test 2-77 a platinum support screen was used for the oxygen electrode but the spacer screens were of nickel. This test ran more stably, but there was a gradual decline in voltage (approximately 5 mv/100 hours) and increase in cell resistance (0.6 milliohm/100 hours). The remaining tests of the series were run with High-Loading electrodes using gold-plated support screens on the oxygen side. Downward trends in performance were noted in these tests too. Test 2-86 was terminated after 24 hours because the cell had flooded due to an incorrect gas flow setting. In test 2-88, voltage dropped rapidly from .94 to .81 volts in 24 hours, and then more slowly. Cell resistance rose initially from .011 to .018 ohms and then stayed nearly constant. After approximately 200 hours the gas pressures were dropped to atmospheric on the hydrogen side and 2 psig on the oxygen side. Cell resistance dropped sharply to about .007 ohms and the voltage improved slightly. Thus, under these particular conditions, better performance was obtained at essentially atmospheric pressure than at 25 psig.

In the final test of this series (2-98) the initial performance was high but again a downward trend in voltage (2.5 mv/100 hours) and an upward trend in resistance (2 milliohms/100 hours) were evident.

In these tests the initial improvement in performance obtained by operating under pressure has not been sustained over a prolonged period. In general, there has been a sharp drop of 10-20 millivolts or more at the beginning of the test followed by a more gradual decline in voltage and increase in cell resistance. The latter trends may be associated with oxidation of the nickel spacer screens used in these tests, although tests at atmospheric pressure under similar conditions of temperature and current density (2-46, 2-72) gave stable performance with unplated spacer screens.

5.3.3 Carbonate Build-Up During Life Tests

Data obtained during this investigation(2K,3F) on the effect on cell performance of carbonate in the KOH electrolyte are shown in Table 5-5. These data indicate that in the range 0-200 ma/cm^2, performance is governed largely by the total KOH concentration but changes little for KOH concentrations above 15%. For a cell with an initial KOH concentration of 30-35%, operating at 100 to 200 ma/cm^2, conversion of approximately half of the hydroxide to carbonate should cause a loss in performance of not more than about 40-50 millivolts. Conversion of more than half of the hydroxide to carbonate would probably result in a major loss in performance.

In the life-testing program, gas flows as high as 4 to 8 times stoichiometric were used, depending on cell temperature and degree of saturation of the inlet gases. Since these gases were not recirculated, even trace quantities of carbon dioxide passing the Ascarite scrubbers in the inlet gas lines could lead to a considerable build-up of carbonate in very long tests, or in tests at very high current densities. To determine how much carbonate does build up under varying test conditions, analyses were made at the end of a number of life tests. The results are shown

in Table (5-6). In test 2-24, which ran at 100 ma/cm^2 for 5008 hours, nearly 40% of the KOH was converted to carbonate. Undoubtedly this high level of carbonate was a significant factor contributing to the somewhat reduced stability of this test toward the end of the 5000 hour period.

The data in Table 5-6 show an approximately linear relationship between the total gas flow during the test and conversion of KOH to carbonate. From this relationship it may be estimated that the carbonate build-up is equivalent to removal of approximately 2 ppm carbon dioxide from the inlet gases.

The above analytical results show that build-up of carbonate can be a significant factor in very long tests particularly at high current densities. For these conditions the use of an aqueous KOH scrubber is recommended.

5.3.4 Examination of Electrodes Used in Life Tests

During the course of the life-testing program, it was observed that the hydrogen electrode almost invariably developed a rather uniform grey discoloration on the side facing the electrode. This "greying" was not observed on the gas side of the hydrogen electrode, or on either side of the oxygen electrode. An electron microscope study(3G) of the surfaces of used electrodes showed that only on the matrix side of the hydrogen electrode was there any discernible difference between used and unused electrodes. At this surface the platinum particles appeared coarser and more compact than on the other surfaces, and indicated that some sintering of the platinum in the hydrogen electrode surface may occur under life test conditions.

To determine what changes in electrode activity may have occurred during life-testing, polarization data were obtained on a number of used electrode pairs. The data were obtained on one-inch discs cut from the water-washed electrodes and reassembled in a cell with a new matrix and fresh electrolyte. Table 5-7 summarizes the polarization data obtained on used electrodes, in terms of the difference between the voltage obtained at 100 ma/cm^2 with the used electrodes and that expected for new electrodes of the same type, using the same matrix and operating conditions.

Also reported in Table 5-7 are surface area values determined for some of the used electrodes, using the BET nitrogen adsorption method. Surface areas were measured directly on a piece cut from the electrode. The amount of platinum present was estimated from the weight of the sample piece, allowing for the weight of the screen and the Teflon content.

As shown in Table 5-7, "greying" of the hydrogen electrodes appears to be a function of both time and temperature, a very grey appearance being noted even in relatively short tests at 100°C. At 70°C, there appears to have been very little loss in activity of the electrodes, even for long tests in which the matrix side of the hydrogen electrode became very grey. The magnitude of the voltage differences indicated for tests at 70°C, 12 millivolts or less, is within experimental error. Since all the values are downward, however, a slight loss in performance is indicated. This does not necessarily mean a loss in activity of the catalyst. Other factors, such as small losses of platinum on removing and reassembling the electrodes, or partial blockage of electrode area by traces of asbestos may influence these results.

At higher temperatures, the data are somewhat inconsistent. In several cases, apparently significant losses in performance are indicated. In at least one case (2-95), the loss in performance appears to be associated with the oxygen rather than the hydrogen electrode. On the other hand, in life test 2-63, which ran for 1000 hours at 100°C, very little loss in performance is indicated for either electrode.

The platinum black used in making the electrodes for these tests has a surface area consistently in the range 27-32 m^2/g. Area measurements on fresh electrodes generally range from about 22 to 29 m^2/g Pt. In a group of eleven new electrode samples ranging in loading from 9 to 40 mg/cm^2, the average measured surface area was 25 m^2/g.Pt, with standard deviation of 2.6 m^2/g. Uncertainty with respect to the tare weight of the screen and to the exact ratio of Teflon to platinum in the catalyst solids, as well as the small sample size contribute to the variability of the data.

Most of the surface area data on used electrodes shown in Table 5-7 fall in the range 18-33 m^2/g Pt and should probably not be considered significantly different from that for fresh electrodes. In several cases, however, the surface area measured for the hydrogen electrode was in the range 10-13 m^2/g. A value this low appears to be beyond the range of experimental uncertainty, and to indicate a true loss of surface area. These low values were observed in test 2-24, which was run for 5000 hours at 70°C, and tests 2-33 and 2-63, each of which was run for 1000 hours at 100°C. None of the oxygen electrodes checked showed a significant loss of surface area.

There appears to be no direct relationship between loss of surface area and loss of performance. In tests 2-24 and 2-63, for which a significant loss in surface area at the hydrogen electrode is indicated, there was very little loss in performance. Further, in test 2-65 there appears to have been a significant decrease in performance without a corresponding decrease in surface area.

The overall picture shown by these studies on used electrodes is by no means clear. It does appear, however, that changes in appearance and in surface area occur at the hydrogen electrode, and that these changes become more pronounced as the temperature and duration of test are increased. The effect of these changes on performance has not been firmly established, but does not, in general, appear to be serious for tests up to several thousand hours duration in the temperature range 70-100°C.

TABLE 5-1

Performance of High-Loading Electrodes vs. Electrolyte Concentration and Temperature at 100-200°C

Run	Matrix	Pressure (psig)	Temp. (°C)	Solubility KOH (%)	KOH Conc. (N)	KOH Conc. (%)	Cell Resistance ohms	Working Voltage at Current Density (ma/cm) of 0	40	100	200	300	400	500	600	800	1000	1200
6800-170	ACCO Asbestos	0	100	64	13	50	.017	1.08	-	.98	.94	.90	.87	.85	.82	.77	.72	.64
-198	"	"	120	67	13	50	-	1.05	-	.98	.94	.90	.8	.85	.82	.77	.66	-
-162	"	"	120	67	18	64	-	-	-	.98	.94	.90	.85	.80	.75	.63	.50	.40
151-161	"	"	140	72	15	55	-	-	-	1.00	.95	.90	.86	.83	.79	.72	.64	.51
"	"	"	140	72	16	58	-	-	-	.98	.94	.90	.88	.85	.82	.74	.67	.56
"	"	"	140	72	17	61	-	1.05	-	.98	.96	.93	.90	.88	.84	.77	.73	.59
"	"	"	140	72	19	67	-	1.12	-	1.02	.99	.95	.95	.88	.84	.76	.61	.53
6964-67	"	30	100	64	13	50	-	1.11	1.00	.96	.92	.88	.85	-	-	-	-	-
"	"	"	120	67	13	50	-	1.09	1.00	.96	.92	.89	.86	-	-	-	-	-
"	"	"	140	72	13	50	-	1.07	1.00	.96	.92	.89	.86	-	-	-	-	-
	Fuel Cell																	
-137	Asbestos	45	100	64	13	50	.040	1.14	1.06	1.03	.98	.94	.91	.89	.86	.81	.76	-
"	"	"	140	72	18	64	068	1.13	-	1.04	1.00	.96	.91	.89	.80	.72	.64	-
-140	"	45	100	64	13	50	.049	-	-	1.01	-	-	-	-	-	-	-	-
"	"	"	120	67			.040	-	-	1.02	-	-	-	-	-	-	-	-
"	"	"	140	72			.045	-	-	1.03	-	-	-	-	-	-	-	-
"	"	"	165	-			.073	-	-	1.03	-	-	-	-	-	-	-	-
"	"	"	180	-			.115	-	-	1.01	-	-	-	-	-	-	-	-
"	"	"	193	-			.205	-	-	.90	-	-	-	-	-	-	-	-
"	"	"	200	>85	Approx. 75		.720	-	-	.72 Falling	-	-	-	-	-	-	-	-

TABLE 5-2

Performance vs. Gas Pressure

Run	Electrodes	Matrix	Temp. (°C)	Normality KOH	Pressure (psig)	Working Voltage at Current Density (ma/cm²) of 0	40	100	200	300	400	500	600	800	1000	1200
24	High-Loading	ACCO	100	3	0	1.01	.90	.86	.76	x	x	x	x	x	x	x
13	"	Asbestos	"	"	7.5	.96	.90	.87	.83	.78	.74	.67	.58	x	x	x
16	"	"	"	"	15	1.04	.95	.92	.89	.86(i)	.83	.81(i)	.78(i)	.73	-	.61
93	"	"	100	13	0	-	-	.97	.91	.87	.80	.74	.68	.48	x	x
"	"	"	"	"	15	-	-	.99	.94	.91	.88	.84	.80	.74	x	x
67	"	"	100	13	0	1.08	.96	.92	.87	.83	.80	-	-	-	-	-
"	"	"	"	"	15	1.09	.99	.95	.91	.87	.84	-	-	-	-	-
"	"	"	"	"	30	1.11	1.00	.96	.92	.88	.85	-	-	-	-	-
108	"	"	100	13	0	-	-	.94	.88	.83	.76	.69	.60	x	x	x
"	"	"	"	"	30	1.09	1.01	.97	.93	.88	.85	.80	.75	x	x	x
"	"	"	"	"	45	1.11	1.04	1.01	.98	.94	.92	.89	.86	.80	.71	x
112	"	"	100	13	0	1.07	.97	.93	.88	.81	.75	.67	.56	x	x	x
"	"	"	"	"	15	1.07	.98	.94	.88	.82	.76	-	x	x	x	x
"	"	"	"	"	30	1.07	-	.95	-	-	.86	-	-	-	-	-
"	"	"	"	"	45	1.08	-	.97	-	-	.88	-	-	-	-	-
129	"	"	140	13	0	1.09	-	1.01	.98	.95	.92	.89	.87	.79	.70	.61
"	"	"	"	"	15	1.10	-	1.03	.99	.97	.94	.92	.90	.86	.81	.77
"	"	"	"	"	30	-	-	1.03	.99	.96	‡					
137	"	Fuel Cell	100	13	0	-	-	.97	.90	.84	.77	.70	.60	x	x	x
"	"	Asbestos	"	"	45	1.14	1.06	1.03	.98	.94	.91	.89	.86	.81	.76	-
125	Standard AB-1	ACCO	100	13	0	1.07	.95	.89	.76	x	x	x	x	x	x	x
"	"	Asbestos	"	"	15	1.09	.98	.94	.86	.78	.67	x	x	x	x	x
"	"	"	"	"	30	1.10	1.00	.96	.90	.84	.76	x	x	x	x	x
"	"	"	"	"	45	1.12	1.01	.97	.91	.85	.76	x	x	x	x	x

(i) Interpolated Linearly

x Current Did Not Hold
‡ Cell Failed Abruptly

TABLE 9-3

Life Test Conditions, 2" x 2' Cells

Test No.	Notebook Reference	Electrodes[2] Catalyst Loading (3) mg/cm²		Remarks[4]	Matrix	Cell Temp. °C	Gas Pressure (psig)	Current Density (ma/cm²)	Initial KOH Concentration (N)	Inlet Gas Condition	Inlet Gas Flow Ratio, H_2/O_2	Test Duration (Hrs.)
		H_2	O_2									
2-1	6582-4	9	9		ACCO[5]	70	0	100	5.0	Dry		46
2-2	6582-8	"	"		"	"	"	"	"	"	varied	67
2-3	6582-18	"	"		"	"	"	"	"	"		720
2-4	6582-40	"	"		"	"	"	"	"	"		500
2-5	6582-56	"	"		FCAB[6]-30	"	"	"	7.2	"		1295
2-7	6582-78	"	"		Quinterra[7]	"	"	"	"	"		468
2-8	6582-86	"	"		ACCO	"	"	200	"	"		597
2-10	6582-104	"	50 Ag		"	"	"	100	"	"		285
-	6582-120	"	9		FCAB-30	100	"	"	8.0	Sat. @ 79°C		303
2-11	6582-134	"	"		" "	70	"	"	5.0	Dry		184
2-12	6582-150	"	"		2 ACCO	"	"	"	"	"		502
1-1	6582-162	55 Ni	"	1" Cell	FCAB-20	100-115	"	"	"	"		287
-	6582-172	9	"		FCAB-30	100	"	"	"	"		114
2-13	6582-178	"	"		" "	"	"	"	"	"		115
2-15	6582-190	"	"		" "	"	"	"	"	"		212
2-17	6735-15	"	"		" "	70	"	"	7.2	"	0.7	2245
2-19	6708-33	"	"		FCAB-10	"	"	"	"	"	1.0	1532
2-20	6597-7	40	40		" "	"	"	"	"	"	0.7	1184
2-21	6718-2	9	9		FCAB-30	"	"	"	"	Sat. @ 47°C		1336
2-22	6718-16	9	40 Ag		" "	"	"	"	"	Dry		1176
2-23	6708-47	"	9		ACCO	"	"	"	"	"	0.8	253

TABLE 5-3 (Cont'd)

Life Test Conditions, 2" x 2" Cells

Test No.	Notebook Reference	Electrodes[2] Catalyst Loading[3] mg/cm H_2	Electrodes[2] Catalyst Loading[3] mg/cm O_2	Remarks[4]	Matrix	Cell Temp. °C	Gas Pressure (psig)	Current Density (ma/cm²)	Initial KOH Concentration (N)	Inlet Gas Condition	Inlet Gas Flow Ratio, H_2/O_2	Test Duration (Hrs.)
2-24	6708-57	9	9		FCAB-20	70	0	100	7.2	dry	0.7	5008
2-27	6597-26	"	"		FCAB-30	"	"	"	"	Sat. @ 47°C	0.6	1014
2-29	6597-33	"	"		FCAB-20	"	"	400	5.0	dry	0.8	338
2-30	6708-76	"	"		B-2[8]	"	"	100	"	"	0.8	1317
2-31	6597-42	"	"		FCAB-30	"	"	"	"	H_2: Sat.@47°C O_2: Dry	13.0[9]	1223
2-32	6597-44	"	"		FCAB-20	"	"	400	"	Sat. @ 50°C	0.8	112
2-33	6708-111	"	"		" "	100	"	100	7.2	Sat. @ 70°C	1.2	1030
2-34	6597-54	40	40		ACCO[10]	70	"	400	5.0	Dry	0.8	295
2-36	6597-58	9	9	Electrodes previously used in test 2-27	FCAB-30	"	"	100	"	Sat. @ 47°C	0.8	1012
2-38	6597-66	40	40	14% Teflon binder	FCAB-20	"	"	"	"	Dry	1.2	779
2-39	6708-129	10	10	Pt support, spacer screens, Pt foil lining face plates	" "	"	"	"	7.2	"	1.3	1110
2-40	6597-74	40	40		ACCO	"	"	400	5.0	"	1.1	1682
2-42	6708-147	10	10	50% Teflon binder	FCAB-20	"	"	100	8.0	"	1.1	835
2-43	6597-80	40	40		" "	"	"	"	"	"	1.1	1032
2-45	6597-92	"	"		ACCO	100	"	"	"	Sat. @ 70°C	1.1	354
2-46	6597-83	10	10	Pt support screens	FCAB-20	70	"	"	"	Dry	1.1	1056
2-47	6597-94	9	9		" "	"	"	"	"	"	1.1	143
2-48	6597-95	"	"		" "	"	"	"	"	"	1.1	161
2-50	6597-100	"	"		" "	"	"	"	"	"	1.1	380
2-51	6597-106	"	"		ACCO	100	"	"	"	Sat. @ 70°C	1.4	212

TABLE 5-3 (Cont'd)

Life Test Conditions, 2" x 2" Cells

Test No.	Notebook Reference	Electrodes[2] Catalyst Loading[3] mg/cm² H_2	Electrodes[2] Catalyst Loading[3] mg/cm² O_2	Remarks[4]	Matrix	Cell Temp. °C	Gas Pressure (psig)	Current Density (ma/cm²)	Initial KOH Concentration (N)	Inlet Gas Condition	Inlet Gas Flow Ratio, H_2/O_2	Test Duration (Hrs.)
2-53	6708-134	10	10	Teflon support screens	FCAB-20	70	0	100	8.0	Dry	1.0	528
2-54	6597-120	40	40	Expanded nickel support screens	" "	"	"	"	"	"	1.1	1002
2-56	6708-152	10	10	Pt support, spacer screens, Pt foil lining face plates	" "	"	"	"	"	"	1.1	143
2-57	6597-114	40	40		2 ACCO	"	"	100	"	"	1.1	1002
2-59	6597-108	40	40		FCAB-20	100	"	"	"	Sat. @ 70°C	1.0	1002
2-60	6708-155	10	10	Pt support, spacer screens, Pt foil lining face plates	" "	87	"	200	"	Dry	1.2	1053
2-63	6597-110	9	9		" "	100	"	100	"	Sat. @ 70°C	1.3	1007
2-65	6708-179	10	10	Pt support screens, nickel spacer screens	" "	92	"	300	"	Dry	1.3	478
2-68	6708-183	10	10	Teflon support screens	FCAB-30	70	25	100	"	"	1.1	335
2-70	6597-102	40	40	Sn-Ni plated support, spacer screens, and face plates	FCAB-20	"	0	"	"	"	1.1	571
2-71	6708-186	9	9		FCAB-20	"	"	"	"	"	1.0	1657
2-72	6708-192	9	10	Pt support screen, O_2 side only	" "	"	"	"	"	"	1.1	1099
2-73	6597-124	40	40	Gold-plated support, spacer screens,	" "	"	"	"	"	"	1.1	1460
2-74	6597-131	10	10	Teflon support screens	" "	"	"	"	"	"	1.1	2014
2-75	6597-135	40	10	Pt support screen, O_2 side only	2 ACCO	80	"	300	"	"	1.1	1000
2-76	6597-139	10	10	Teflon support screens	FCAB-20	100	"	100	"	Sat. @ 70°C	0.9	161
2-77	6708-198	9	10	Pt support screen, O_2 side only	" "	70	15	100	"	Dry	1.0	287
2-79	6597-145	40	40	Gold-plated support screen, O_2 side only	" "	87	0	200	"	"	1.3	666
2-86	7060-10	40	40	" " " " " " "	ACCO	70	25	100	"	"	1.0	24
2-88	7060-13	40	40	" " " " " " "	FCAB-20	"	"	"	"	"	1.5	196
2-89	7060-17	40	40	Gold-plated support, spacer screens, O_2 side only	ACCO	"	0	"	"	"	1.0	1079

TABLE 5-3 (Cont'd)

Life Test Conditions, 2" x 2" Cells

Test No.	Notebook Reference	Electrodes[2] Catalyst Loading[3] mg/cm² H_2	Electrodes[2] Catalyst Loading[3] mg/cm² O_2	Remarks[4]	Matrix	Cell Temp. °C	Gas Pressure (psig)	Current Density (ma/cm²)	Initial KOH Concentration (N)	Gas Condition	Inlet Gas Flow Ratio, H_2/O_2	Test Duration (Hrs.)
2-91	6597-152	40	40	Gold-plated support, spacer screens, O_2 side only	FCAB-20	85	0	200	8.0	H_2 Sat. @ 40°C O_2 Dry	11.2[9]	30
2-92	6597-153	40	40	Rhodium-plates support, spacer screens, O_2 side only	ACCO	100	"	300	11.5	Sat. @ 50°C	1.2	70
2-93	6597-155	40	40	Gold-plated support, spacer screens O_2 side only	FCAB-20	85	"	200	8.0	H_2 Sat. @ 40°C O_2: Dry	9.8[9]	790
2-94	6597-159	40	40	Gold-plated support, spacer screens O_2 side only	2 ACCO	80	"	300	"	Dry	1.2	1000
2-95	6597-163	40	40	Rhodium-plated support, spacer screens O_2 side only	ACCO	100	"	300	11.5	Sat. @ 50°C	1.1	427
2-98	7060-30	40	40	Gold-plated support screen, O_2 side only	FCAB-20	90	25	100	8.0	Dry	1.4	738

Notes:

(1) For performance data, see Table 5-4
(2) Electrodes formulated with 25% Teflon binder unless otherwise noted
(3) Catalyst is platinum unless otherwise noted
(4) Nickel electrode supported and spacer screens unless otherwide noted
(5) Proprietary asbestos matrix, 20-25 mils thick
(6) Johns Manville Fuel Cell Asbestos in nominal 10, 20 or 30 mil thickness
(7) Johns Manville Quinterra Asbestos, nominal 10 mil thickness
(8) Proprietary membrane
(9) Slow oxygen purge: essentially all water removal on H_2 side
(10) Unleached

TABLE 5-4

Life Test Performance[1], 2" x 2" Cells

Test No.	Notebook Reference	Test Duration (hours)	Cell Voltage			Cell Internal Resistance			Remarks
			Initial	Max.	Final	Initial	Min.	Final	
2-1	6582-4	46	.877			-	-	-	
2-2	6582-8	67	.875	.875	.805	-	-	-	Ratio of gas flows varied to study concentration gradients
2-3	6582-18	720	.866	.866	.789	-	-	-	
2-4	6582-40	500	.875	.875	.77	-	-	-	
2-5	6582-56	1295	.856	.856	.52	-	-	-	
2-7	6582-78	468	.834	.834	.6	0.0170	0.0170	0.0550	
2-8	6582-86	597	.845	.845	.564	-	0.0083	.0125	
2-10	6582-104	285	.854	.854	.482	0.0100	0.0100	0.0137	
-	6582-120	303	.859	.859	.587	0.0125	0.0125	0.0420	
2-11	6582-134	184	.830	.830	.491	0.0174	0.0125	0.090	
2-12	6582-150	502	.860	.860	.706	0.0115	0.0115	0.0225	
1-1	6582-162	287	.86	.86	.28	-	-	-	Voltage above 0.8 for 250 hours
-	6582-172	114	.864	.864	.62-.75	-	-	-	
2-13	6582-178	115	.821	.821	.406	-	-	-	
2-15	6582-190	212	.815	.815	.736	-	0.0130	0.0252	
2-17	6708-19	2245	.843	.847	.60	0.0145	0.0116	0.0525	Gases reversed at 808, 1850 hours
2-19	6708-33	1532	.887	.887	.812	0.0153	0.0073	0.0195	Gases reversed at 1225 hours
2-20	6597-7	1184	.892	.894	.482	0.0105	0.0052	-	
2-21	6718-2	1336	.847	.847	.695	0.0165	0.0125	0.0208	
2-22	6718-16	1176	.782	.782	.700	0.0200	0.0200	0.0410	
2-23	6708-47	253	.822	.822	.791	0.0050	0.0050	-	

TABLE 5-4 (Cont'd)

Life Test Performance[1], 2" x 2" Cells

Test No.	Notebook Reference	Test Duration (hours)	Cell Voltage			Cell Internal Resistance			Remarks
			Initial	Max.	Final	Initial	Min.	Final	
2-24	6708-57	5008	.845	.845	.805	.0160	.0082	.0123	Gases Reversed at 50, 613, 2100 and 3205 hours
2-27	6597-26	1014	.800	.844	.79	.0215	.0108	.0248	
2-29	6597-33	338	.715	.715	.534	.011	.0077	.0135	
2-30	6708-76	1317	.891	.891	.815	.0055	.0055	.0085	Gases reversed at 575 hours
2-31	6597-42	1223	.822	.822	.77	.0160	.0160	.0294	
2-32	6597-44	112	.666	.666	.558	.0083	.0075	.0075	
2-33	6708-111	1030	.849	.849	.817	.0080	.0060	.0133	
2-34	6597-54	295	.794	.794	.641	.0058	.0058	.0065	
2-36	6597-58	1012	.665	.834	.74	.0160	.0150	.0210	
2-38	6597-66	779	.848	.854	.818	.0128	.0110	.0156	Gases reversed at 165 hours
2-39	6708-129	1110	.867	.869	.72	.0092	.0078	.0165	Voltage over .86 for 800 hours
2-40	6597-74	1677	.778	.778	0.617	.0065	.0053	.0063	Gases reversed at 440 hours
2-42	6708-147	835	.822	.847	.73	0.0143	0.0093	0.158	Gases reversed at 330 hours
2-43	6597-80	1032	.880	.888	.787	.0087	.0087	.0270	
2-45	6597-92	354	.871	.901	.73	.0069	.0069	.041	
2-46	6597-83	1056	.876	.876	.861	.0140	.0062	.0072	
2-47	6597-94	143	.876	.876	.806	.0105	.0078	.0130	Cell heater failed
2-48	6597-95	161	.883	.889	.886	.0108	.0068	.0082	Sudden failure
2-50	6597-100	380	.876	.882	.842	.0080	.0080	.0155	
2-51	6597-106	212	.880	.904	.75	.0063	.0063	.046	Rapid drop after 60 hours

TABLE 5-4 (Cont'd)

Life Test Performance[1], 2" x 2" Cells

Test No.	Notebook Reference	Test Duration (hours)	Cell Voltage			Cell Internal Resistance			Remarks
			Initial	Max.	Final	Initial	Min.	Final	
2-53	6708-134	528	.831	.840	.763	.0118	.0088	.0110	
2-54	6597-120	1002	.906	.907	.829	.0076	.0063	.0160	
2-56	6708-152	143	.824	.824	.72	.0094	.0071	.0109	
2-57	6597-114	1002	.895	.902	.803	.0066	.0062	.0182	
2-59	6597-108	138	.840	.868	.690	.0105	.0103	.0205	
2-60	6708-155	1053	.788	.809	.778	.0080	.0068	.0075	
2-63	6597-110	1007	.862	.884	.798	.0068	.0068	.0265	
2-65	6708-179	478	.760	.760	.5	.0063	.0048	.0094	
2-68	6708-183	335	.894	.894	.764	.0135	.0135	.0282	
2-70	6597-102	571	.865	.870	.801	.0126	.0126	.0252	
2-71	6708-186	1657	.859	.859	.816	.0084	.0084	.0137	
2-72	6708-192	1099	.866	.867	.861	.0107	.0072	.0072	
2-73	6597-124	1460	.886	.897	.892	.0114	.0062	.0072	
2-74	6597-131	2014	.853	.855	.831	.0114	.0084	.0120	Gases reversed after 460 hours
2-75	6597-135	1000	.788	.788	.737	.0100	.0060	.0063	
2-76	6597-139	161	.828	.841	.658	.0090	.0075	.037	
2-77	6708-198	287	.888	.888	.865	.0093	.0093	.0107	
2-79	6597-145	666	.806	.839	.740	.0105	.0080	.0132	
2-86	7060-10	24	.942	.946	.915	.0130	.0068	.0072	
2-88	7060-13	196	.937	.937	.865	.0110	.0068	.0068	
2-89	7060-17	1079	.902	.908	.893	.0072	.0051	.0058	
2-91	6597-152	30	.825	.866	.710	-	-	-	
2-92	6597-153	70	.843	.843	.748	.0105	.0072	.0072	
2-93	6597-155	790	.835	.835	.772	.0102	.0084	.0086	
2-94	6597-159	1000	.784	.796	.743	.0090	.0080	.0095	
2-95	6597-163	427	.832	.833	.790	.0060	.0040	.0048	
2-98	7060-30	738	.932	.932	.900	.0103	.0080	.0155	

Notes:

(1) For test conditions, see Table 5-3.

TABLE 5-5

Effect of Carbonate Concentration on Cell Performance

Electrodes: Standard AB-1 (9 Mg Pt/Cm^2)
Matrix: 20 Mil Fuel Cell Asbestos
Temperature: 70°C
Pressure: 1 Atm.

Wt.% KOH	Wt.% K_2CO_3	Volts at Indicated Current Density			
		40	50	100	200 ma/cm^2
38.5	0	.925	-	.875	.79
34	0	-	.915	.875	.81
30	0	.91	-	.865	.80
30	3	-	.915	.875	.81
27	6	-	.91	.86	.765
23	0	-	.89	.845	.775
19	15	-	.90	.84	.77
16.5	7	-	.885	.835	.76
15	0	.875	-	.825	.76
14	20	.86	-	.61	.51
0	34	.62	-	.34	-

TABLE 5-6

Carbonate Build-Up in Life Tests

Life Test No.	Time (hrs)	Current Density (ma/cm^2)	Gas Flow Rate[a] cc/min	Total Gas Flow during Test (liters)	Conversion to Carbonate,[b] (%)
2-32	112	400	850	5700	2.9
2-29	354	400	310	6600	7.9
2-72	1099	100	132	8700	7.4
2-75	1000	300	294	17,600	20.0
2-24	5008	100	120	36,000	39.4

(a) Total rate for hydrogen and oxygen.

(b) % of total K^+ present as carbonate.

TABLE 5-7

Examination of Electrodes Used in Life Tests

Life Test No.	Nominal Electrode Loading (mg Pt/cm²)	Test Conditions: Temp. °C	Test Conditions: Current Density (ma/cm²)	Test Conditions: Time (hrs)	Appearance of Hydrogen Electrode, Matrix Side	Performance,(1) ΔV a 100 ma/cm² (millivolts): Used H_2 Used O_2	Performance,(1) ΔV a 100 ma/cm² (millivolts): Used H_2 New O_2	Performance,(1) ΔV a 100 ma/cm² (millivolts): New H_2 Used O_2	(m²/g Pt) Surface Area: H_2	(m²/g Pt) Surface Area: O_2
2-24	9	70	100	5008(2)	Very Grey	10	-	-	13	-
2-20	40	"	"	1184	- -	1	-	-	-	-
2-57	40	"	"	1002	Mod. Grey	4	-	-	21	28
2-42	10(3)	"	"	835	Very Grey	12	-	-	-	-
2-70	40	"	"	571	Slightly Grey	11	-	-	-	33
2-50	9	"	"	380	" "	-	-	-	-	-
2-88	40	"	"	267	Mod. Grey	5	-	-	-	-
2-23	9	"	"	253	- -	7	-	-	-	-
2-47	9	"	"	143	V. Slt. Grey	-	-	-	22	-
2-40	40	70	400	1682	Very Grey	4	-	-	18	-
2-94	40	80	300	1000	" "	13	-	-	22	-
2-93	40	85	200	790	Mod. Grey	- 20	-	-	-	-
2-79	40	87	200	666	" "	10	-	-	-	-
2-65	10	92	300	478	Very Grey	61	-	-19	31	20
2-33	9	100	100	1030	Very Grey	(4)	-58	-	13	-
2-63	9	"	"	1007	" "	20	-6	-9	10, 11	28
2-95	40	"	300	427	" "	28	+4	-26	19	21
2-45	40	"	100	354	" "	10	-	-	-	-

(1) ΔV: Average voltage at 100 ma/cm² for fresh electrodes minus voltage obtained for used electrodes minus voltage obtained for used electrodes using the same matrix and test conditions.

(2) Gases reversed five times during this test. Each electrode used approximately 2500 hours as a hydrogen electrode and 2500 hours as an oxygen electrode.

(3) Electrodes made with 50% Teflon

(4) Very poor performance. Very low Pt loading (ca. 4 mg/cm²) on oxygen electrode as recovered from life test.

GASKETING ARRANGEMENTS – 2" x 2" CELL
(Schematic – not to scale)

TYPE I CELL – SILICONE RUBBER GASKETS

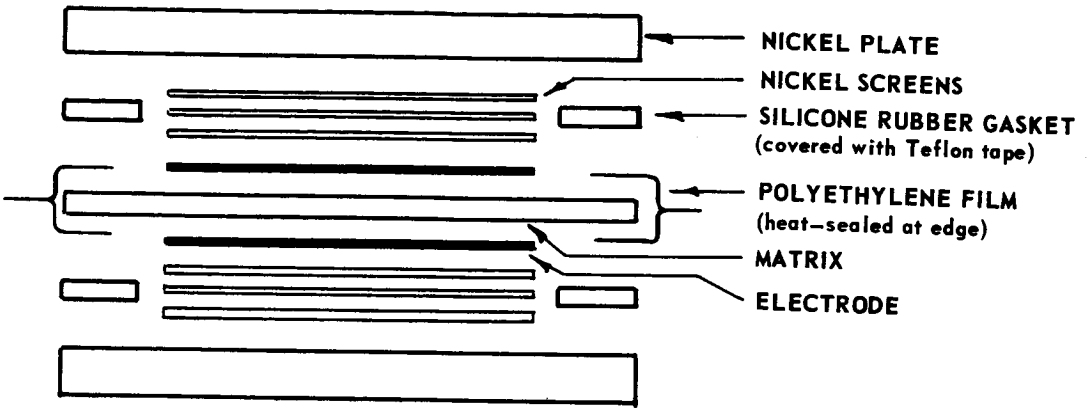

TYPE II CELL – TEFLON GASKETS

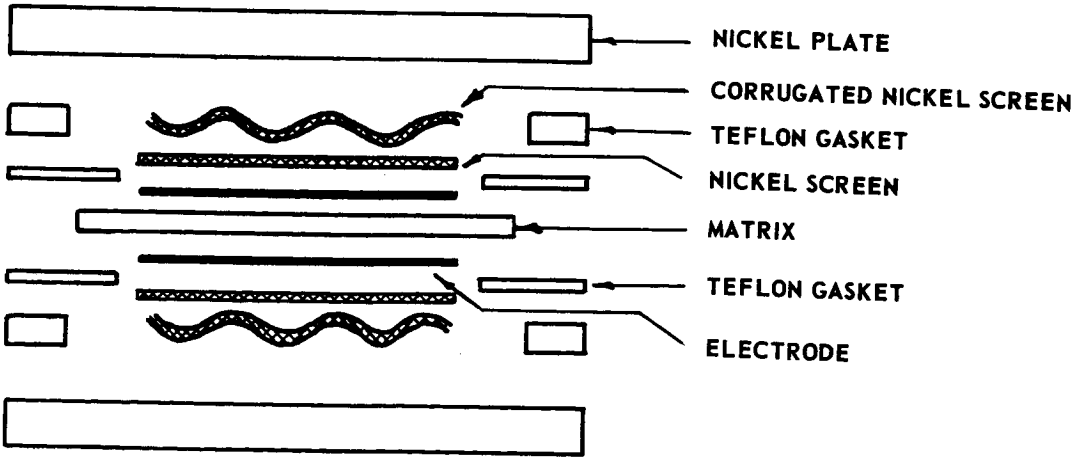

FIGURE 5–1

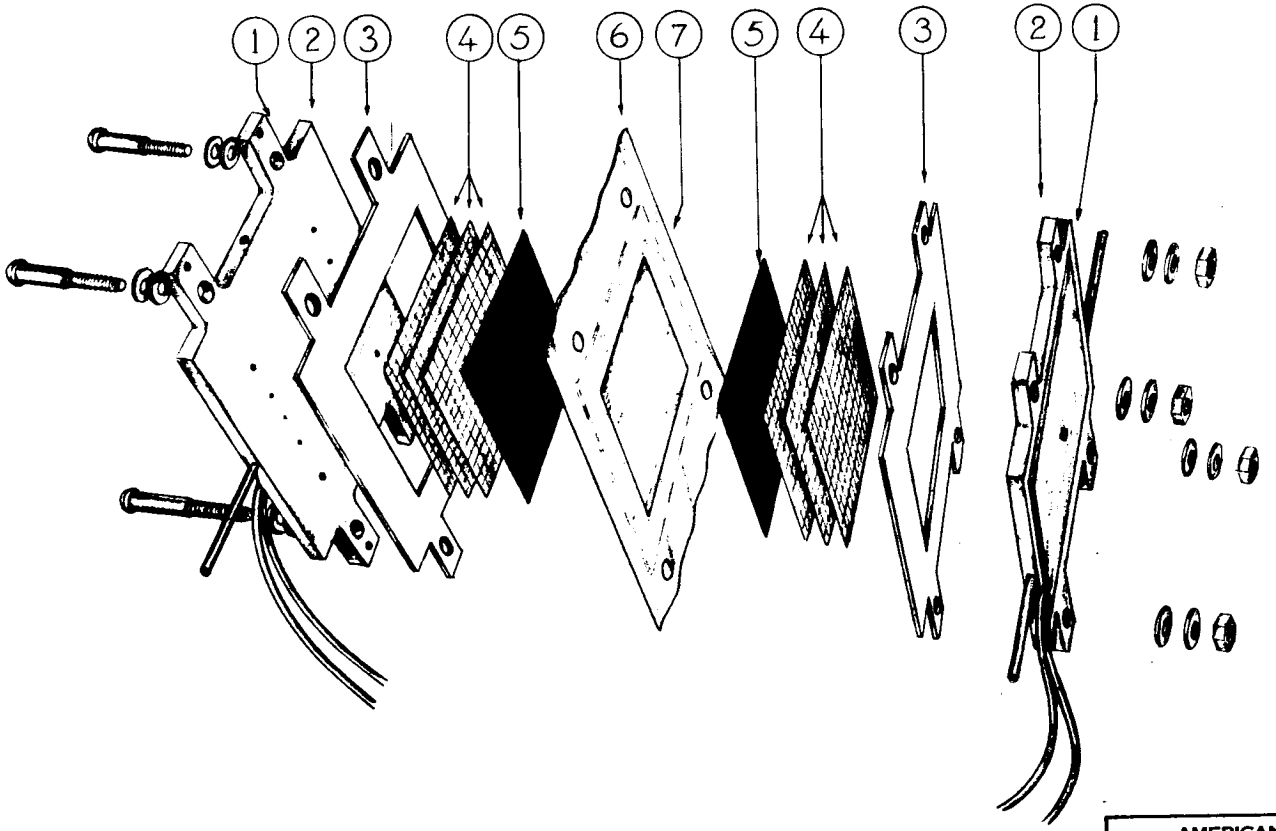

N°	PARTS DESCRIPTION
1	HEATING ELEMENT
2	FACE PLATE
3	GASKET
4	SPACER SCREENS
5	ELECTRODE
6	MEMBRANE ENVELOPE
7	MEMBRANE

AMERICAN CYANAMID CO.
RESEARCH DEPT.
STAMFORD, CONN.

2"x2" TEST CELL
- EXPLODED VIEW -

DRAWN	DATE	SCALE:		
AP		JOB NO.	DWG. NO.	ISSUE
CHECKED	DATE			
APP'D				

FIGURE 5–2

FACE PLATE DESIGN 2" x 2" CELL

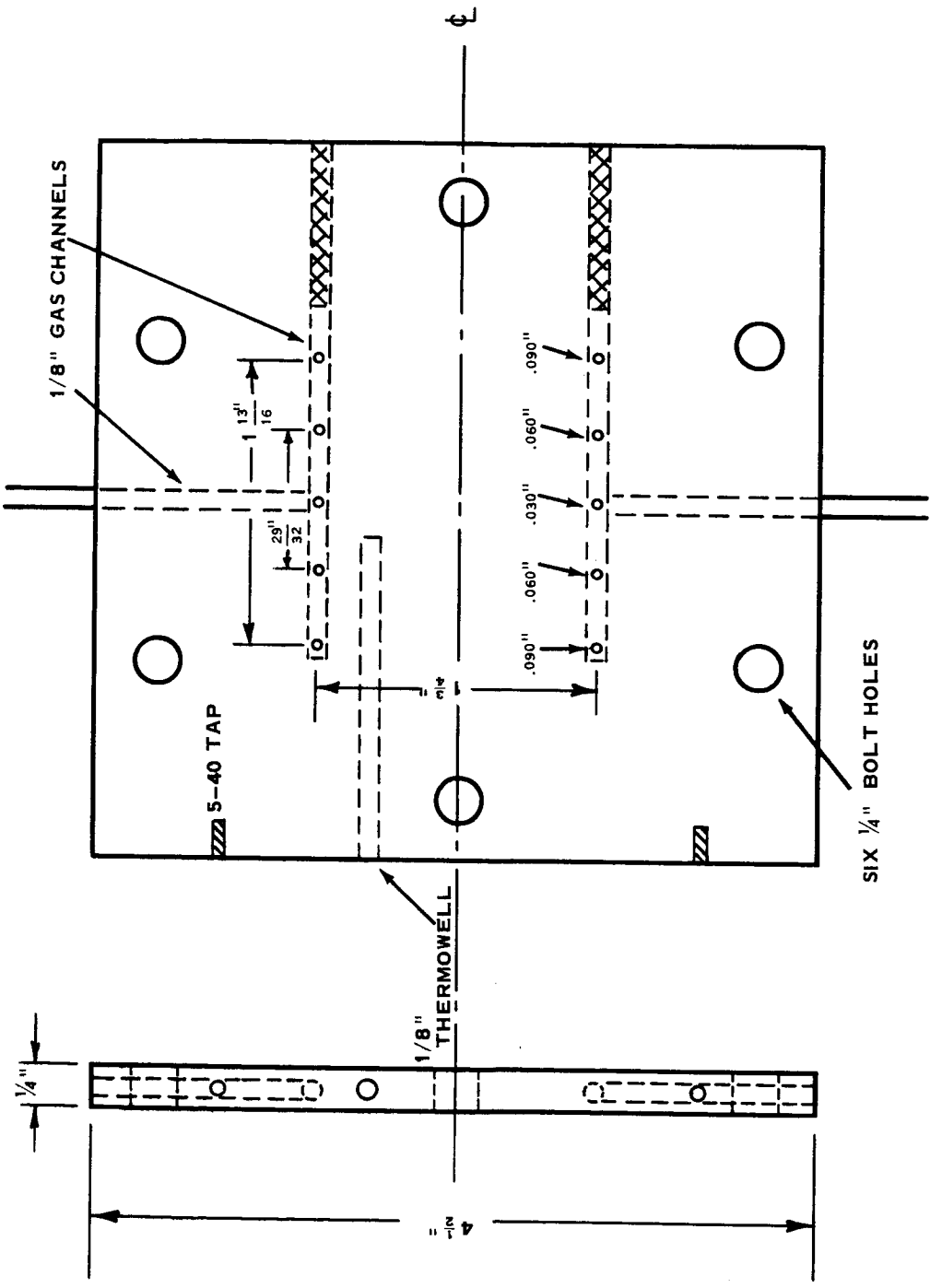

FIGURE 5-3

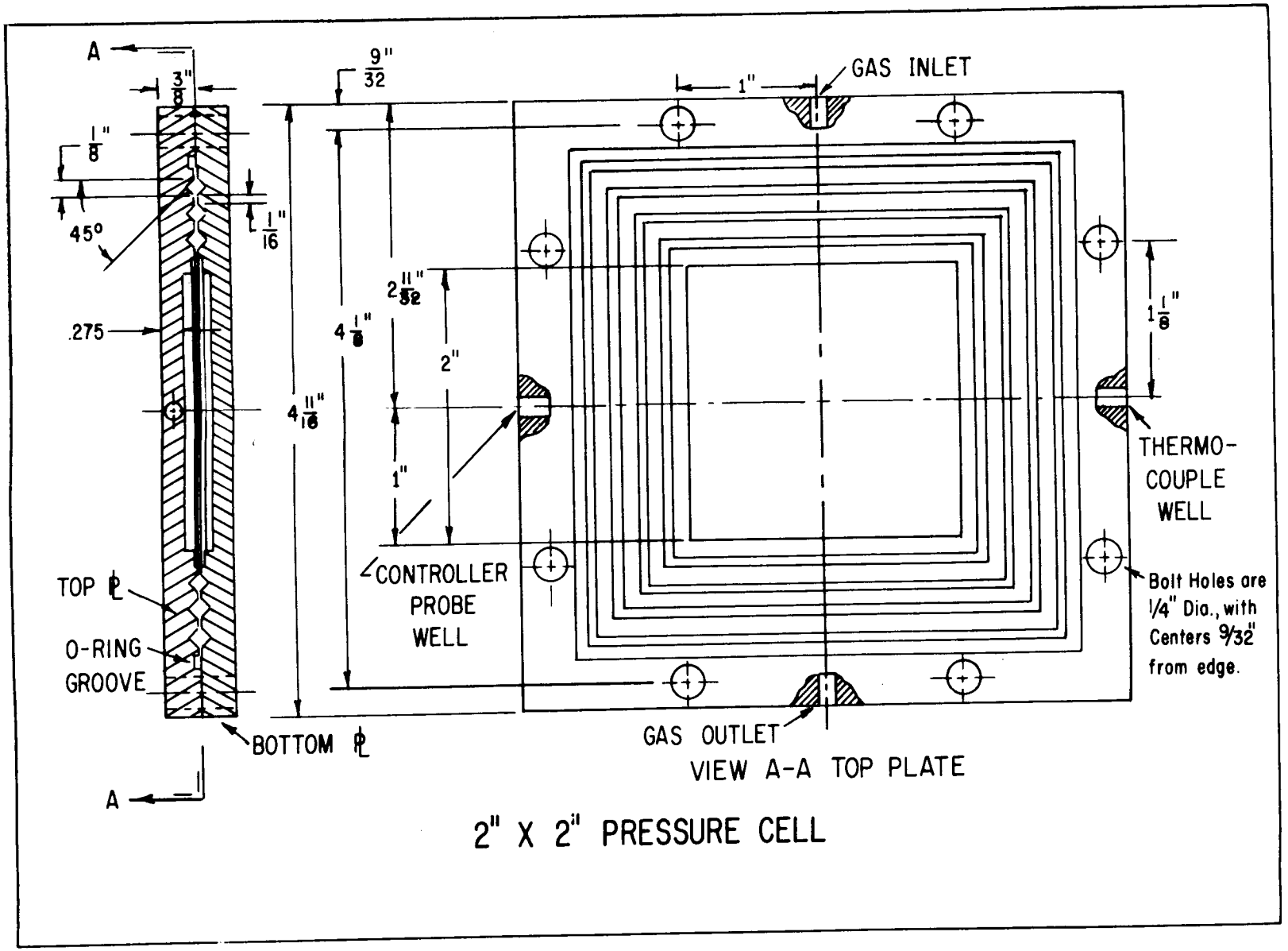
A
3/8"
9/32"
1"
GAS INLET
1/8"
45°
1/16"
.275
2 11/32"
4 1/8"
2"
4 11/16"
1 1/8"
THERMO-
COUPLE
WELL
1"
CONTROLLER
PROBE
WELL
TOP ℄
O-RING
GROOVE
Bolt Holes are
1/4" Dia., with
Centers 9/32"
from edge.
BOTTOM ℄
GAS OUTLET
A
VIEW A-A TOP PLATE
2" X 2" PRESSURE CELL

FIGURE 5-4

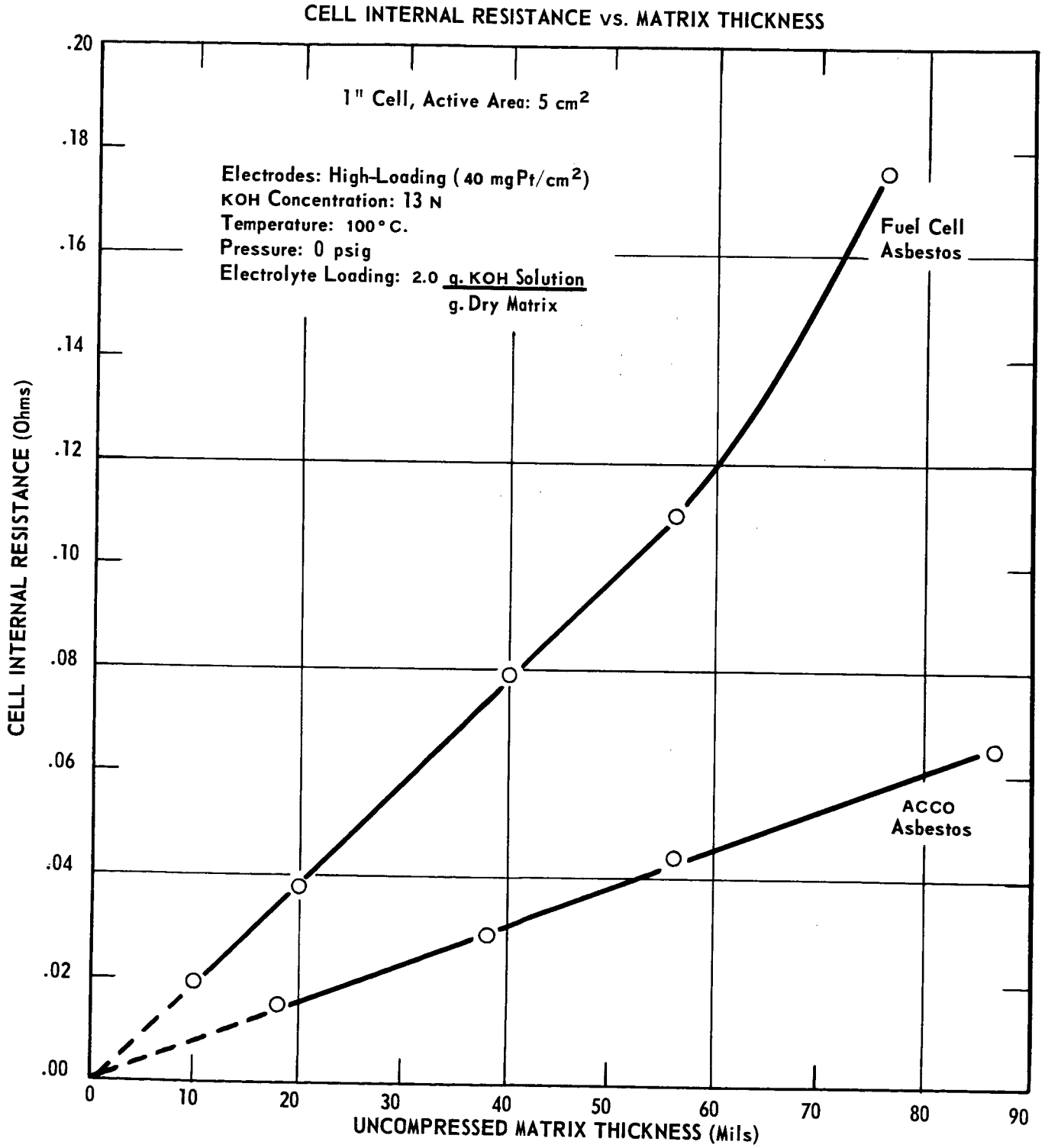
CELL INTERNAL RESISTANCE vs. MATRIX THICKNESS
1" Cell, Active Area: 5 cm²
Electrodes: High-Loading (40 mgPt/cm²)
KOH Concentration: 13 N
Temperature: 100° C.
Pressure: 0 psig
Electrolyte Loading: 2.0 g. KOH Solution / g. Dry Matrix
Fuel Cell Asbestos
ACCO Asbestos
CELL INTERNAL RESISTANCE (Ohms)
.20
.18
.16
.14
.12
.10
.08
.06
.04
.02
.00
0
10
20
30
40
50
60
70
80
90
UNCOMPRESSED MATRIX THICKNESS (Mils)

FIGURE 5-5

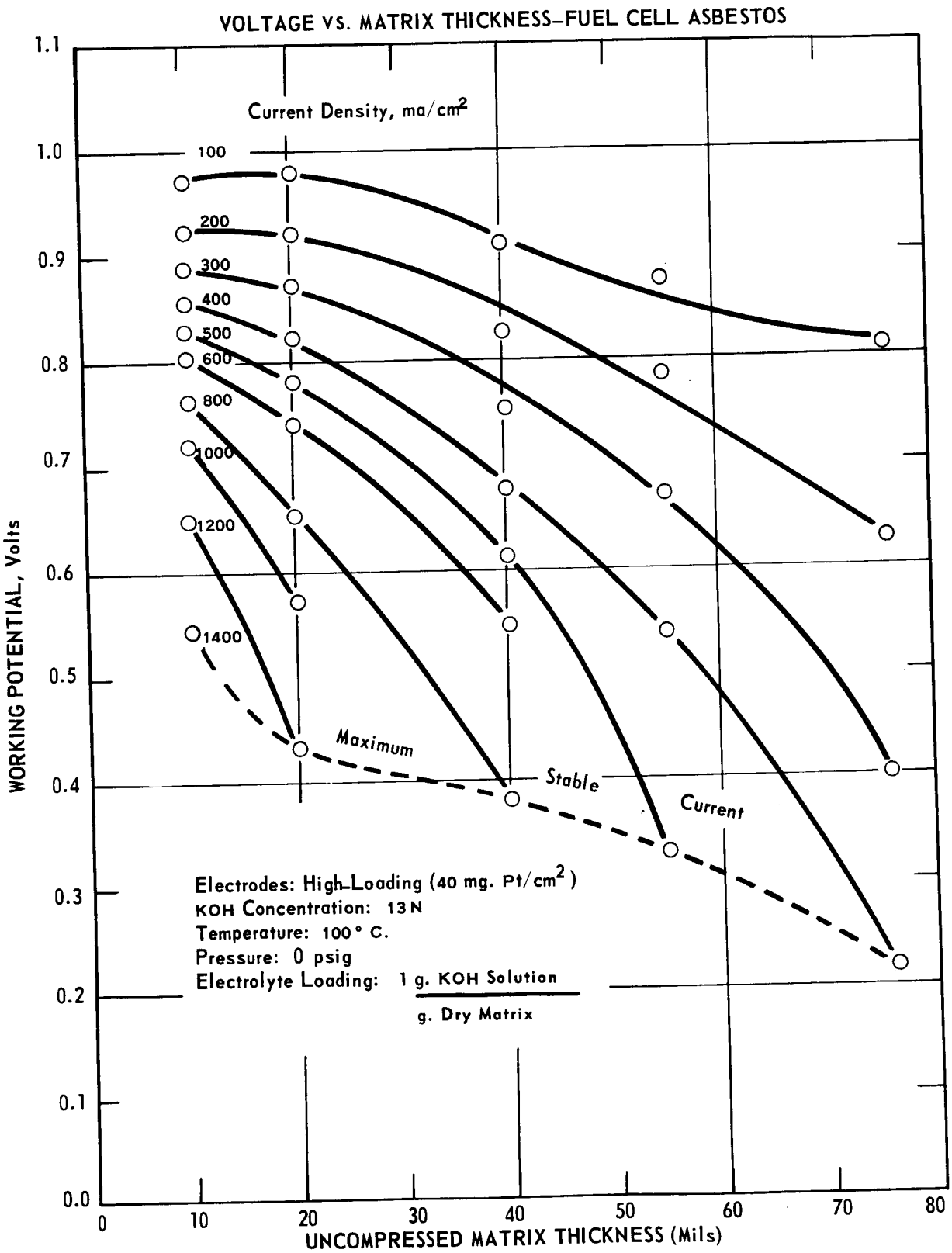
VOLTAGE VS. MATRIX THICKNESS–FUEL CELL ASBESTOS
Current Density, ma/cm²
100
200
300
400
500
600
800
1000
1200
1400
Maximum Stable Current
Electrodes: High-Loading (40 mg. Pt/cm²)
KOH Concentration: 13 N
Temperature: 100° C.
Pressure: 0 psig
Electrolyte Loading: 1 g. KOH Solution / g. Dry Matrix
WORKING POTENTIAL, Volts
1.1
1.0
0.9
0.8
0.7
0.6
0.5
0.4
0.3
0.2
0.1
0.0
0
10
20
30
40
50
60
70
80
UNCOMPRESSED MATRIX THICKNESS (Mils)

FIGURE 5–6

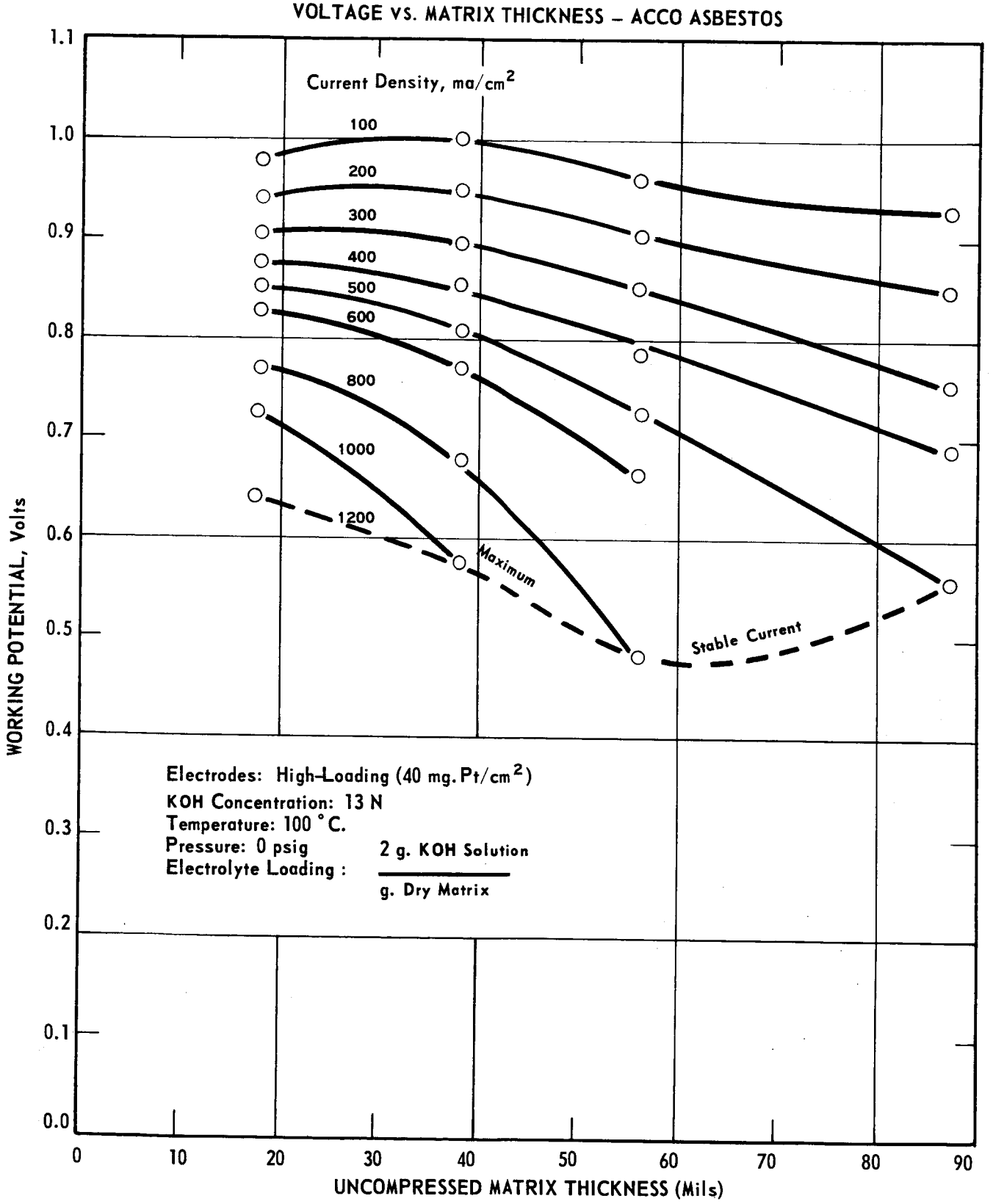
VOLTAGE vs. MATRIX THICKNESS – ACCO ASBESTOS
Current Density, ma/cm²
100
200
300
400
500
600
800
1000
1200
Maximum
Stable Current
Electrodes: High-Loading (40 mg. Pt/cm²)
KOH Concentration: 13 N
Temperature: 100 °C.
Pressure: 0 psig
Electrolyte Loading : 2 g. KOH Solution / g. Dry Matrix
WORKING POTENTIAL, Volts
1.1
1.0
0.9
0.8
0.7
0.6
0.5
0.4
0.3
0.2
0.1
0.0
0
10
20
30
40
50
60
70
80
90
UNCOMPRESSED MATRIX THICKNESS (Mils)

FIGURE 5–7

CELL INTERNAL RESISTANCE *vs.* KOH CONCENTRATION – 70° C

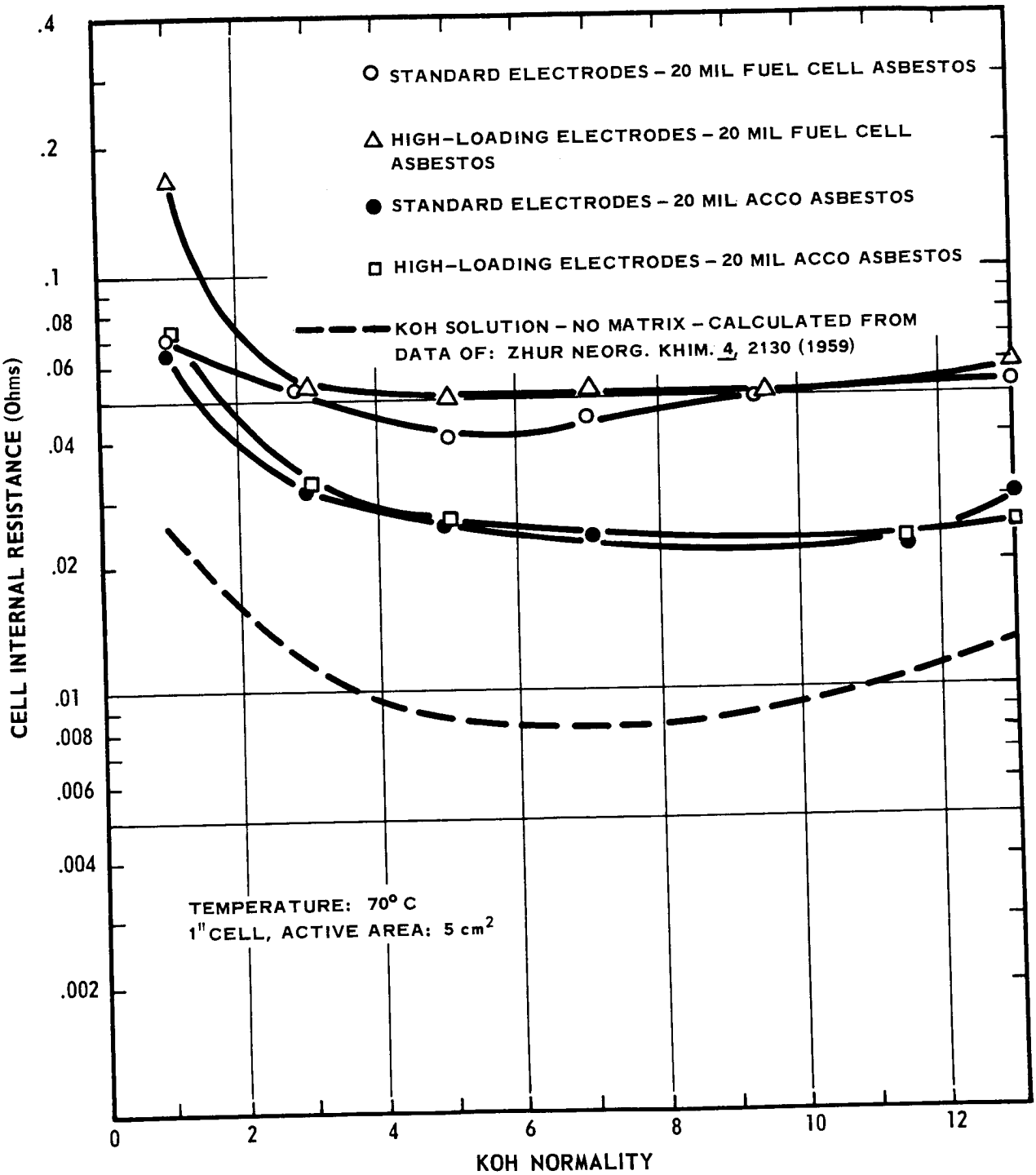

FIGURE 5–8

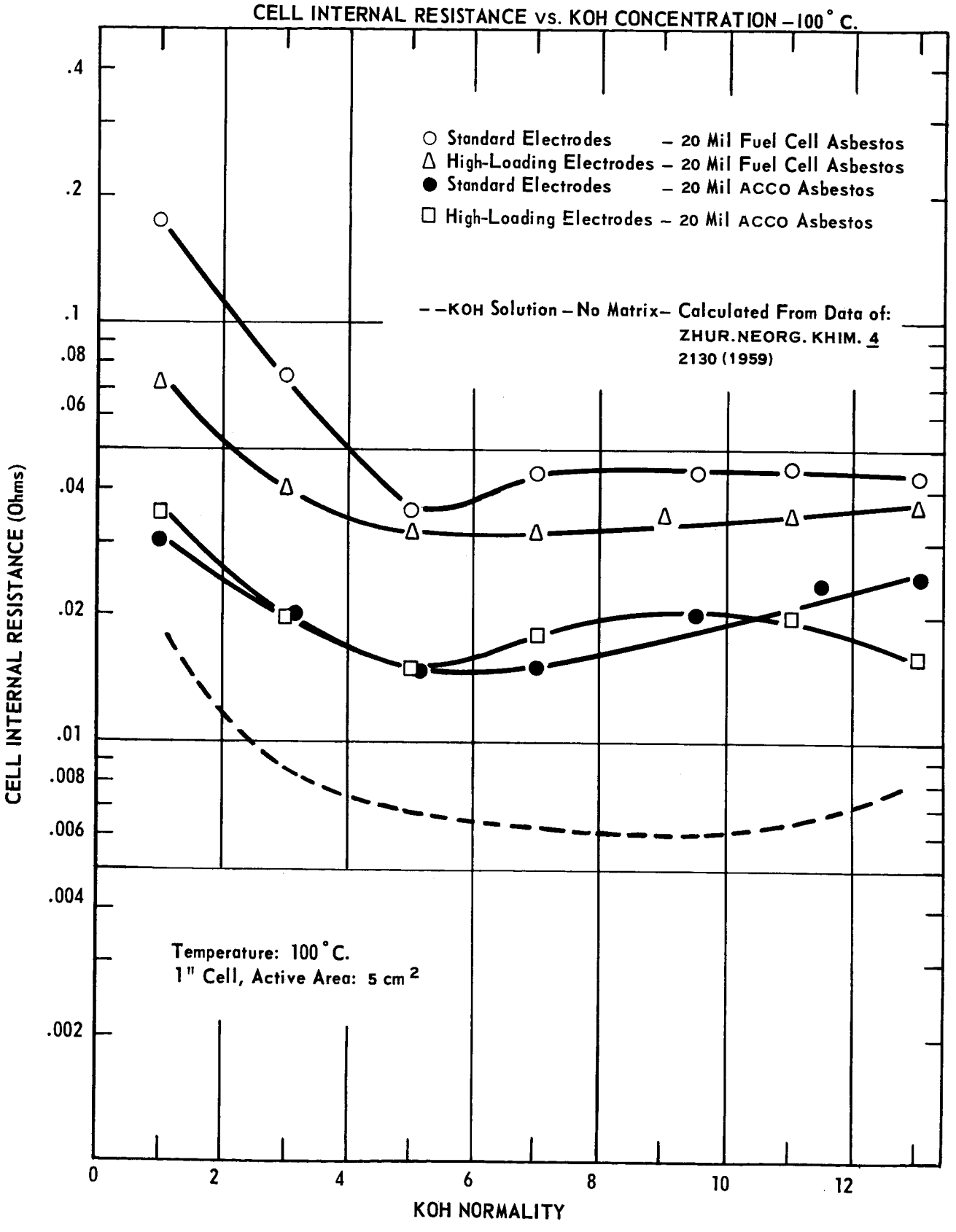
CELL INTERNAL RESISTANCE vs. KOH CONCENTRATION – 100° C.
CELL INTERNAL RESISTANCE (Ohms)
.4
.2
.1
.08
.06
.04
.02
.01
.008
.006
.004
.002
0
2
4
6
8
10
12
KOH NORMALITY
○ Standard Electrodes – 20 Mil Fuel Cell Asbestos
△ High-Loading Electrodes – 20 Mil Fuel Cell Asbestos
● Standard Electrodes – 20 Mil ACCO Asbestos
□ High-Loading Electrodes – 20 Mil ACCO Asbestos
– –KOH Solution – No Matrix– Calculated From Data of:
ZHUR.NEORG. KHIM. 4
2130 (1959)
Temperature: 100° C.
1" Cell, Active Area: 5 cm 2

FIGURE 5–9

CELL PERFORMANCE vs. KOH CONCENTRATION

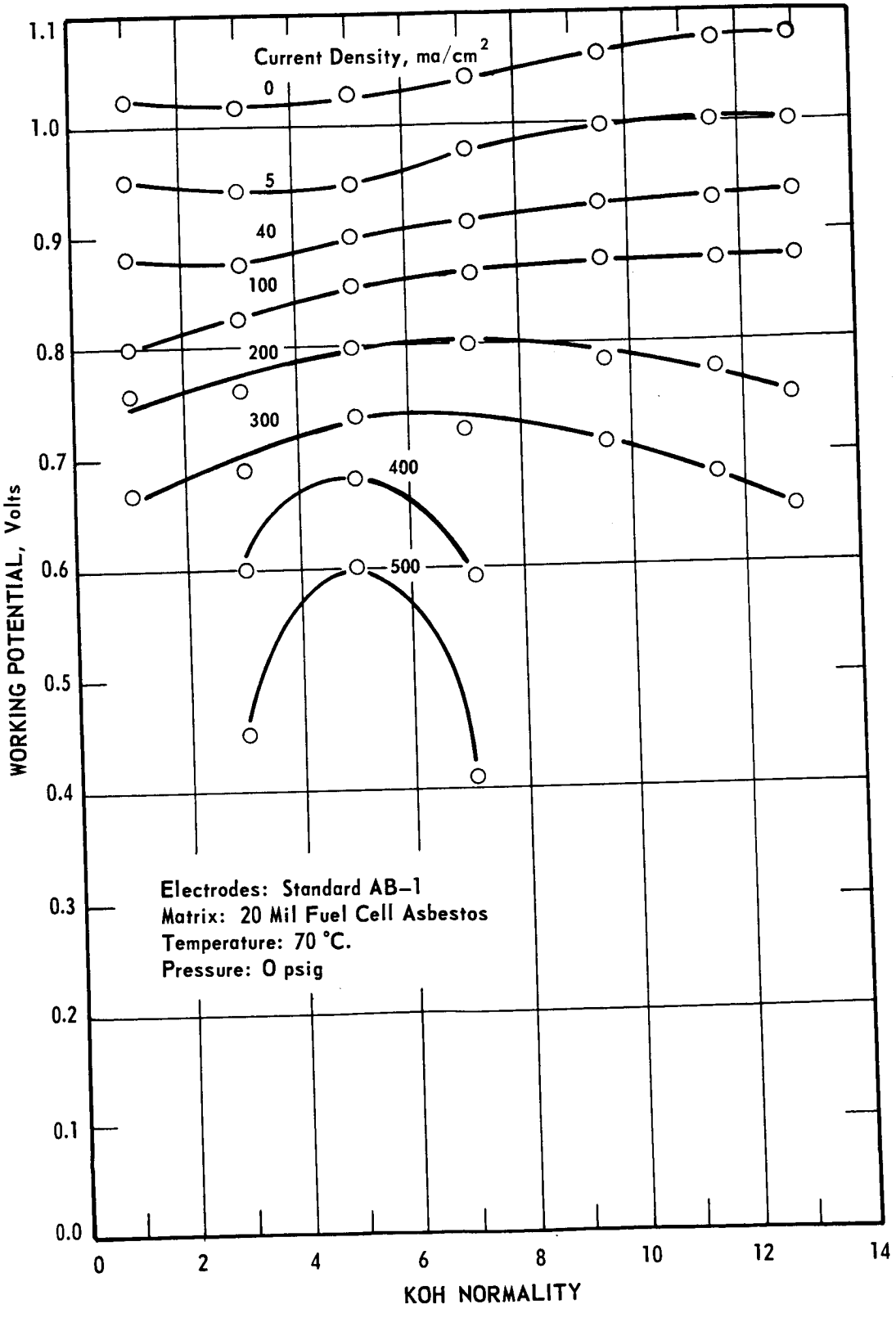

FIGURE 5-10

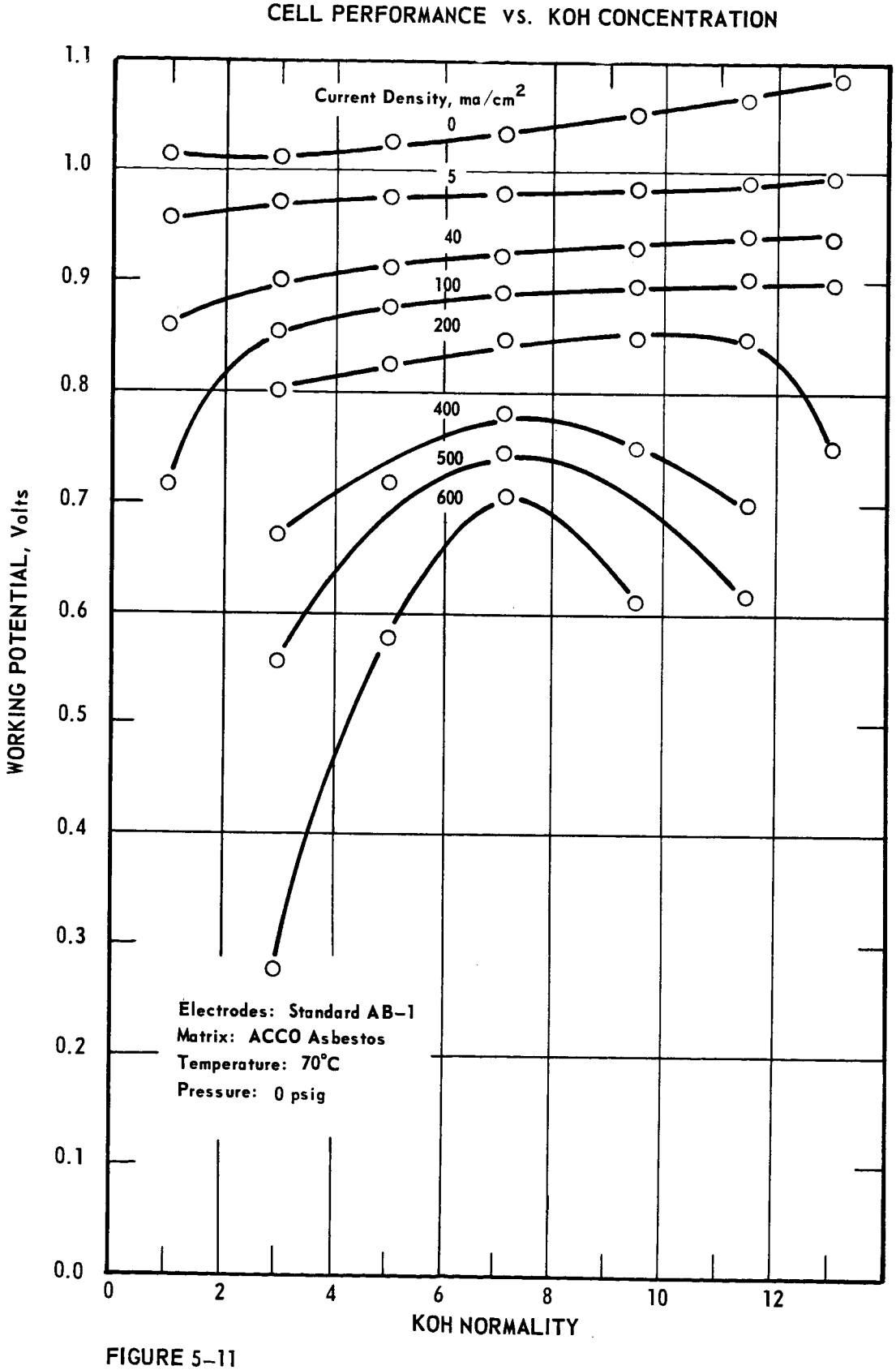
CELL PERFORMANCE VS. KOH CONCENTRATION
Current Density, ma/cm²
0
5
40
100
200
400
500
600
Electrodes: Standard AB-1
Matrix: ACCO Asbestos
Temperature: 70°C
Pressure: 0 psig
WORKING POTENTIAL, Volts
KOH NORMALITY
1.1
1.0
0.9
0.8
0.7
0.6
0.5
0.4
0.3
0.2
0.1
0.0
0
2
4
6
8
10
12

FIGURE 5-11

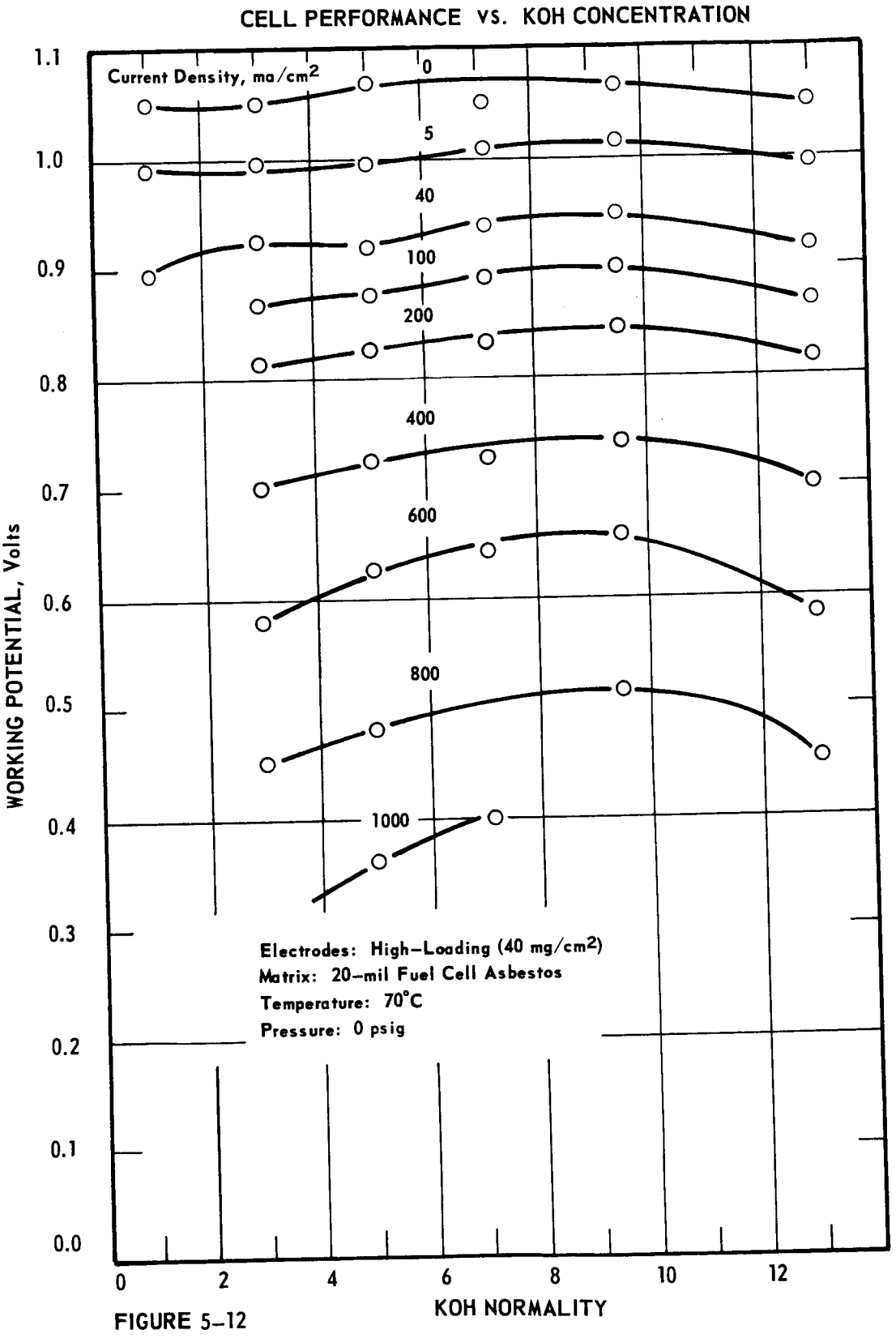
CELL PERFORMANCE VS. KOH CONCENTRATION
Current Density, ma/cm2
0
5
40
100
200
400
600
800
1000
Electrodes: High-Loading (40 mg/cm2)
Matrix: 20-mil Fuel Cell Asbestos
Temperature: 70°C
Pressure: 0 psig
WORKING POTENTIAL, Volts
1.1
1.0
0.9
0.8
0.7
0.6
0.5
0.4
0.3
0.2
0.1
0.0
0
2
4
6
8
10
12
KOH NORMALITY

FIGURE 5-12

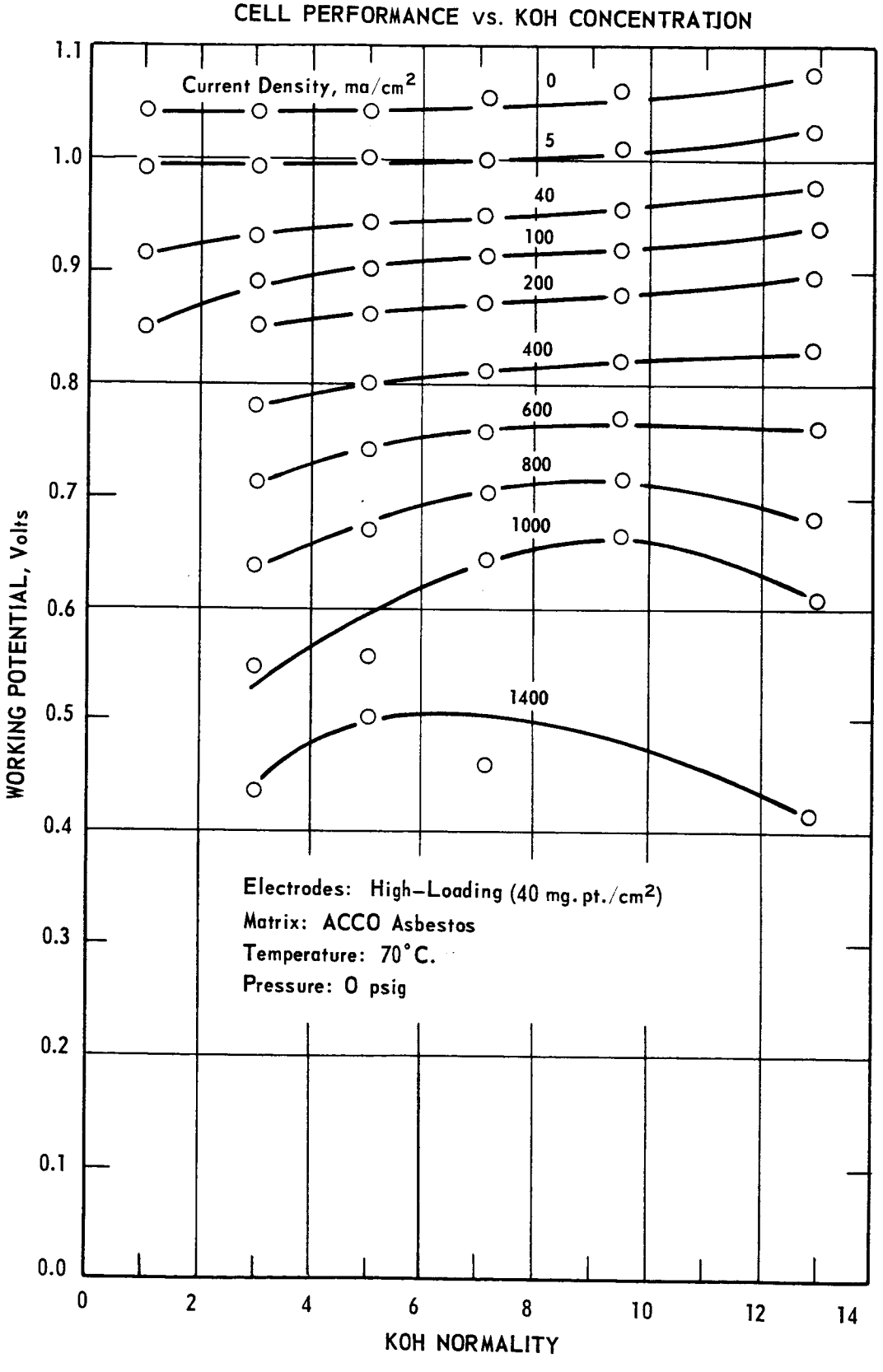
CELL PERFORMANCE vs. KOH CONCENTRATION
Current Density, ma/cm²
0
5
40
100
200
400
600
800
1000
1400
Electrodes: High-Loading (40 mg. pt./cm²)
Matrix: ACCO Asbestos
Temperature: 70°C.
Pressure: 0 psig
WORKING POTENTIAL, Volts
1.1
1.0
0.9
0.8
0.7
0.6
0.5
0.4
0.3
0.2
0.1
0.0
0
2
4
6
8
10
12
14
KOH NORMALITY

FIGURE 5-13

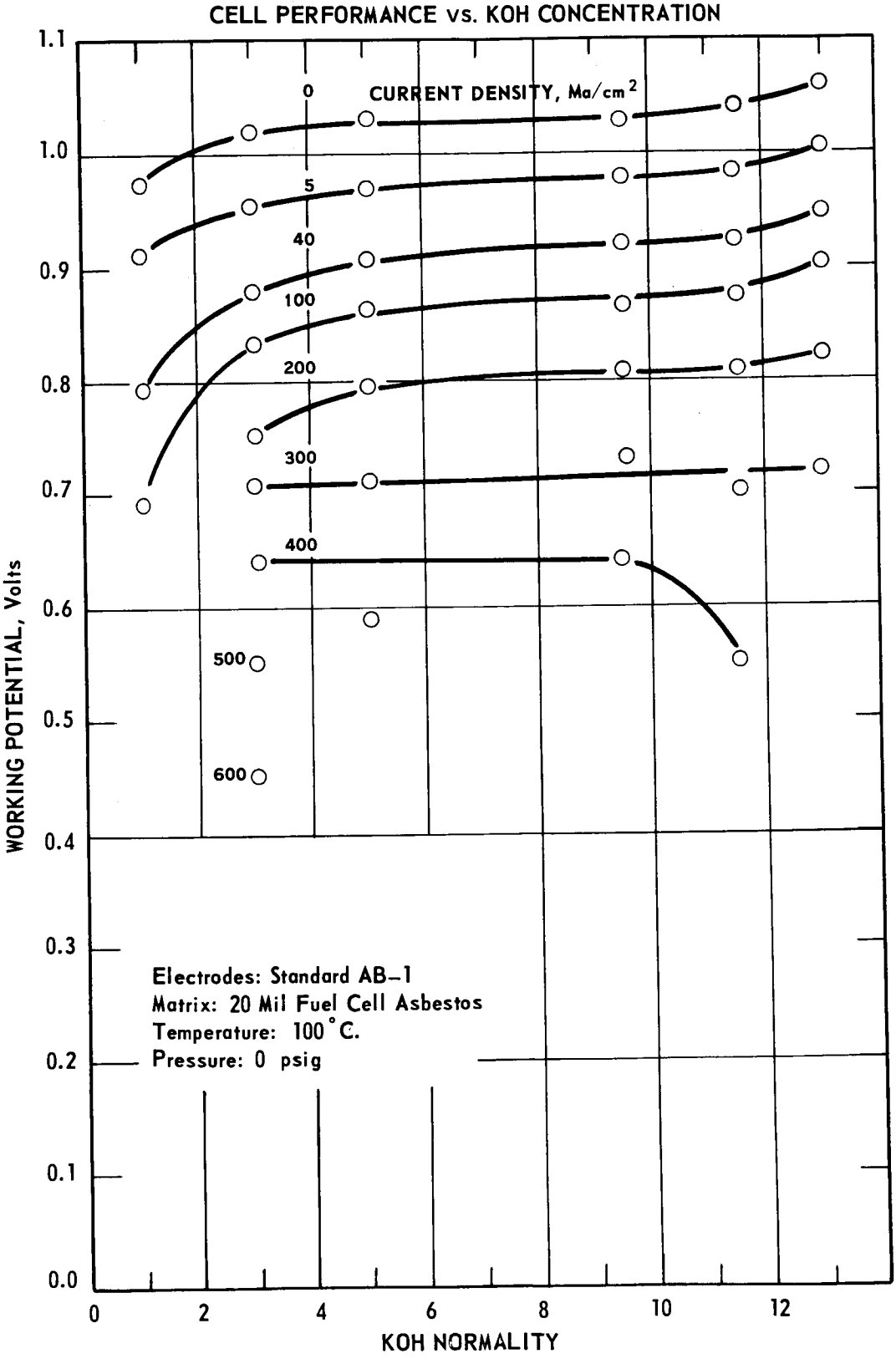
CELL PERFORMANCE vs. KOH CONCENTRATION
CURRENT DENSITY, Ma/cm 2
0
5
40
100
200
300
400
500
600
WORKING POTENTIAL, Volts
KOH NORMALITY
1.1
1.0
0.9
0.8
0.7
0.6
0.5
0.4
0.3
0.2
0.1
0.0
0
2
4
6
8
10
12
Electrodes: Standard AB-1
Matrix: 20 Mil Fuel Cell Asbestos
Temperature: 100 °C.
Pressure: 0 psig

FIGURE 5-14

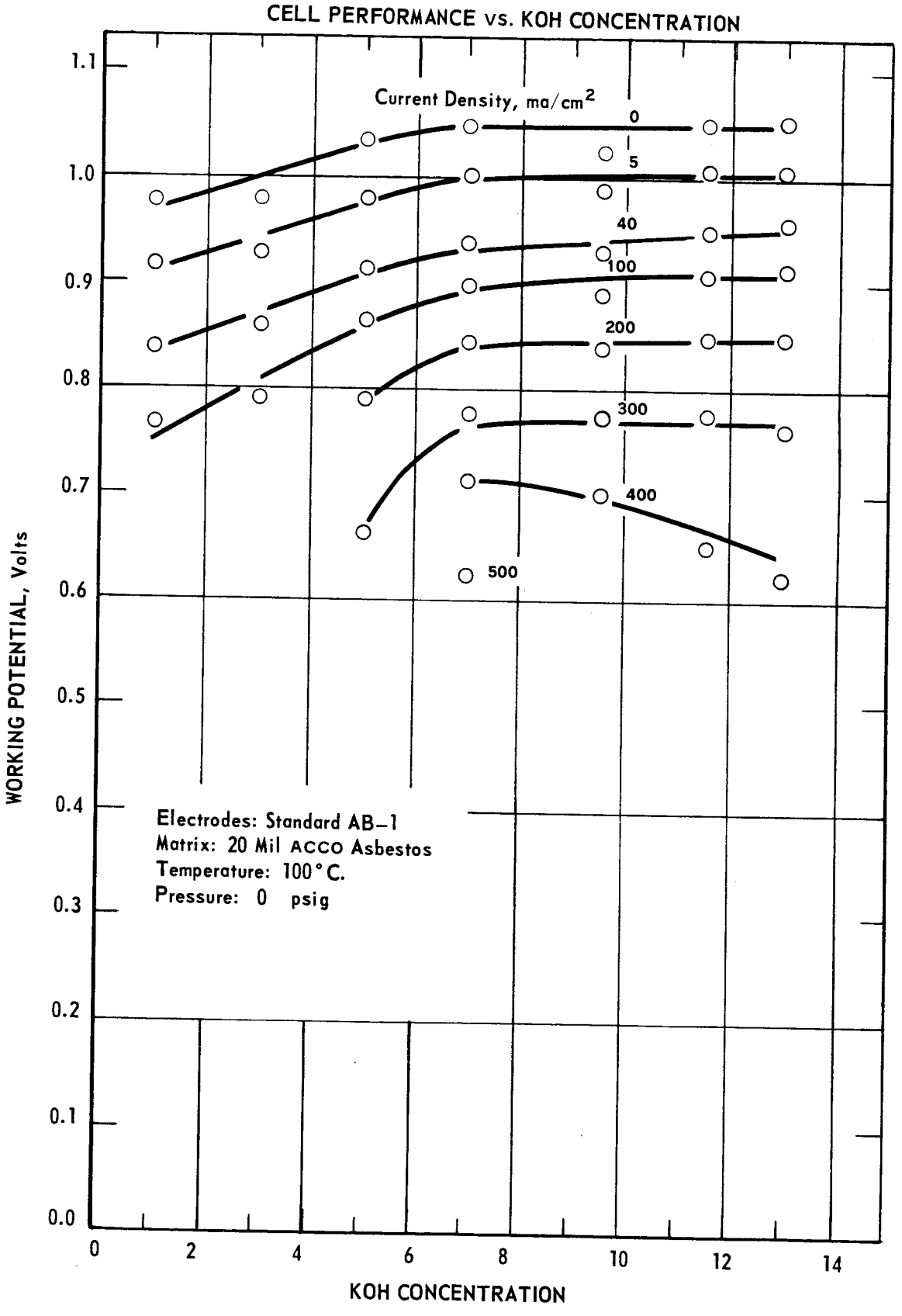
CELL PERFORMANCE vs. KOH CONCENTRATION
Current Density, ma/cm2
0
5
40
100
200
300
400
500
Electrodes: Standard AB-1
Matrix: 20 Mil ACCO Asbestos
Temperature: 100°C.
Pressure: 0 psig
WORKING POTENTIAL, Volts
KOH CONCENTRATION
1.1
1.0
0.9
0.8
0.7
0.6
0.5
0.4
0.3
0.2
0.1
0.0
0
2
4
6
8
10
12
14

FIGURE 5-15

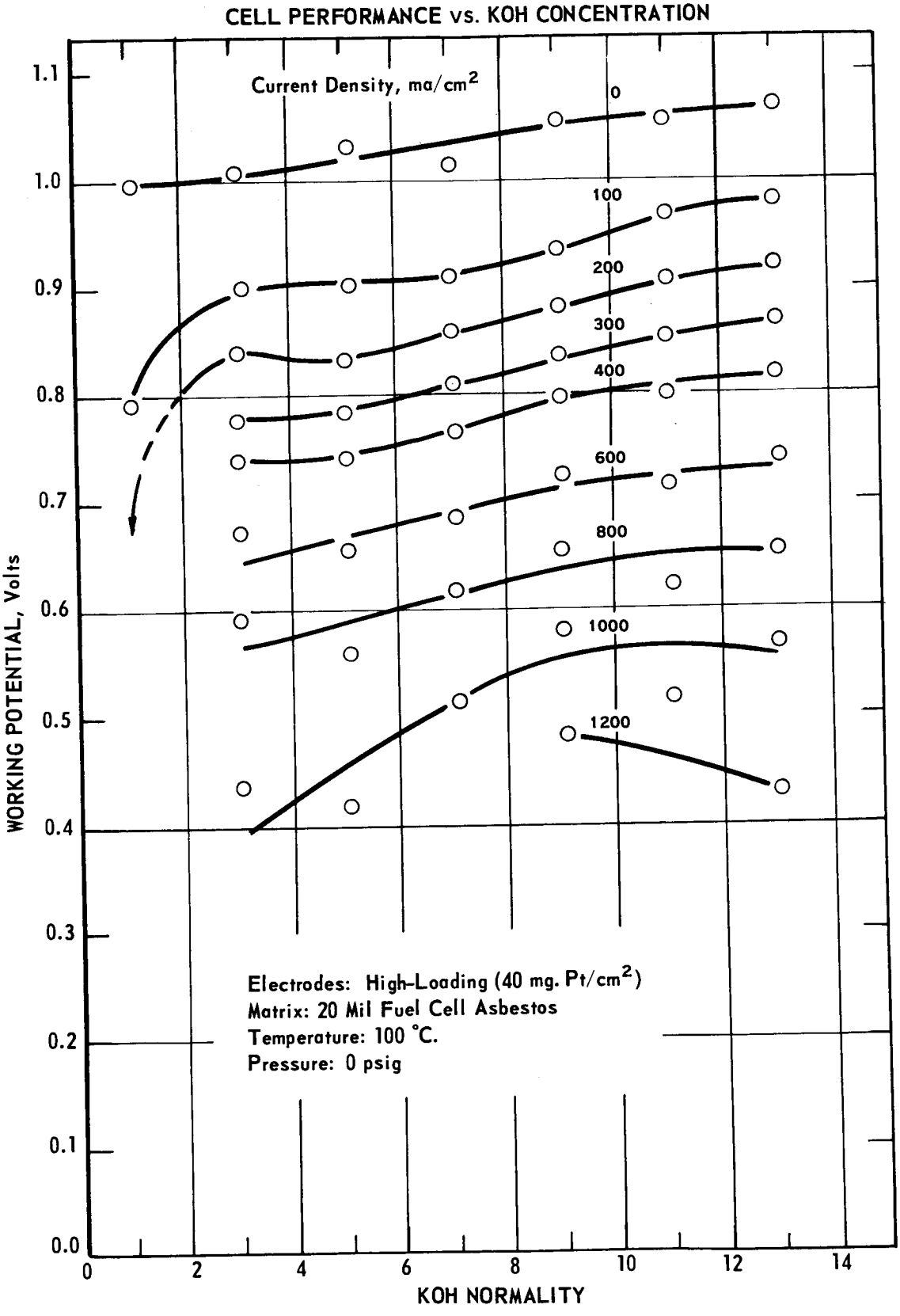
CELL PERFORMANCE vs. KOH CONCENTRATION
Current Density, ma/cm2
0
100
200
300
400
600
800
1000
1200
WORKING POTENTIAL, Volts
1.1
1.0
0.9
0.8
0.7
0.6
0.5
0.4
0.3
0.2
0.1
0.0
0
2
4
6
8
10
12
14
KOH NORMALITY
Electrodes: High-Loading (40 mg. Pt/cm2)
Matrix: 20 Mil Fuel Cell Asbestos
Temperature: 100 °C.
Pressure: 0 psig

FIGURE 5-16

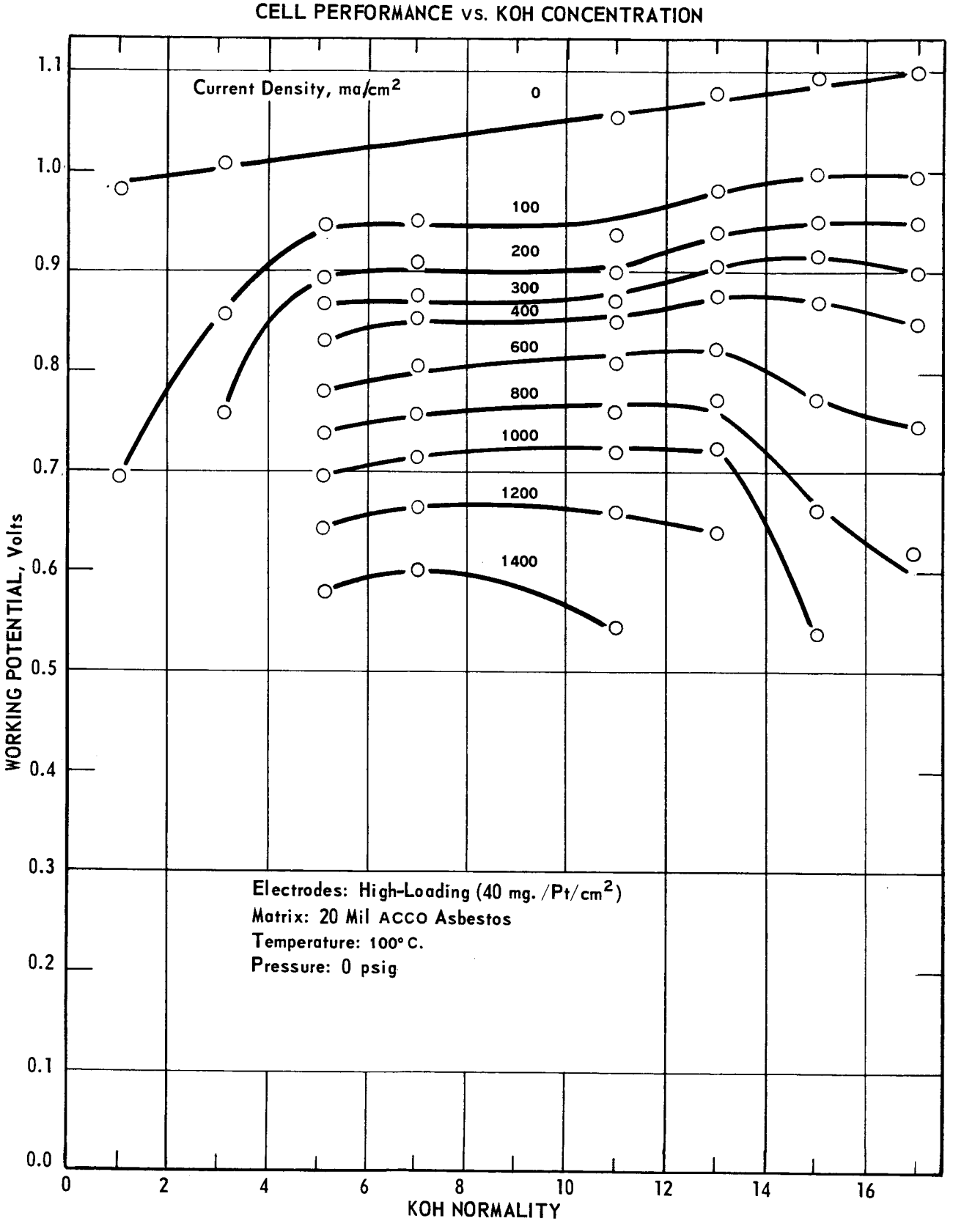
CELL PERFORMANCE vs. KOH CONCENTRATION
Current Density, ma/cm²
0
100
200
300
400
600
800
1000
1200
1400
WORKING POTENTIAL, Volts
1.1
1.0
0.9
0.8
0.7
0.6
0.5
0.4
0.3
0.2
0.1
0.0
0
2
4
6
8
10
12
14
16
KOH NORMALITY
Electrodes: High-Loading (40 mg. /Pt/cm²)
Matrix: 20 Mil ACCO Asbestos
Temperature: 100° C.
Pressure: 0 psig

FIGURE 5–17

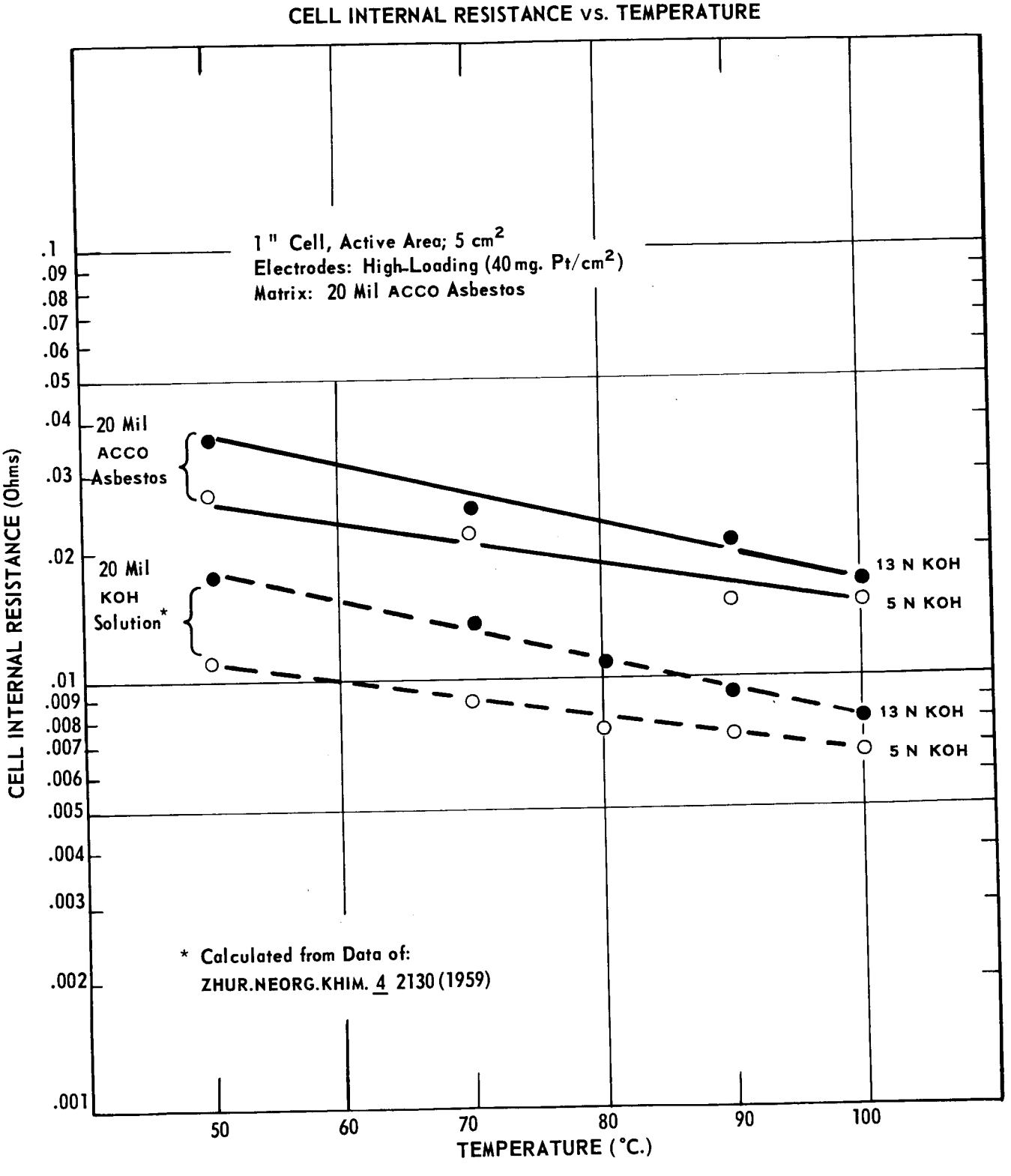
CELL INTERNAL RESISTANCE vs. TEMPERATURE
1" Cell, Active Area; 5 cm²
Electrodes: High-Loading (40 mg. Pt/cm²)
Matrix: 20 Mil ACCO Asbestos
20 Mil ACCO Asbestos
20 Mil KOH Solution*
13 N KOH
5 N KOH
13 N KOH
5 N KOH
* Calculated from Data of:
ZHUR.NEORG.KHIM. 4 2130 (1959)
CELL INTERNAL RESISTANCE (Ohms)
.1
.09
.08
.07
.06
.05
.04
.03
.02
.01
.009
.008
.007
.006
.005
.004
.003
.002
.001
50
60
70
80
90
100
TEMPERATURE (°C.)

FIGURE 5-18

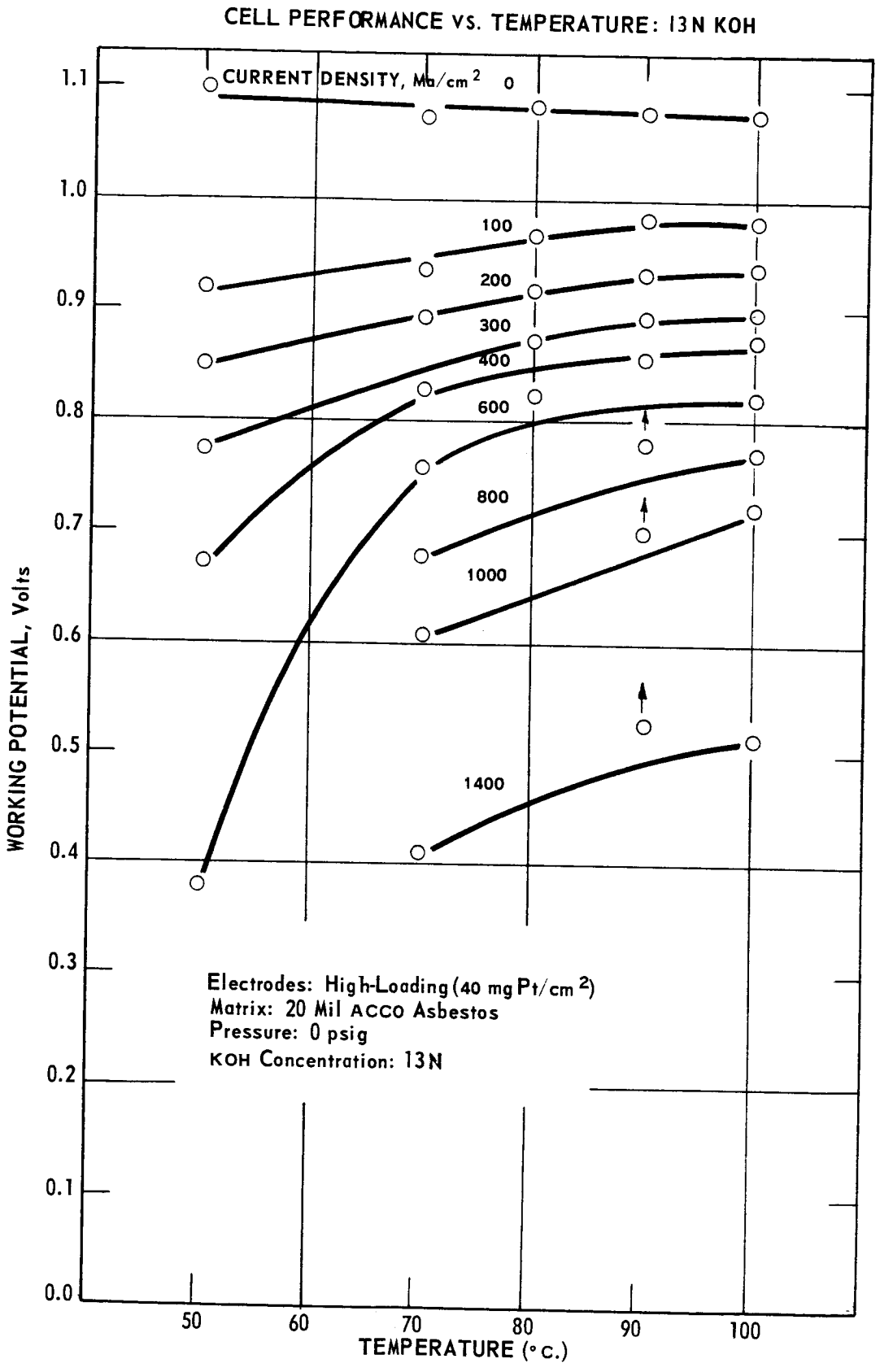
CELL PERFORMANCE VS. TEMPERATURE: 13N KOH
CURRENT DENSITY, Ma/cm 2
0
100
200
300
400
600
800
1000
1400
WORKING POTENTIAL, Volts
1.1
1.0
0.9
0.8
0.7
0.6
0.5
0.4
0.3
0.2
0.1
0.0
50
60
70
80
90
100
TEMPERATURE (°C.)
Electrodes: High-Loading (40 mg Pt/cm 2)
Matrix: 20 Mil ACCO Asbestos
Pressure: 0 psig
KOH Concentration: 13N

FIGURE 5-19

CELL PERFORMANCE vs. TEMPERATURE: 5N KOH

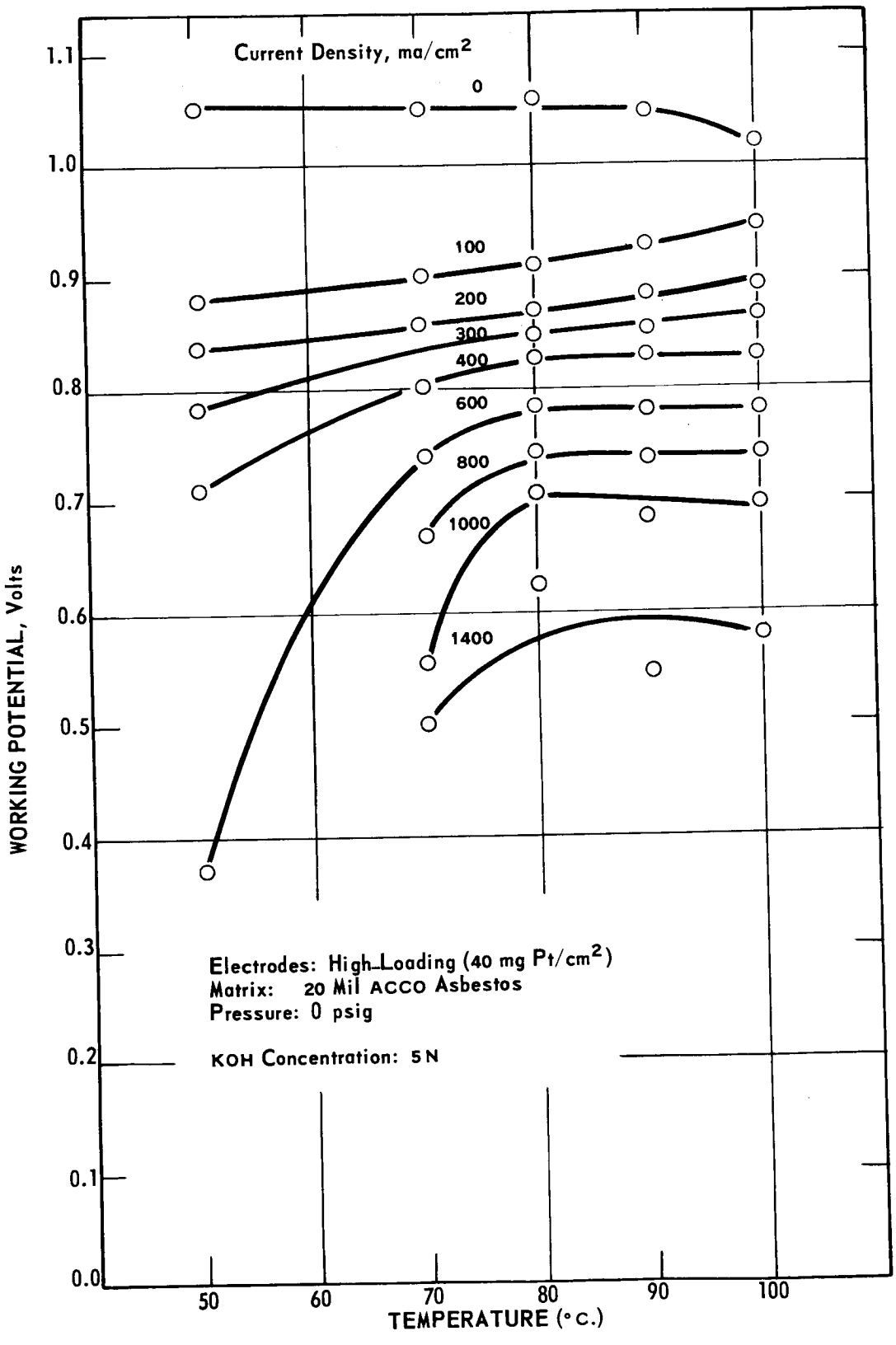

FIGURE 5-20

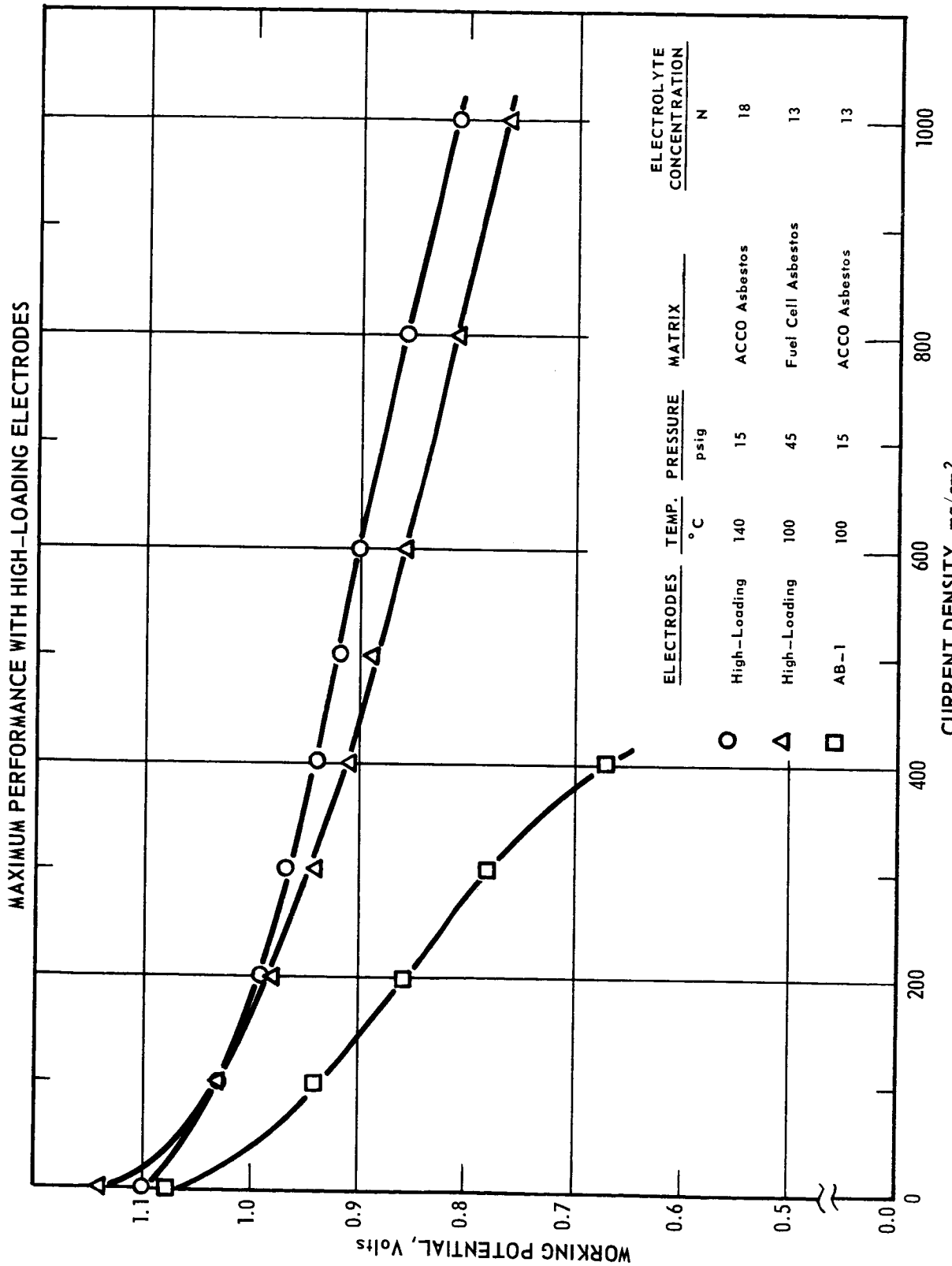
MAXIMUM PERFORMANCE WITH HIGH-LOADING ELECTRODES
WORKING POTENTIAL, Volts
CURRENT DENSITY, ma/cm²
ELECTRODES
TEMP. °C
PRESSURE psig
MATRIX
ELECTROLYTE CONCENTRATION N
High-Loading 140 15 ACCO Asbestos 18
High-Loading 100 45 Fuel Cell Asbestos 13
AB-1 100 15 ACCO Asbestos 13

FIGURE 5-21

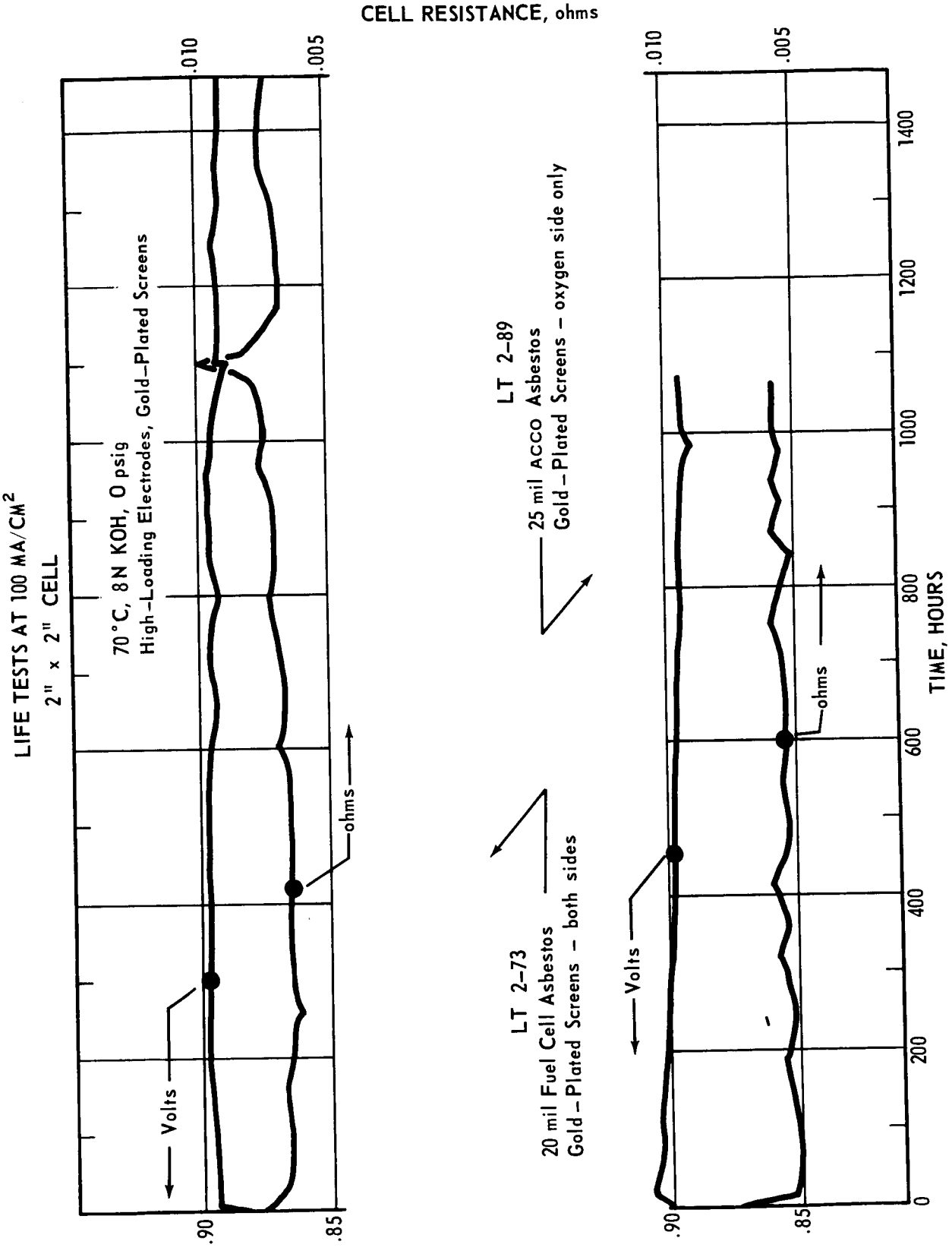
LIFE TESTS AT 100 MA/CM²
2" x 2" CELL
70°C, 8N KOH, 0 psig
High-Loading Electrodes, Gold-Plated Screens
Volts
ohms
.90
.85
.010
.005
LT 2-89
25 mil ACCO Asbestos
Gold-Plated Screens – oxygen side only
LT 2-73
20 mil Fuel Cell Asbestos
Gold-Plated Screens – both sides
0
200
400
600
800
1000
1200
1400
TIME, HOURS
CELL RESISTANCE, ohms
WORKING POTENTIAL, Volts

FIGURE 5-22

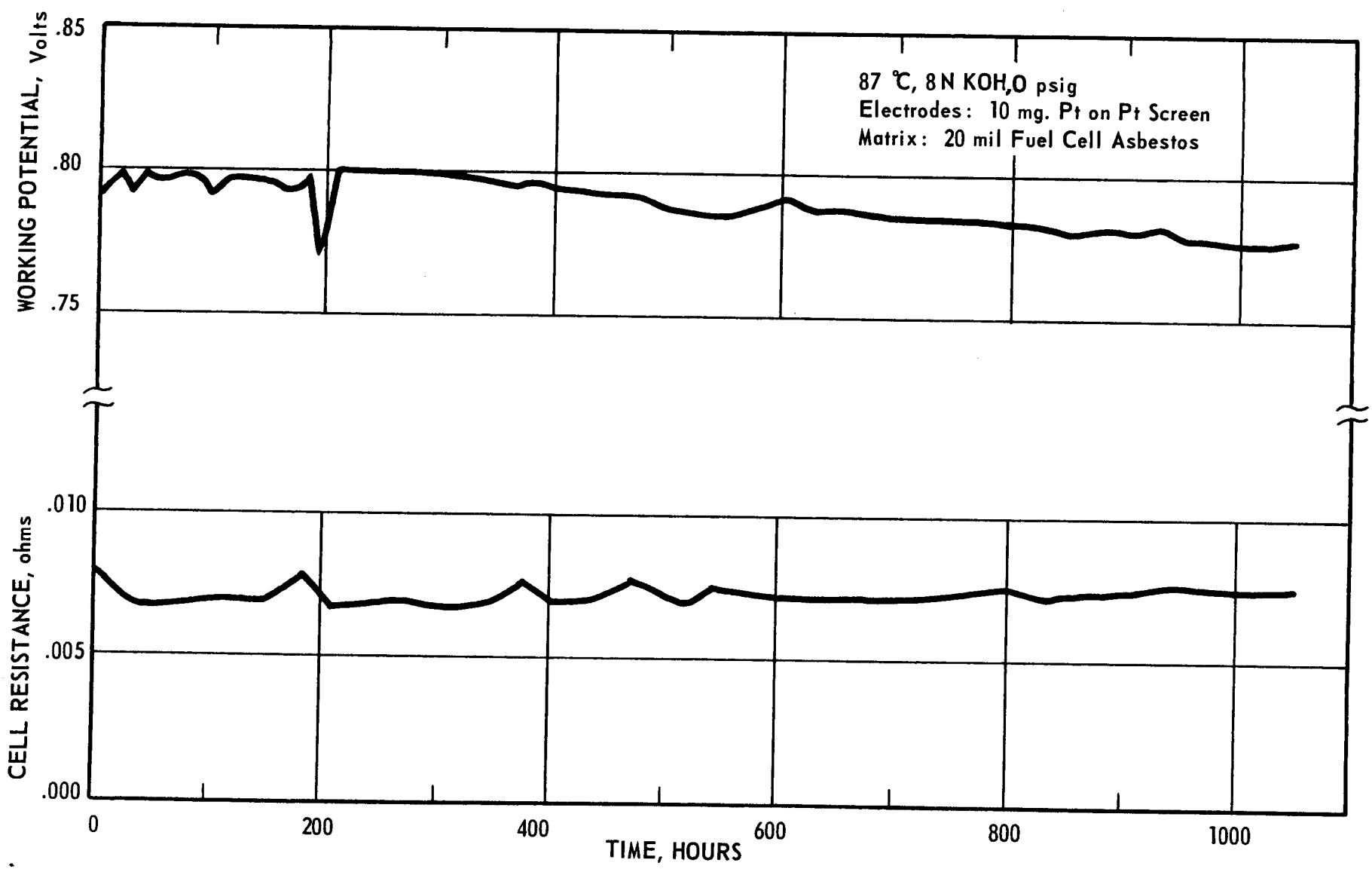
LIFE TEST 2-60 AT 200 MA/CM 2
2" x 2" CELL
87 ℃, 8 N KOH, 0 psig
Electrodes: 10 mg. Pt on Pt Screen
Matrix: 20 mil Fuel Cell Asbestos
WORKING POTENTIAL, Volts
.85
.80
.75
CELL RESISTANCE, ohms
.010
.005
.000
0
200
400
600
800
1000
TIME, HOURS

FIGURE 5-23

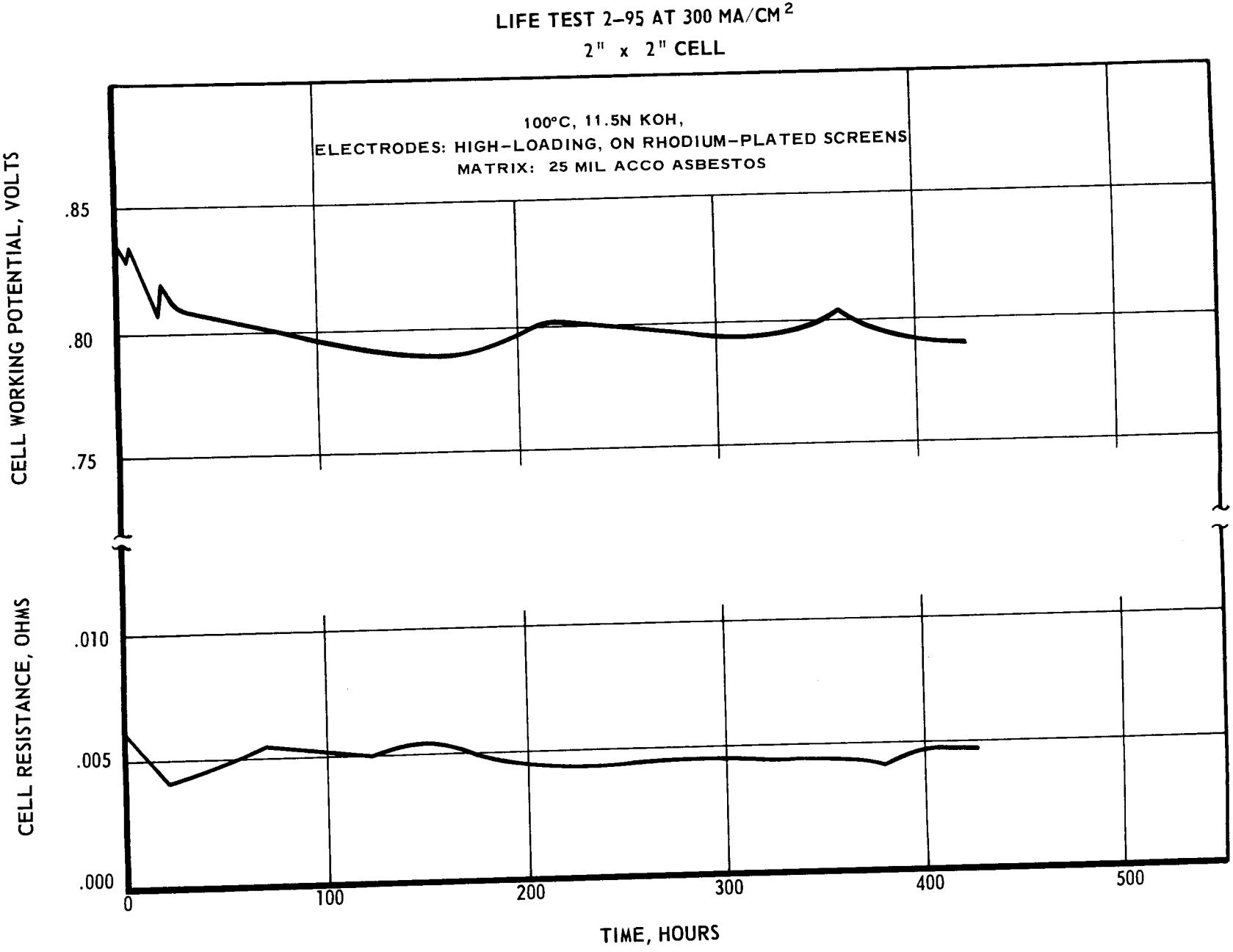
LIFE TEST 2-95 AT 300 MA/CM 2
2" x 2" CELL
100°C, 11.5N KOH,
ELECTRODES: HIGH-LOADING, ON RHODIUM-PLATED SCREENS
MATRIX: 25 MIL ACCO ASBESTOS
CELL WORKING POTENTIAL, VOLTS
.85
.80
.75
CELL RESISTANCE, OHMS
.010
.005
.000
0
100
200
300
400
500
TIME, HOURS

FIGURE 5-24

6. BATTERY SIZE CELL OPERATION

6.1 Choice of Operating Conditions

It is desirable to select an electrode-matrix system, cell assembly conditions, and operating conditions which will lead to minimum weight/net power of an entire battery system, including battery, all auxiliary equipment (for heat and water removal and power control), and fuel plus associated tankage. Where the weight of fuel plus associated tankage is an overriding factor in system weight (long missions), maximum voltage output at reasonable current density is desired. Where fuel and associated tankage weight is not an overriding factor, the higher battery humidity obtainable with lower KOH concentrations is desirable (even though cell performance is slightly lower) because of lower weight and power consumption of equipment for removing battery heat and water.

With these two cases in mind, Table 6-1 summarizes the combinations of electrode-matrix system, cell assembly and operating conditions which the performance data, described in Section 5, indicates to be at or near optimum. The reasons for the choice of the electrode-matrix system, matrix thickness, cell assembly pressure, and electrolyte loading have been discussed.

The temperature (100°C) was selected from the point of view of achieving maximum performance and maximum battery humidity at a given KOH concentration. At this temperature stable operation can be expected without excessive material problems. While the data of Section 5.1.7 shows that still higher initial performance may be attained with high KOH concentrations at temperatures above 100°C, this regime must be explored in detail before adaption to battery operation can be considered.

A gas pressure of at least 45 psig is specified since, compared with atmosphere pressure, operation at 45 psig yields higher performance and in addition should decrease the weight and parasitic power consumption of the gas recycle pump. While increased pressure tends to increase the weight of the battery, design considerations indicate that this increase would be insignificant at pressures up to 45 psig. At higher pressures, the optimum pressure would be determined by a trade-off between battery weight, fuel plus related tankage weight, and the weight and power consumption of the hydrogen recycle pump. Nevertheless, operation at atmospheric pressure might still be attractive since it would avoid the safety problem posed by possible matrix rupture as the result of a differential pressure control failure during pressure operation.

Two electrolyte concentrations, 5N and 13N are shown. The higher concentration corresponds to maximum performance and low battery humidity, hence to minimum weight/net power of a battery and its fuel plus related tankage. The lower concentration corresponds to performance somewhat below the maximum, but to maximum practical battery humidity, hence to minimum weight/net power of equipment for removing battery heat and product water. At both concentrations, performance data are shown at both pressures (0 psig and 45 psig) which, for the different reasons discussed above, would be attractive.

6.2 Design of 6" x 6" Cell

A fuel cell was designed and constructed for evaluating the performance of scaled-up electrodes (6 inch square) at pressures above atmospheric(3H). The nickel face plates were designed to provide uniform gas distribution over the electrodes by manifolding from a 1/4 inch diameter header through evenly spaced 1/8 inch diameter channels, and then through 1/32 inch diameter orifices spaced at 1 inch intervals along the length of each channel (Figure 6-1). Gas discharge is through an identical manifold with channels running parallel to and alternate with the channels of the inlet manifold. The nominal path of gas flowing through each inlet orifice over the electrodes is 1 inch. Experimental work with 1 inch diameter and 2 inch square electrodes indicates that this path length is sufficient to saturate each gas with water vapor without causing electrolyte concentration gradients large enough to affect cell voltage adversely.

Gas distributions were measured experimentally in a plastic model of the face plates of the scaled-up cell over the entire expected range of total hydrogen and oxygen flow rates (70-8000 cc/min.). The flow rates among the manifold channels were found to vary by a maximum of 15% at 1000-8000 cc/min. total flow, and by a maximum of 20% at 70-400 cc/min. The flow rates among the rows of orifices varied by a maximum of 15% at average flows of 487-1130 cc/min. in the channels. Only at very low flows in the channels (15-167 cc/min.), was the variation among the rows of orifices as high as 25-30%. These experimental data indicate that the 6" x 6" cell design affords sufficiently uniform gas distribution.

6.3 Operation

An initial study was made of the operation of the High-Loading electrodes - ACCO Asbestos matrix system in the battery-size cell.

Each electrode was separated from its face plate by one flat nickel screen pressed against the electrode and by one corrugated nickel screen pressed against the face plate. The gaskets were of silicone rubber, encased in 3 mil thick Teflon tape. The dimensions of internal cell components are listed below.

Electrodes:	6" x 6" x 29 mils thick
Matrix:	8" x 8" x 20 mils thick - peripheral 3/4" encased in polyethylene film.
Spacer Screens:	Flat: 40 mesh - 6" x 6" x 25 mils thick corrugated: 60 mesh - 6" x 6" x 16 mils thick
Gaskets:	10" x 11 3/4" x (65-70) mils thick, with a 6" square opening in center

Each face plate was heated by a flat 8" square heating element (5 watts/in^2). Cell temperature was measured by thermocouples in the face plates and controlled by an on-off controller to within $\pm$ 1°C.

Provision was made for humidifying the inlet hydrogen stream by sparging through a saturator containing a 12 inch column of water at a temperature controlled to $\pm$ 0.4°C. Preliminary work showed that hydrogen left the saturator saturated with water vapor at the liquid temperature, over the range of flow rates required for operation of the cell.

Currents up to 110 amps (480 ma/cm^2) could be drawn through a load circuit comprising one variable resistor and six fixed resistors in parallel. The latter could be put into the circuit through knife switches.

The cell was first assembled and operated at atmospheric pressure under conditions which had been shown previously to give highest initial performance. These conditions are given below:

Electrolyte (KOH) concentration - 13N

Electrolyte loading - 2.2 g KOH solution/g dry matrix

Cell assembly pressure - 180 psi

Temperature - 100°C

The flow of hydrogen and oxygen was countercurrent. Initial operation was on dry gases at flow rates set to maintain the electrolyte concentration at 13N.

The initial performance is shown in Table 6-2 and compared with the initial performance obtained with the same electrode sample and under the same operating conditions in a one-inch cell (1 in. in diameter electrodes). Although the internal resistance (in ohm-cm^2) of the 6 inch cell was slightly higher than that of the 1 inch cell, performance was essentially the same.

The performance of the 6 inch cell during 420 hours on both dry and humidified hydrogen and at varying current densities is shown in Figure 6-2. A condition of "dead-ended" oxygen was approximated by using an oxygen flow rate only slightly in excess of the stoichiometric requirement; 90-95% of the product water was removed by the hydrogen stream. Operating with dry gases, the voltage at a current density of 100 ma/cm^2 declined by 25 mv during 66 hours, following which a reversal of gases (in both polarity and direction), immediately increased the voltage by 35 mv. Following gas reversal, the voltage declined by 22 mv over a 44 hour period. From then on, the cell was operated with hydrogen

saturated with water at 45°C, simulating battery operation with a recycle hydrogen stream from which water is condensed at 45°C. At 100 and 200 ma/cm^2, the performance was relatively steady, at 0.90 and 0.84 volts respectively, during successive 30 and 20 hour periods. During this time, the hydrogen flow was set to maintain the KOH concentration at 11.6-12.8N. At 300 ma/cm^2, a potential of 0.815-0.805 volts was maintained over a 60 hour period by operating at 8N KOH. At 400 ma/cm^2, the voltage in this test fluctuated between 0.75 and 0.78 volts over a 7 hour period and was extremely sensitive to small changes in flow rate. Voltage decline at 400 ma/cm^2 was not caused by any electrode deterioration since lowering the current density to 300 ma/cm^2 gave steady performance during a 12 hour period at the same voltage level as had been maintained earlier. Likewise, as seen in Figure 6-2, the initial voltages at 200 and 100 ma/cm^2 were the same as at the conclusion of the earlier periods of operation at these current densities. Further operation at 100 ma/cm^2 produced a decline of 20 mv over a 165 hour period. During the total 420 hour period the cell internal resistance was maintained between 0.5 and 0.85 milliohms, with no apparent trend with time. This run demonstrates the ability of High-Loading electrodes to give high and reasonably stable performance over prolonged periods at current densities at least up to 300 ma/cm^2, in a battery-sized single cell operating with dynamic water removal in the hydrogen stream. As discussed in Section 5.3 life test data obtained in 2" x 2" cells indicate that time dependent voltage declines of the magnitude encountered here can be eliminated by the use of gold-plated nickel screens on the oxygen side.

6.4 Pressure Drop

To aid in the design of a prototype 6" x 6" bipolar plate, pressure drops through the cell were measured at dry hydrogen flows up to 5 c.f.m. and at dry oxygen flows up to 2.5 c.f.m. These flows are equivalent to approximately 130 (for hydrogen) and 65 (for oxygen) times the total stoichiometric gas requirement (hydrogen plus oxygen) for a current density of 400 ma/cm^2. Three different spacer screen configurations were used; flat 20 mesh screen (30 mils thick), flat 40 mesh screen (20 mils thick), and a flat 40 mesh screen backed up by a corrugated 60 mesh screen on each side of the cell. Measurements were made at 100°C with no current being drawn from the cell. To keep the matrix from drying out, the flow of gas was maintained only while pressure measurements were made, generally for 10-15 seconds per measurement. The effect of flow rate on pressure drop is shown in a logarithimic plot (Figure 6-3). Except at hydrogen pressure drops below about 0.15 psi the pressure drop varied as the 1.7 power of the flow rate. This is reasonably close to the theoretical value of 2 for flow through orifices. At a given volumetric flow rate the pressure drop for oxygen was generally 8 times that of hydrogen.

TABLE 6-1

Operating Conditions For Scale-Up

Electrodes:	High-Loading (40 mg Pt/cm^2)
Matrix:	ACCO Asbestos, 20 mils thick
Cell Assembly Pressure:	150 psi
Electrolyte Loading:	2g Solution/g Dry Matrix
Temperature:	100°C

Polarization Data:

Electrolyte Concentration	5N(1)		13N(2)	
Gas Pressure, psig	0	45	0	45
Current Density, ma/cm^2	Working Voltage			
100	0.94	0.98	0.98	0.01
200	0.89	0.94	0.94	0.98
300	0.87	0.91	0.90	0.94
400	0.83	0.88	0.88	0.92
500	0.80	0.84	0.85	0.89

(1) For minimum weight/net power of battery and auxiliaries except fuel and tankage.

(2) For minimum weight/net power including fuel and tankage.

Table 6-2

Initial Performance in Six-Inch Cell
Compared with One-Inch Cell

High-Loading Electrodes - 20 mil ACCO Asbestos Matrix
13N KOH, 100°C, 0 psig

	Internal Resistance ($ohm\text{-}cm^2$)	Working Voltage at Indicated Current Density (ma/cm^2)				
		0	100	200	300	400
Six Inch Cell	0.118	1.06	0.93	0.89	0.84	0.78
One Inch Cell	0.071	1.07	0.94	0.89	0.83	0.74

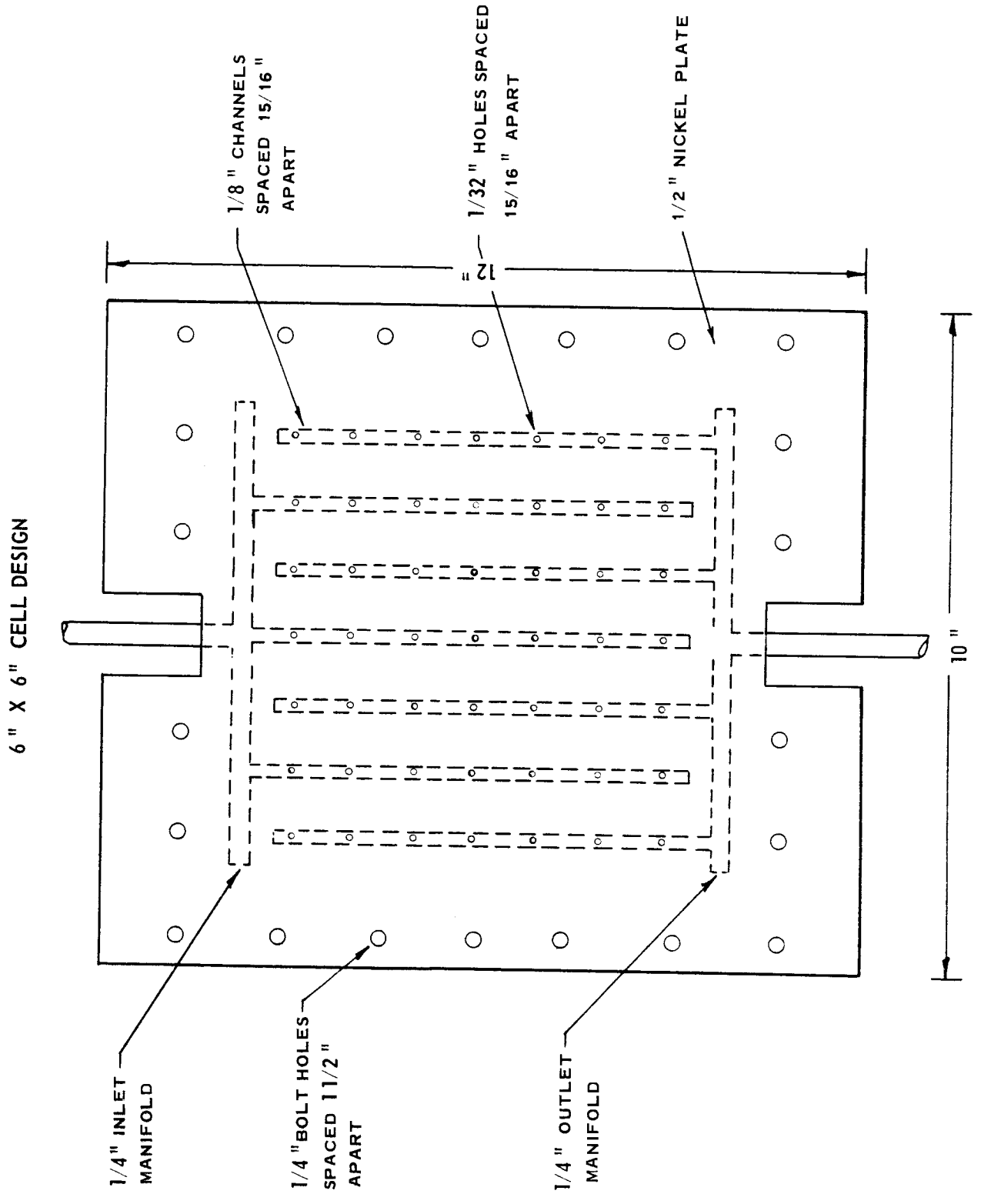
6 " X 6" CELL DESIGN
1/8 " CHANNELS SPACED 15/16 " APART
1/32 " HOLES SPACED 15/16 " APART
1/2 " NICKEL PLATE
12 "
10 "
1/4" INLET MANIFOLD
1/4 "BOLT HOLES SPACED 11/2 " APART
1/4 " OUTLET MANIFOLD

FIGURE 6-1

LIFE TEST, 6" x 6" CELL

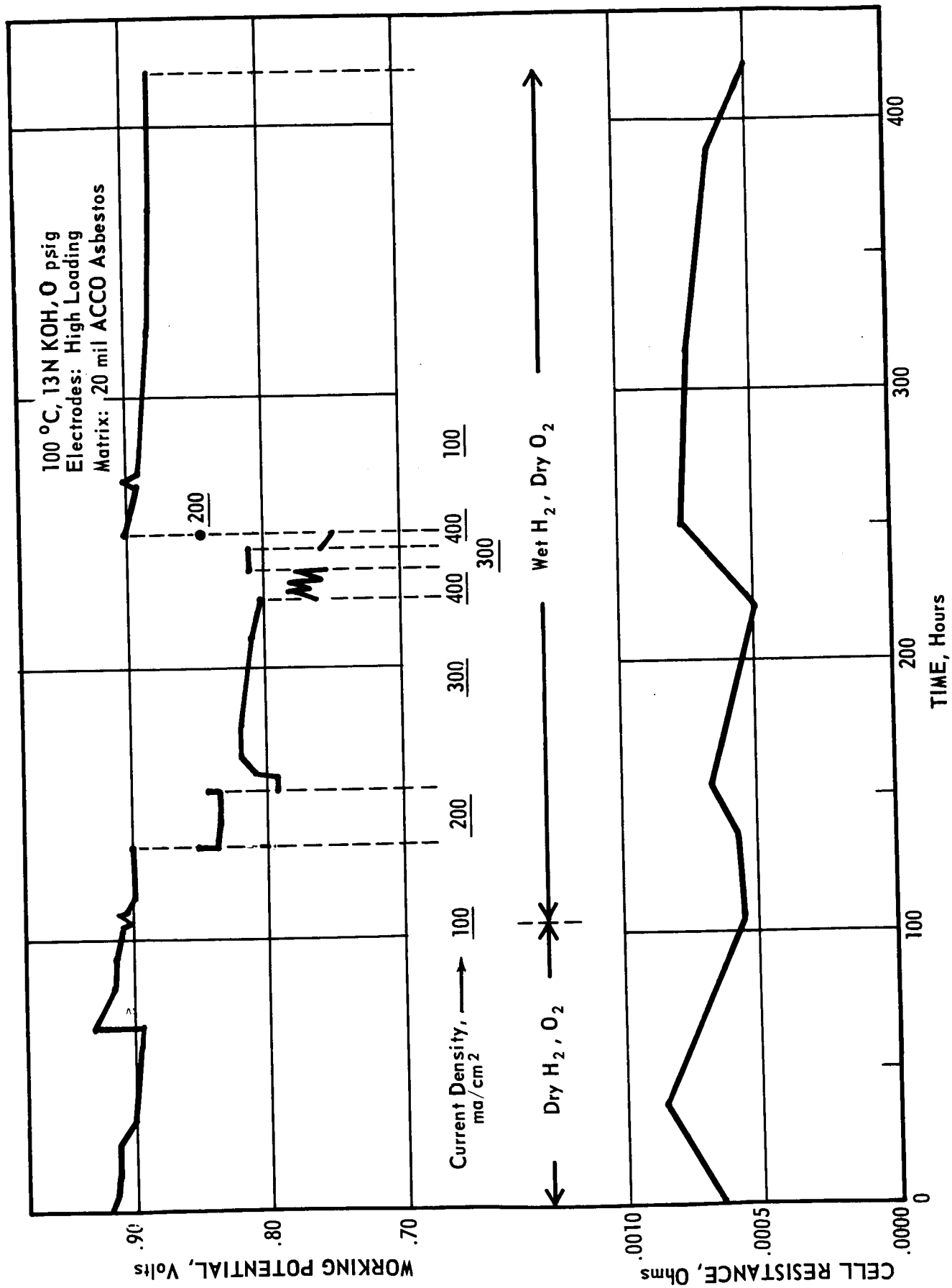

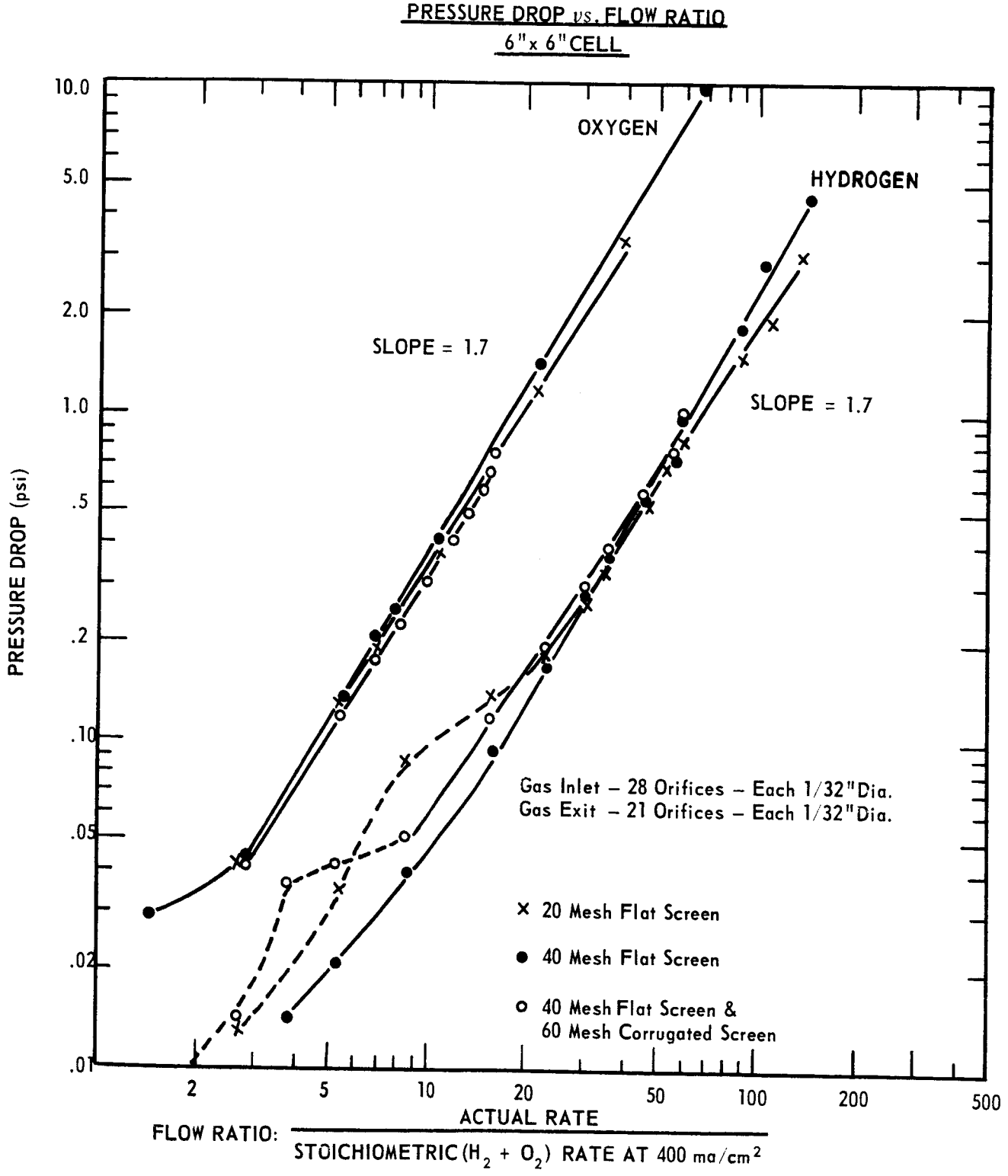
PRESSURE DROP vs. FLOW RATIO
6"x 6" CELL
OXYGEN
HYDROGEN
SLOPE = 1.7
SLOPE = 1.7
Gas Inlet – 28 Orifices – Each 1/32"Dia.
Gas Exit – 21 Orifices – Each 1/32"Dia.
× 20 Mesh Flat Screen
● 40 Mesh Flat Screen
○ 40 Mesh Flat Screen &
60 Mesh Corrugated Screen
PRESSURE DROP (psi)
10.0
5.0
2.0
1.0
.5
.2
.10
.05
.02
.01
2
5
10
20
50
100
200
500
FLOW RATIO: ACTUAL RATE / STOICHIOMETRIC (H2 + O2) RATE AT 400 ma/cm2

FIGURE 6-3

7. BATTERY SYSTEM

7.1 System Design

Two battery systems which could incorporate the thin, lightweight electrodes of this study were designed. These systems are based on dynamic removal of product heat and water from the battery into a recycle hydrogen stream, either with or without auxiliary liquid cooling. As described in Section 5, the performance of a battery system, operated at a given total pressure, would depend on the electrolyte loading, electrolyte concentration, and temperature. It is expected that during steady state battery operation, gradients in these three variables will exist over the face of the electrodes and through the thickness of the electrode-matrix sandwich. For optimum performance of the battery system, the battery should be designed and operated to limit these gradients within the boundaries defined by the data of Section 5.

The effect of battery design and operation on the magnitude of these gradients was simulated by a mathematical model. General differential mass and energy balance equations were derived. Solution of these equations, and a computer estimation of temperature and electrolyte concentration gradients in the battery for both types of cooling are reported.

Weight per net power was estimated for both battery systems. The estimate was based on the detailed battery design, on the mathematical simulation of temperature and electrolyte concentration gradients, on detailed performance data, and on the weight and power consumption of a special hydrogen blower.

Figure 7-1 shows schematically the arangement of the fuel cell battery with its auxiliares, in the system using auxiliary cooling. The actual physical picutre of the battery system is given in the design drawings shown in Figures 7-2 through 7-5.

The battery itself is composed of thirty-four individual fuel cells connected electrically in series. The bipolar plates separating the cells (Figure 7-2) not only serve to make this connection but also act as the distributor channels for the hydrogen and oxygen. For the case of auxiliary cooling, the liquid coolant is also introduced through channels in this bipolar plate. The hydrogen and oxygen streams are manifolded through the cells in parallel. This also applies to the coolant stream when auxiliary cooling of the fuel cell is used. To provide room for manifolds and fittings and to increase the mechanical stability of the battery stack, the orientation of the individual cells is alternated through ninety degrees (Figure 7-3).

The battery stack and hydrogen blower are encased in a shell (Figure 7-4) which allows operation of the system at four atmospheres pressure absolute. The gas space inside this shell also serves to manifold the hydrogen which is being fed to the battery. Hydrogen leaving the cells is collected by a manifold and taken outside the shell. A portion of this stream is admitted to the annular space of a finned double pipe heat exchanger and the remaining portion is introduced back into the gas space of the shell on the suction side of the hydrogen blower.

Make-up hydrogen is added to the shell behind the blower. These three streams, the cooled and by-passed streams and the make-up hydrogen, then pass through the hydrogen blower which restores the pressure lost across the system. The cage or fan space of the blower unit fills the entire cross section of the shell.

Additional components of the system include the oxygen inlet and outlet manifolds and the cooling system. In practice the oxygen is dead-ended; however, an occasional purge is used to avoid build up of impurities. For the case in which all heat removal from the cell is by excess gas flow only the single pass of coolant through the inside tube of the condenser is used. When auxiliary cooling is added a portion of the coolant leaving the condenser is added to a loop which recycles coolant through the cell. The coolant flow is shown schematically in Figure 7-1, while the actual piping and pump arrangement is shown in Figure 7-4. A high recycle of the coolant through the cell is used to control closely the coolant temperature (and maintain a small temperature rise in the coolant across the cell). For this latter case an additional pump is required. The power for this pump and the blower must be subtracted from the gross power output of the battery.

7.2 System Operation

A mixture of hydrogen and water vapor enters through the open ends of the hydrogen "in" distribution channels (Figure 7-2). The mixture enters the individual cell hydrogen compartments along the center line of the cell and flows outward. As it travels through the cell a portion of the hydrogen reacts at the electrode surface to yield electrical

power, water, and heat. Part of the heat is removed by vaporization of the water into the hydrogen-water vapor stream. The remaining heat is removed as sensible heat. If no liquid coolant is used all of the additional heat leaves with the hydrogen. Coolant channels can be provided and in this case some of the sensible heat is transferred from the electrode to the hydrogen stream and through to the coolant. Use of coolant minimizes the temperature gradients, and consequently the concentration gradients, in the electrolyte across the cell. In order to avoid condensation of water vapor in the hydrogen stream within the cell, and yet to insure that the coolant can pick up heat, the coolant temperature must obey the restrictions:

$$T_{\text{hydrogen stream dew point}} < T_{\text{coolant}} < T_{\text{hydrogen stream}}$$

To maintain the coolant temperature within these limits a portion of the coolant is recycled through the cell.

The hydrogen and water vapor content of the hydrogen stream, as well as its temperature, change along the path through the cell. The magnitude of these changes and their dependence on operating conditions are treated in section 7.3.

7.3 Mathematical Simulation

7.3.1. Development of the Model

7.3.1.1. Physical Picture and Assumptions

The actual cell design has not been chosen at this point so it will be necessary to utilize a suitable general model which can be easily adapted to different designs. The cell configuration, flow scheme,

and coordinate system chosen for this simulation are shown in Figure 7-6. It is assumed that the hydrogen enters from a channel which distributes gas uniformly along the line x = 0. Similarly, gas is removed unifromly along the edges of the cell at x = $\pm$ a. Equations will be written for one unit of this cell, i.e., from x = 0 to x = a. Other cell configurations, which may contain more inlet and exit channels, can then be built up from this single unit.

An actual fuel cell battery will consist of a number of individual cells in series. At present, a twenty-eight volt unit with approximately thirty cells is envisioned. This simulation will cover a single cell in the midst of such a battery: that is, there will be no transfer of heat to adjoining cells. Referring to Figure 7-6, a single cell is composed of:

a. the hydrogen half of the distributor plate;

b. the hydrogen gas space, containing a screen to distribute the flow and also keep the electrode pressed against the electrolyte membrane;

c. the hydrogen electrode;

d. an asbestos membrane containing the electrolyte, a potassium hydroxide solution;

e. the oxygen electrode;

f. oxygen gas space screen;

g. the oxygen side of the distributor plate.

The sandwich formed by the thin electrolyte membrane and the two thin electrodes comprises a compact unit on which heat and mass balances may be taken. Hereafter in this section, this "sandwich" will be referred to as the matrix(a).

The screen in the gas space touches the electrode and distributor at points which are but a small percent of their total surfaces. The screen will, however, increase the effective heat transfer area of these surfaces in the same manner as a fin or other extended surface. The heat and mass transfer coefficients will be increased by the continual mixing action of the screen. It is assumed that all effects of the screen in the gas space can be accounted for by suitable choice of the transfer coefficients.

It is further assumed that the gasket material which separates the cells is a poor conductor of heat and thus that the matrix and distributor plates are insulated at the edges $y = \pm b$ for all values of x. It will be shown that the heat conduction terms will be small compared with the other heat transfer terms so that this assumption will be justified. Concentration gradients through the thickness of the matrix will be neglected: that is, although such a gradient probably does exist, this analysis will be concerned only with the concentration on the hydrogen side which affects the vapor pressure of the water evaporating into the hydrogen stream. The above assumptions greatly aid in the solution of the performance equations because they result in a problem which is one-dimensional.

(a) Elsewhere in this report "matrix" refers to the electrolyte membrane only.

The assumptions are summarized as follows:

1. Hydrogen enters uniformly along the center line and leaves uniformly at the edges.
2. The matrix, consisting of the two electrodes and the electrolyte membrane, can be treated as a single unit.
3. The effects of the screen in the gas space can be accounted for by suitable mass and heat transfer coefficients.
4. The matrix is insulated against mass and heat transfer at all boundaries.
5. Concentration and temperature gradients through the thickness of the matrix are neglected.
6. The distributor plate is insulated along $y = \pm b$. Thus, there are no gradients normal to the direction of flow.
7. The cell is one of a stack comprising a battery.

7.3.1.2 Derivation of the Performance Equations

The six differential equations which describe the temperature and concentration profiles in the fuel cell were obtained by making energy and mass balances on differential elements across the cell and perpendicular to the direction of hydrogen flow. Energy balances were written for the matrix, the hydrogen stream, and the distribution plate. Mass balances were written for the hydrogen stream, the water in the hydrogen stream and the

water in the matrix. These statements are summarized in the following table which also shows the equation numbering system which will be used in the subsequent derivations.

Energy Balances	Mass Balances	
	Hydrogen	Water
Matrix (Equation 1)	--	Matrix (Equation 2)
Hydrogen Stream (Equation 3)	Hydrogen Stream (Equation 4)	Hydrogen Stream (Equation 5)
Distributor Plate (Equation 6)	--	--

A table defining the nomenclature used in this mathematical analysis is given in the Appendix.

1. Energy balance on the matrix. (Equation 1)

It will be recalled that the matrix refers to the "sandwich" composed of the hydrogen electrode, the membrane filled with electrolyte, and the oxygen electrode. Consider a volume element of this matrix which is t centimeter thick, one centimeter wide in the y direction, and of length Δx. The heat entering this volume element is given by

$$-k_m \frac{dT_m}{dx}\bigg|_x + G_R(I) \cdot \Delta x + c_h(T_h - R)If + c_o(T_o - R)I\frac{f}{2} - c_w(T_m - R)If$$

The first term represents heat in by conduction. The second is the irreversible heat of the reaction. This term depends on the current density, I ma/cm^2, directly in that this sets the rate of reaction and indirectly since the irreversibility is measured by the difference between open cell voltage and the actual cell voltage. The latter is read from a polarization curve which is a function of the operating conditions, particularly current density. R is a reference temperature for the heat of reaction, and the last three terms represent the heat required to heat the hydrogen and oxygen up to this temperature and then leave the liquid water product at the temperature of the matrix. The factor f converts current density to gram moles per hour per square centimeter.

The heat leaving this volume element is given by

$$-k_m \frac{dT_m}{dx}\Bigg|_{x+\Delta x} + h_2\Delta x(T_m - T_h) + h_3\Delta x(T_m - T_o) + k_2 \cdot \Delta x \left[P(N,T_m) - P_{wh}\right] \left[\Delta H_v + c_w(T_m - T_h)\right]$$

The first term is the conduction out at $x + \Delta x$. The second and third terms are convective losses to the hydrogen and oxygen streams. Since the oxygen is dead-ended and the stoichiometrically required oxygen is very small, this latter term will be small compared to the convective losses to the hydrogen stream. Since we are first considering cases with hydrogen flows several times stoichiometric, we will neglect the oxygen convective term for the present. The last term represents the heat lost by vaporizing the water in the matrix at point x and transferring it into the hydrogen stream at T_h and partial pressure of water P_{wh}. $P(N,T_m)$ is the vapor pressure of water at the matrix temperature T_m and over a KOH solution of normality N. Since the oxygen is dead-ended, there is no vaporization on that side of the matrix.

Since we are looking for a steady state solution, the accumulation of heat in this volume element must be zero. Setting the heat out equal to the heat in, dividing by Δx, and taking the limit as Δx approaches zero gives the first differential or performance equation

$$k_m \frac{d^2T_m}{dx^2} = G_R(I) + c_h(T_h - R)If + c_o(T_o - R)I\frac{f}{2} - c_w(T_m - R)If$$

$$- h_2(T_m - T_h) - h_3(T_m - T_o) - k_2 \Delta H_v [P(N,T_m) - P_{wh}]. \qquad (1\text{-}1)$$

The heat of reaction varies slightly with temperature over the range of temperature in a particular battery. Thus, if we take the reference temperature equal to the local matrix temperature, the only approximation involved is that of using a heat of reaction based on an average matrix temperature. Accordingly, our equation becomes

$$k_m \frac{d^2T_m}{dx^2} = G_m(I) - (c_hIf + h_2)(T_m - T_h) - (C_o I\frac{f}{2} + h_3)(T_m - T_o)$$

$$-k_2 [P(N,T_m) - P_{wh}] [\Delta H_v + c_w(T_m - T_h)]. \qquad (1\text{-}2)$$

This equation can be simplified by considering the magnitude of certain of the terms. The heat capacity of hydrogen or oxygen is about 7 cal/g-mole ^{o}C. Current densities have been measured up to 1400 ma/cm^2, but the usual operating range will probably be less than 500 ma/cm^2. The hydrogen consumed is

$$3600\frac{sec}{hr} \cdot \frac{1\text{-g-equivalent}}{96494\ amp.sec} \cdot \frac{1\ g\text{-mole}}{2\ g\text{-equivalent}} \frac{1\ amp}{1000\ ma} \ I\ \frac{ma}{cm^2}$$

$$= 1.865 \times 10^{-5} I\ \frac{g\text{-mole}}{hr \cdot cm^2},$$

thus the conversion factor

$$f = 1.865 \times 10^{-5}\ \frac{g\text{-mole}}{hr \cdot ma}$$

and the quantity

$$\mathbf{c}If = 7 \times 1400 \times 1.865 \times 10^{-5} = 0.18\ \frac{cal}{hr \cdot cm^2 {}^{o}C}$$

as a maximum. For laminar flow between parallel plates the quantity

$$hD_e/k \simeq 8 \tag{1-3}$$

The equivalent diameter for parallel plates is twice the spacing or 0.4 centimeters maximum. For hydrogen, k = 1.82 cal/hr·cm ^{o}C, so that

$$h_{min} = 8\ \frac{1.82}{0.4} = 36\ \frac{cal}{hr \cdot cm^2 {}^{o}C} \tag{1-4}$$

or

$$h \gg \mathbf{c}If. \tag{1-5}$$

In addition, the sensible heat required to raise the vaporized water from the matrix temperature to the stream temperature is small compared with the latent heat, that is

$$\Delta H_v \gg \mathbf{c}_w(T_m - T_h) \tag{1-6}$$

since $T_m - T_h$ will certainly be less than ten degrees. Inequalities (1-5) and (1-6) state that the sensible heat terms involving reactants and product going between the stream and matrix temperatues are negligible.

The performance equation becomes

$$k_m \frac{d^2T_m}{dx^2} = G_m(I) - h_2(T_m - T_h) - k_2 \Delta H_v \left[P(N,T_m) - P_{wh} \right] \tag{1-7}$$

The cell is **symmetric** at x = 0 and the matrix is clamped in place with gaskets so that it is essentially insulated at x = a. Thus we have the boundary conditions

$$\frac{dT_m}{dx} = 0 \qquad x = \begin{cases} o \\ a \end{cases} \tag{1-8}$$

2. Water balance in the matrix **(Equation 2)**

Let N_w be the flux of water in the matrix in the x-direction, **g**-moles/hr·cm^2. Then, considering the same matrix volume element, the water formed is fI and the total entering is given by

$$N_w t \Big|_x + fI\Delta x$$

The water leaving is

$$N_w t \Big|_{x + \Delta x} + k_2 \cdot \Delta x \left[P(N,T_m) - P_{wh} \right]$$

Again, setting these two expressions equal, dividing by Δ x, and taking the limit as Δ x approaches zero gives the second performance equation

$$t \frac{dN_w}{dx} = fI - k_2 \left[P(N,T_m) - P_{wh} \right] \tag{2-1}$$

Now,

$$N_w = - \phi D_w \frac{dX_w}{dx} + X_w(N_w + N_{KOH}) \tag{2-2}$$

At steady state, the molar flux of KOH, N_{KOH}, will equal zero. Thus,

$$N_w = - \frac{\phi D_w}{1 - X_w} \cdot \frac{dX_w}{dx}, \tag{2-3}$$

and the performance equation becomes

$$\frac{t\phi D_w}{1-X_w} \left[\frac{d^2X_w}{dx^2} - \frac{1}{1-X_w} \frac{dX_w}{dx} \right] = fI - k_2 \left[P(N,T_m) - P_{wh} \right] \tag{2-4}$$

with boundary conditions

$$\frac{dX_w}{dx} = 0 \qquad \text{at} \quad x = \begin{cases} o \\ a \end{cases}, \tag{2-5}$$

since the matrix is insulated at the edges and the cell is **symmetric.**

3. Energy balance on the hydrogen stream. **(Equation 3)**

Consider next an element of the hydrogen stream of unit width and of length Δx flowing between the distributor plate and the electrode or matrix surface.

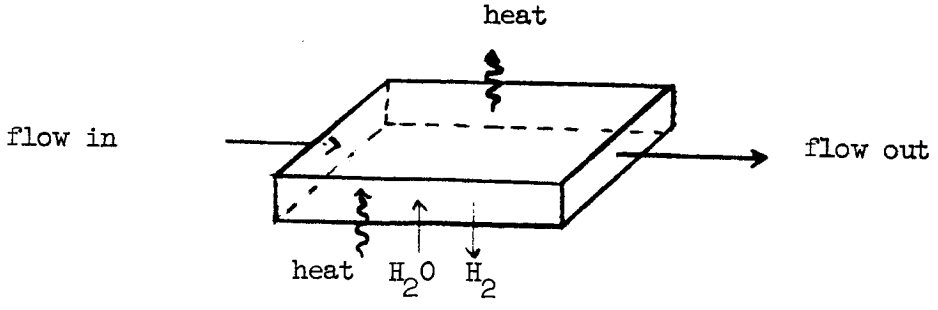

The enthalpy in is given by

$$(W_h H_h + W_{wh} H_w)\Big|_x + h_2 \cdot \Delta x (T_m - T_h) + k_2 \Delta X \left[P(N,T_m) - P_{wh}\right] H_w,$$

where the terms represent the enthalpy in with the flowing stream, the convective transfer from the matrix, and the enthalpy associated with the water evaporating into the stream, respectively. The enthalpy out is

$$(W_h H_h + W_{wh} H_w)\Big|_{x+\Delta x} + h_1 \Delta x (T_h - T_d) + fI \cdot \Delta x \cdot H_h,$$

where the terms represent the enthalpy out with the flowing stream, the convective transfer to the distributor, and the enthalpy out with the reacting hydrogen. Equating these two expressions, dividing by Δx and letting Δx approach zero gives

$$\frac{d(W_h H_h + W_{wh} H_w)}{dx} = h_2(T_m - T_h) - h_1(T_h - T_d) + k_2 \left[P(N,T_m) - P_{wh}\right] H_w - fIH_h \qquad (3\text{-}1)$$

Differentiating the left side gives

$$W_h \frac{dH_h}{dx} + W_{wh} \frac{dH_{wh}}{dx} + H_h \frac{dW_h}{dx} + H_w \frac{dW_{wh}}{dx} \cdot$$

Now,

$$\frac{dH}{dx} = \frac{dH}{dT} \cdot \frac{dT}{dx} = c\frac{dT}{dx} \qquad (3\text{-}2)$$

and from the hydrogen and water balances on the hydrogen stream

$$\frac{dW_h}{dx} = -fI \qquad (4\text{-}2)$$

$$\frac{dW_{wh}}{dx} = k_2 \left[P(N,T_m) - P_{wh}\right]. \qquad (5\text{-}1)$$

Thus the performance equation becomes simply

$$(W_h c_h + W_{wh} c_w) \frac{dT_h}{dx} = h_2(T_m - T_h) - h_1(T_h - T_d). \tag{3-3}$$

The inlet hydrogen stream temperature will be known so that the boundary condition is

$$T_h = T_h(in) \text{ at } x = 0 \tag{3-4}$$

4. Mass balance on the hydrogen stream. **(Equation 4)**

The flow rate of hydrogen per unit width, W_h g-moles/hr·cm, decreases in the direction of flow as the hydrogen is consumed in the electrode reaction. Referring to the same unit volume used in the previous section, a steady-state hydrogen balance may be written

$$W_h \Big|_x = W_h \Big|_{x + \Delta x} + fI \cdot \Delta x \tag{4-1}$$

or

$$\frac{dW_h}{dx} = -fI, \tag{4-2}$$

with the boundary condition

$$W_h = W_h(in) \text{ at } x = 0. \tag{4-3}$$

The solution to this equation is simply

$$W_h = W_h(in) - fIx. \tag{4-4}$$

If we define the flow rate in terms of the parameter

$$F = \frac{\text{hydrogen fed to the cell}}{\text{hydrogen consumed in the reaction}}, \tag{4-5}$$

then the solution becomes

$$W_h = fI(aF - X), \tag{4-6}$$

where a is the length of the cell in the direction of flow. The change in flow rate across the cell becomes negligible for the case when all cooling is done by excess hydrogen flow.

5. Water balance on the hydrogen stream. **(Equation 5)**

The product water from the cell reaction is removed by evaporation into the hydrogen stream. The flow rate of water in this stream, W_{wh} g-moles/hr·cm, increases with x. Considering the same volume element, a water balance gives

$$W_{wh}\Big|_{x+\Delta x} = W_{wh}\Big|_{x} + k_2 \Delta x \left[P(N,T_m) - P_{wh}\right],$$

which yields the differential equation

$$\frac{dW_{wh}}{dx} = k_2 \left[P(N,T_m) - P_{wh}\right]. \tag{5-1}$$

This is a nonlinear equation since the partial pressure of water in the hydrogen stream, P_{wh}, is a function of the water and hydrogen flow rates and the total pressure, π, i.e.,

$$P_{wh} = \frac{W_{wh}}{W_h + W_{wh}}\pi . \tag{5-2}$$

The partial pressure of water in the inlet stream will be known so that the boundary condition for equation (5-1) is

$$W_{wh} = W_{wh}(in) \qquad \text{at } x = 0 \tag{5-3}$$

6. Energy balance on the distributor plate. **(Equation 6)**

Heat can be transferred to the distributor plate from both the hydrogen and oxygen streams. If coolant is being pumped through channels in the distributor plate, there will be transfer to this stream also. This will apply only to those points along x where coolant is flowing. To denote these areas let the function S(x) be defined such that

$$S(x) = \begin{cases} 0 \text{ if there is no coolant flowing at } x \\ 1 \text{ if there is coolant flowing at } x . \end{cases} \tag{6-1}$$

Let l be the distributor thickness and k_d be an effective thermal conductivity in the x direction. Then the heat input to a volume element of unit width, l thickness, and Δ x length is given by:

$$- k_d \cdot l \left.\frac{dT_d}{dx}\right|_x + h_1 \Delta x(T_h - T_d) + h_4 \Delta x(T_o - T_d).$$

The heat out is given by

$$- k_d l \left.\frac{dT_d}{dx}\right|_{x + \Delta x} + S(x)h_c \Delta x(T_d - T_c)$$

This leads to the performance equation

$$k_d l \frac{d^2T_d}{dx} = h_1(T_d - T_h) + h_4(T_d - T_o) + S(x)h_c(T_d - T_c) \qquad (6\text{-}2)$$

There is a restriction on this equation and therefore also on the hydrogen stream equations which must be mentioned at this point. If the coolant which is flowing in the distributor is too cold it will cause the water in the hydrogen stream to condense. This must be avoided from an operational viewpoint, so we introduce the restriction

$$T_d > T_h(\text{sat}), \qquad (6\text{-}3)$$

where $T_h(\text{sat})$ is the dew point of the hydrogen stream.

Since the hydrogen enters from a channel in the distributor at x = 0, a reasonable estimate for the initial condition on T_d is

$$T_d(0) = T_h(\text{in}) \qquad \text{at } x = 0 \qquad (6\text{-}4)$$

The boundary condition at x = a will depend on the final design. For some type of fin extended from the distributor or for a coolant in a channel along the edge, the end condition might read

$$T_d = T_d(a) \qquad \text{at } x = a . \qquad (6\text{-}5)$$

For the cases of gas cooling alone or gas cooling with internal coolant channels the end condition becomes

$$\frac{dT_d}{dx} = 0 \quad \text{at } x = a.$$

7.3.2 Solutions of the Equations

7.3.2.1 Gas Cooling

For this case, the flow rate of hydrogen can be from twenty to one hundred-fifty times the stoichiometric requirement. The heat transfer terms on the oxygen side may be safely neglected. In addition, there is no coolant flowing in the distributor plates so that these terms in the performance equation (6-2) are deleted.

The performance equations developed in the preceding section lend themselves to considerable simplification. As a first approximation to the solution, all the diffusion terms were neglected. This leads to the linear solution described in the next section. These approximations are not as severe as it first appears. The cross sectional area available for diffusion of heat and mass in the matrix is very small. The thickness of this unit is only about 0.06 inches. In its present state of development, the distributor plate is conceived to be of thin sheet metal with comparatively large gas spaces. Thus, its effective thermal conductivity in the x-direction is quite low. An analog computer was used to solve the complete performance equations. The results of this simulation verify the assumptions of negligible water diffusion in the matrix and negligible heat conduction in the distributor plate, and show that the linear solution can correctly be used in the design of a gas-dried gas-cooled fuel cell system.

7.3.2.1.1 Linear Solution

For this solution it is assumed that the diffusion of water and heat in the matrix and the conduction of heat in the distributor plate are negligible. The performance equations become

$$G_m = h_2(T_m - T_h) + \Delta H_v fI \tag{1-9}$$

$$fI = k_2 \left[P(N,T_m) - \frac{W_{wh}}{W_h + W_{wh}} \pi \right] \tag{2-6}$$

$$\frac{dT_h}{dx} = \frac{h_2(T_m - T_h) - h_1(T_h - T_d)}{W_h c_h + W_{wh} c_w} \tag{3-3}$$

$$T_h = T_h(in) \quad \text{at} \quad x = 0 \tag{3-4}$$

$$W_h = W_h(in) - fIx \tag{4-4}$$

$$\frac{dW_{wh}}{dx} = k_2 \left[P(N,T_m) - P_{wh} \right] \tag{5-1}$$

$$W_{wh} = W_{wh}(in) \quad @ \quad x = 0 \tag{5-3}$$

$$0 = h_1(T_d - T_h) \tag{6-2}$$

Combining (5-1) and (2-6) gives

$$\frac{dW_{wh}}{dx} = fI \tag{7-1}$$

and solving, using (5-3),

$$W_{wh} = W_{wh}(in) + fIx \,. \tag{7-2}$$

Combining (1-9), (3-3) and (6-2) yields

$$\frac{dT_h}{dx} = \frac{G_m - \Delta H_v fI}{W_h c_h + W_{wh} c_w} \tag{7-3}$$

and using the results (4-4) and (7-2)

$$\frac{dT_h}{dx} = \frac{G_m - \Delta H_v fI}{\left[W_h(in) c_h + W_{wh}(in) c_w \right] + fI(c_w - c_h)x} \,. \tag{7-4}$$

This equation can be solved, but a further simplification is possible. For gas cooling, the hydrogen rate is at least twenty times stoichiometric, i.e.,

$$W_h(in) > 20a(fI).$$

In order to avoid drying the membrane, a high water content of the hydrogen stream is maintained so that W_{wh} is usually greater than twenty percent of W_h. In addition, $\mathbf{c}_w$ = 8.1 cal/g-mole°C and $\mathbf{c}_h$ = 6.95, but $(\mathbf{c}_w - \mathbf{c}_h) = 1.15$ so that in the range of x under consideration,

$$\left[W_h(in)\mathbf{c}_h + W_{wh}(in)\mathbf{c}_w\right] \gg fI(\mathbf{c}_w - \mathbf{c}_h)x \ . \tag{7-5}$$

Thus, the solution to equation (7-4) is simply

$$T_h = T_h(in) + \frac{G_m - \Delta H_v fI}{W_h(in)\mathbf{c}_h + W_{wh}(in)\mathbf{c}_w} x \ . \tag{7-6}$$

The temperature of the matrix is found by solving Equation (1-9) to give

$$T_m = T_h + \frac{G_m - \Delta H_v fI}{h_2} \ . \tag{7-7}$$

The vapor pressure of water over the matrix, $P(N,T_m)$, is given by a polynomial in N times the vapor pressure of pure water at T_m (Ref. 7)

$$P(N,T_m) = P_N \cdot P_o(T_m) \tag{7-8}$$

$$= \left\{ \begin{array}{ll} 1 - 0.0350N - 0.003415N^2, & N < 6 \\ 1.1836 - 0.0962N + 0.001685N^2, & N > 6 \end{array} \right\} P_o(T_m) \ . \tag{7-9}$$

A curve of P_N versus N is given in Figure 7-7. Solution of (2-6) for $P(N,T_m)$ gives

$$P(N,T_m) = \left(\frac{W_{wh}}{W_{wh} + W_h}\right)\Pi + \frac{fI}{k_2} \ .$$

So the quantity

$$P_N = \frac{\left(\frac{W_{wh}}{W_{wh} + W_h}\right)\Pi + \frac{fI}{k_2}}{P_o(T_m)},$$

can be computed for any point x and then N can be determined by reference to Figure 7-7.

7.3.2.1.2 Analog Solution

To obtain an actual solution, the set of differential performance equations was programmed for an analog computer. The results of this solution verified that the diffusion of water in the matrix and diffusion of heat in the distributor plate were completely negligible. The effect of heat conduction in the matrix was slight. Temperature profiles given by the analog began with a zero slope (dictated by the boundary conditions), but quickly became linear. The temperature of the distributor was equal to the temperature of the hydrogen stream and the temperature difference between the matrix and hydrogen was the same as in the linear solution. For the case of gas-cooling gas-drying, the temperature and concentration profiles are monotonic, with their extreme values at the end conditions. These values are the same in both solutions. The differences in the actual profile are small and it is concluded that the linear solution may be correctly used in design of this fuel cell system.

7.3.2.2 Gas-Liquid Cooling

For this case it is assumed that coolant will be introduced directly into the cell through channels in the bipolar plate. A possible construction for the bipolar plate was shown in Figure 7-2. The larger channels in the center of each half of the plate are the coolant channels. The area available for cooling is limited by the required space for hydrogen and oxygen distribution channels.

Figure 7-8 is a schematic representation of this structure. From the hydrogen inlet (x=0) to the point where the coolant channel begins (x=A2) the performance equations are exactly the same as for the case of gas cooling. Thus we can use the linear solution of the previous case directly. The same holds for the region from the end of the coolant channel (x=A4) to the hydrogen outlet (x=AEND).

In the case of gas cooling the diffusion terms were shown to be negligible due to the very small available cross-sectional areas. In that case, however, the profiles were monotonic and large gradients did not exist. For the present case the same assumptions may be made at all points except the discontinuity points where the coolant channel begins and ends. The inclusion of the diffusion terms, however, makes the solution and subsequent analysis extremely complex. The assumption that diffusion terms may be neglected will again be made. It is justified at this point when the emphasis is on finding satisfactory region of cell operation. This will be a conservative assumption since in all cases diffusion would tend to smooth the profiles slightly.

In the region of coolant flow (x=A2 to x=A4) the parameter S(x) equals one, by definition. The performance equations for this region become:

$$G_m(I) - \Delta H_v \, fI = h_2 (T_m - T_h) + h_3 (T_m - T_o) \qquad (8\text{-}1)$$

for the water in the matrix

$$fI = k_2 \left[P(N,T) - \frac{W_{wh}}{W_{wh} + W_h} \pi \right] \qquad (2\text{-}6)$$

and for the hydrogen stream temperature

$$\frac{dT_h}{d_x} = \frac{h_2 (T_m-T_h) - h (T_h-Td)}{W_h c_h + W_{wh} c_w} \quad . \qquad (3-3)$$

The equations and solutions for the water and hydrogen content of the hydrogen stream remain the same; namely.

$$W_h = W_h(in) - fIx \qquad (4-4)$$

and

$$W_{wh} = W_{wh}(in) + fIx \quad . \qquad (7-2)$$

A modification must be made to the equation for the bipolar or distributor plate temperature. Due to the construction of this plate there are two distributor plate temperatures of interest, one on the hydrogen side, T_{dh}, and one on the oxygen side, T_{do}. (See Figure 7-8).

Since we are neglecting resistance to heat transfer in the metal, we can write for the heat transfered to the coolant from the hydrogen side

$$Q_h = h_1 (T_h-T_{dh}) = h_c (T_{dh}-T_c) \quad . \qquad (8-2)$$

Eliminating the bipolar plate temperature and defining an overall heat transfer coefficient on the hydrogen side, U_h, we have

$$Q_h = h_1 (T_h-T_{dh}) = U_h (T_h-T_c) \qquad (8-3)$$

where

$$U_h = \frac{h_1 h_c}{h_1 + h_c} \quad . \qquad (8-4)$$

The flow rate of oxygen is very small and the oxygen stream is essentially adiabatic. Thus the heat transfered to the coolant from the oxygen side can be written

$$Q_o = h_3 (T_m - T_o) = h_4 (T_o - T_{do}) = h_c (T_{do} - T_c) . \qquad (8\text{-}5)$$

Again forming an overall coefficient on the oxygen side, U_o, we have

$$Q_o = h_3 (T_m - T_o) = U_o (T_m - T_c) , \qquad (8\text{-}6)$$

where

$$\frac{1}{U_o} = \frac{1}{h_3} + \frac{1}{h_4} + \frac{1}{h_c} . \qquad (8\text{-}7)$$

Combining Equation (8-1), (3-3), (8-3), and (8-6) gives, for the hydrogen stream temperature in the range A2 to A4

$$\frac{dT_h}{d_x} = \frac{G(I) - \Delta H_v \, fI - U_h (T_h - T_c) - U_o (T_m - T_c)}{W_h c_h + W_{wh} c_w} . \qquad (8\text{-}8)$$

It can be shown[3I] that due to the high rates of heat transfer which occur in a compact fuel cell, the actual values for the heat transfer coefficients have a relatively small effect on the temperature and normality profiles in the cell. Using this fact, it can be shown that the difference between the hydrogen and matrix temperatures is small (about one-half degree or less) and for the system we are considering, the oxygen overall coefficient is about one-fourth the value of the hydrogen overall coefficient. Thus we can make the simplification,

$$U_o (T_m - T_c) \simeq 0.25 \, U_h (T_h - T_c) . \qquad (8\text{-}9)$$

This approximation will later be shown to have negligible effect. Equation (8-8) becomes

$$\frac{dT_h}{d_x} = \frac{G_m(I) - \Delta H_v f I - 1.25\, U_h\, (T_h - T_c)}{W_h c_h + W_{wh} c_w} \quad . \qquad (8\text{-}10)$$

The solution of (8-10) depends on the temperature distribution of the coolant. The temperature of the coolant, and thus of the hydrogen, will vary in both the x and y directions. The complete solution of this problem is not included in this analysis since maximum and minimum temperatures and normalities do not occur in this region (A2 <x<A4). This can be shown by referring to Figure 7-9. The minimum flow ratio corresponds to the case in which the temperature of the hydrogen rises from the inlet temperature to its maximum value (set by the maximum allowable cell temperature) at the point x = A2. At this point the coolant begins and the hydrogen temperature decreases from x = A2 to x = A4. The extent of this drop depends on the coolant temperature distribution at the y coordinate. From x = A4 to the exit the hydrogen temperature again rises.

One restriction on the coolant temperature is that at the point x = A4 and the coolant outlet, the hydrogen must be cooled sufficiently so that it reaches the exit at maximum cell temperature. The other restriction occurs at X = A4 and the coolant entrance. At this point the coolant temperature must be above the dew point of the hydrogen stream. In general, the external heat balance is more easily accomplished if the exit hydrogen stream is as warm as possible. Thus the first restriction generally sets the coolant temperature. In practice the coolant flow rate in the cell would be adjusted to give an exit hydrogen temperature just under the maximum.

To predict the coolant temperatures we can solve Equation 8-10 for one actual coolant temperature distribution. At the coolant entrance the coolant temperature will be constant. Solution 8-10 gives

$$T_h = T_h(A2) + \frac{G_m(I) - \Delta H_v fI}{1.25\ U_h} - [T_h(A2) - T_c]\left(1-\exp\frac{-1.25U_h\ (x-A2)}{W_h c_h + W_w c_w}\right) . \tag{8-11}$$

Substituting numerical values for the case

$$I = 250\ ma/cm^2,\ E = 0.85 \text{ volts and } F = 45 \text{ yields} \tag{8-12}$$

$$T_h = T_h\ (A2) + [0.92 - T_h(A2) + T_c](1-e^{-6.4x}) .$$

Thus the hydrogen temperature reaches an equilibrium value of 0.92 Centigrade degrees warmer than the coolant temperature soon (about one-half a centimeter) after it enters the region of coolant flow. This agrees with our previous observations that the rates of heat transfer within the cell are very high and thus exact values for the heat transfer coefficients are not necessary for analysis of the cell operation. For now we will neglect the exact shape of the profiles within the liquid cooled region and assume a coolant temperature and flow rate sufficient to ensure that the hydrogen leaving the cell does not exceed its maximum value. We can do this by starting with the maximum temperature at the cell outlet, using the linear solution to calculate the hydrogen temperature at x=A4, and then using the equilibrium approach to find the required coolant temperature. Given the above conditions, the exact profiles and coolant flow rates have a negligible effect on regions of operability.

7.3.3 Restrictions on Cell Operation

In attempting to optimize the performance of this fuel cell system it is desirable to minimize the hydrogen recycle rate since this is a major consumer of parasitic power. Let us consider the lower limits imposed on the variable F, the ratio of hydrogen fed to hydrogen consumed.

Consider first the limits set by the water balance, the maximum cell temperature and the available coolant temperature. The focal point of the analysis will be the outlet of the cell. Consider a cell operating at a given current density and with a specified maximum cell temperature, $T_{max.}$. The maximum temperature occurs at the cell outlet. As a parameter, let us now assume the normality at the cell outlet. We can now calculate the vapor pressure of water over the electrolyte at the outlet

$$P(N,Tm)_{outlet} = P_{N\ out} \cdot Po\ (T_{max}) \ . \qquad (9\text{-}1)$$

Since all the water formed must be evaporated,

$P(N,Tm)$ is related to the water flow rate in the hydrogen stream, W_{wh} by Equation 2-6

$$fI = k_2 \left[\overline{P}(N,Tm) - \frac{W_{wh}}{W_h + W_{wh}} \pi\right] \ . \qquad (9\text{-}2)$$

Applying this equation to conditions at the cell outlet,

$$\frac{W_{wh}(out)}{W_h(out) + W_{wh}(out)} \pi_{out} = P_{wh}(out) = P(N,T_m)_{out} - \frac{fI}{k_2} \quad . \qquad (9\text{-}3)$$

Under the conditions we have assumed we can now calculate $P_{wh}(out)$ using the expression on the right.

Consider next the flow rate terms on the left. The hydrogen rate out is

$$W_h(out) = (F\text{-}1)\ W_h\ (consumed) \qquad (9\text{-}4)$$

since W_h (consumed) is the gram moles hydrogen consumed. (F is the ratio hydrogen in/hydrogen consumed.) This term is also equal to the gram moles of water formed so that

$$W_{wh}(out) = W_{wh}(in) + W_h\ (consumed).$$

Solving for the water entering the cell

$$W_{wh}(in) = W_h\ (consumed) \left[(F\text{-}1) \frac{P_{wh}\ (out)}{\pi(out) - P_w\ (out)} - 1 \right]. \qquad (9\text{-}5)$$

The minimum value of F thus corresponds to the minimum value of $W_{wh}(in)$. The minimum amount of water entering the cell would correspond to the case when the entire steam leaving the cell was passed through the condenser and cooled as much as possible by the available coolant. This would condense out the maximum quantity of water. Let us neglect the fact that in most cases the heat balance would not be satisfied since some of the steam would usually have to by-pass the condenser. If we take a five degree Fahrenheit (2.8°C) approach at the condenser exit we can calculate the water content of the hydrogen stream leaving the condenser. Since the hydrogen at this point is W_h (out) and the water rate is W_{wh} (in)

$$\frac{W_{wh}^{(in)}{}_{min}}{W_h^{(out)}{}_{min} + W_{wh}^{(in)}{}_{min}} \pi_{condenser} = Po\ (T_{c\ available} + 2.8). \qquad (9\text{-}6)$$

Solving for $W_{wh}(in)$

$$W_{wh}(in)_{min} = W_h(out) \frac{Po\ (T_{c_{available}} + 2.8)}{\pi_{condenser} - Po\ (T_{c_{available}} + 2.8)} \quad (9\text{-}7)$$

Setting the fraction on the right side equal to B and rewriting in terms of F

$$W_{wh}(in)_{min} = W_h(consumed)\ (F\text{-}1)\ B_{min} \quad (9\text{-}8)$$

The minimum water flow rate can now be eliminated between equations (9-5) and (9-8) to give

$$W_h(consumed)\ (F_{min}\text{-}1)\ B = W_h(consumed) \left[(F_{min}\text{-}1) \frac{P_{w(out)}}{\pi_{(out)} - P_{wh(out)}} - 1 \right] \quad (9\text{-}9)$$

Solving for F_{min} gives

$$F_{min} = 1 + \frac{1}{\frac{P_{w(out)}}{\pi_{(out)} - P_{w_{(out)}}} - B} \quad (9\text{-}10)$$

Note that the hydrogen consumed, $W_h(consumed)$, is cancelled in going from Equation (9-9) to (9-10). If we now neglect the effect of current density given by Equation (9-3), then the minimum flow ratios calculated by Equation (9-10) are independent of current density. This is perhaps more obvious if we consider that we are dealing with the flow ratio, F, and not an absolute flow rate. The last assumption is quite valid since in Equation (9-3) the term involving current density, fI/k_2 equals 0.023 psi for I=250 ma/cm^2 and 0.037 for I=400 whereas the term P(N,Tm) is of the order 3 to 10 psia.

A set of curves for F_{min} as a function of outlet normality at 58 psig for two available coolant temperatures (60°C and 40°C) and for three maximum cell temperatures (90, 100, 110°C) is shown in Figures 7-10 and 7-11. Minimum flow ratio decreases with decreasing coolant temperature, increasing maximum cell temperature, and decreasing outlet normality. For a given coolant temperature and a given maximum cell temperature there is a maximum outlet normality which can be attained.

It will be recalled that, aside from the coolant approach in the condenser, no mention of heat transfer methods or restriction was made. Thus the curves in Figures 7-9 and 7-10 represent limiting flow ratios for both gas cooling and combined gas and auxiliary cooling.

7.3.4 Regions of Battery Operation

The previous section has dealt with restrictions imposed by the water balance on cell operation for gas cooling or gas-liquid cooling. The results of that discussion have been combined with solutions to the performance equations to define the possible regions of cell operation for both cases.

7.3.4.1 Gas Cooling

The performance equations for gas cooling were solved with the aid of the computer for a large number of cases under a variety of operating conditions. For each case the current density, cell voltage, maximum cell temperature, outlet normality and flow ratio were specified. Total pressure for all cases was 58 psia. The program then calculated the normality profile in the cell and the temperatures and flow rates throughout the system. These results showed that the first restriction which was encountered as the flow ratio decreased was an inlet normality below the allowable minimum(3N). The results of these runs are presented in Figures 7-1
7-13, and 7-14 as a plot of inlet normality versus flow ratio and outlet norma

The parameters differentiating these figures are:

Figure number	7-12	7-13	7-14
Current density, ma/cm^2	250	400	400
Cell Voltage	0.85	0.8	0.8
Maximum cell temperature, °C	110	110	100

On each of these figures a curve has been drawn corresponding to an inlet normality of 3.0 and thus also indicating the minimum allowable flow ratios. The possible regions of cell operation are then above this curve and to the left of the curve set by the water balance restrictions. The inlet normality for other conditions within this region may be estimated by drawing lines of constant inlet normality such as those shown for an inlet normality of 6.0.

7.3.4.2 Gas-Liquid Cooling

Using the methods outlined in section 7.3.2.2 the performance equations were solved to give the operating conditions and profiles for six cases. As summarized in Table 7-1, these involve a maximum cell temperature of 100°C and current densities of 250 and 400 ma/cm^2. The results, plotted as inlet normalities as a function of outlet normality and flow ratios, are shown in Figure 7-15. More cases would be needed to define completely the region of operability.

7.3.4.3. Comparison of Gas and Gas-Liquid Cooling

Operating regions for gas and auxiliary cooling have been summarized in Figures 7-12 through 7-15. Although runs have not been made under all possible operating conditions these figures show the

effect of type of cooling, maximum cell temperature, flow ratio, normality level and current density. Based on these figures reasonable estimates of operating regions may be made over a wide range of these variables.

Normality ranges and approximate normality profiles are shown in Figure 7-16 as a function of flow ratio and type of cooling. This figure allows a direct comparison of the flow ratios required by gas and auxiliary cooling under similar conditions. For example, at a current density of 250 ma/cm^2 the flow ratio required to give a normality range of 4 units (5 to 9 for gas cooling, 6 to 10 for auxiliary) is F = 150 for gas cooling and F = 45 for auxiliary cooling. The curves are for a primary coolant temperature of 60°C. A lower coolant temperature would permit operation at higher normalities as can be seen from Figures 7-10 and 7-11.

7.4 Weight Per Net Power

A comparison of the two cooling systems on the basis of estimated weight per net power for a 2 kw battery operating at 250 or 400 ma/cm^2 is shown in Table 7-2. Stable operation has been demonstrated in single cells operating at the lower current density but not as yet at the higher (Section 5.3 and 6.3). The flow ratios shown are those indicated to be reasonable by the mathematical simulation. A maximum cell outlet temperature of 100°C and a system pressure of 58 psia were considered.

For both cooling systems the estimated weight per net power is close to 50 lb/kw. Each system is lighter by 4 lb/kw when operated at 400 ma/cm^2 rather than at 250 ma/cm^2 because of a smaller battery cross section. No accompanying decrease in the weight of the shell casing is indicated since the shell casing size is considered to be limited by the arrangement of auxiliary equipment and pumping.

At both current densities, the estimated weight per net power is nearly the same for both types of cooling. While gas-liquid cooling requires a much lower recycle rate and hence a lighter blower than does gas cooling, this weight-saving is largely offset by the weight of the liquid coolant and its pump. The estimated parasitic power is nearly the same for both cases because (1) the greater parasitic power of the hydrogen blower required by gas cooling is mostly compensated for by the parasitic power of the coolant pump (60 watts), and (2) the parasitic power for pumping gas or gas plus coolant is estimated to be only 35% of the total parasitic power, the remainder being consumed by the static DC/AC inverter. The low parasitic power for gas circulation arises from the low estimated pressure drop for the overall system, including the battery and the condenser. The pressure drop through the battery alone, as estimated from the standard orifice equation combined with pressure drop data obtained in the 6" cell (Section 6.4) was only 0.01-0.15 psi at the flow ratios and current densities considered (Figure 7-17).

The differences in weight per net power between the two cooling methods are not large enough to exclude one at this point. However, the gas-liquid cooled system will be more advantageous if the system pressure drop should be substantially higher than anticipated or if total pressures substantially below 58 psia are considered. Furthermore, as indicated in Figure (7-16), gas-liquid cooling will permit operation at higher average electrolyte concentrations and with lower concentration gradients, factors which should improve performance. If electrode erosion by flowing gas should prove to be significant, the lower recycle rates required by gas-liquid cooling must be considered another potential advantage. Lastly,

although control questions have not been investigated at this time, the extra degree of freedom inherent in gas-liquid cooling should result in closer control of temperature and electrolyte concentration than can be achieved by gas cooling.

TABLE 7-1

Operation of Fuel Cell Battery with Auxiliary Cooling

Current Density, ma/cm²	250			400		
Cell Voltage	0.85			0.8		
Total Pressure, psia	58			58		
Maximum Cell Temperature, °C	100			100		
Available Coolant, °C	60			60		
Outlet Normality	9			9		
Hydrogen Flow Ratio	60	45	30	60	45	30
Maximum Normality (x = Δ2)	9.7	9.9	10.3	9.7	9.9	10.3
Inlet (Minimum) Normality	6.9	6.0	3.9	6.3	5.2	1.8
Inlet Temperature, °C	88.4	84.6	76.8	86.8	82.5	73.7

TABLE 7-2

Battery System-Weight/Net Power

Cell Cooling Medium	Gas	Gas	Liquid + Gas	Liquid + Gas
Total Voltage	28	28	28	28
I, ma/cm^2	250	400	250	400
Electrode Dimensions (inches)	7 x 7	5.5 x 5.5	7 x 7	5.5 x 5.5
E, Volts/Cell	.85	.80	.85	.80
No. of Cells	33	35	33	35
H_2 Ratio	150	150	45	45
Blower Amp. Pump Efficiency (%)	25	25	25	25
Gross KW	2.24	2.22	2.24	2.22
Parasitic KW	.24	.22	.24	.22
New KW	2.00	2.00	2.00	2.00
Weight, Lbs.				
Battery	25.3	17.5	25.0	17.3
Shell Casing	21.4	21.4	21.4	21.4
Exchanger	8.1	8.1	8.1	8.1
Cyclone	4.6	4.6	4.6	4.6
Braces, Piping Etc.	3.3	3.3	5.0	5.0
DC-AC Inverter	14.0	14.0	14.0	14.0
Valves	1.5	1.5	2.0	2.0
Blower (Inc. Motor)	25.0	25.0	10.0	10.0
Pump	-		5.0	5.0
Liquid Coolant	.4	.4	6.0	6.0
Total Weight, Lbs.	103.6	95.8	101.1	93.4
Ratio Weight/Net Power Lbs./KW	51.8	47.9	50.6	46.7

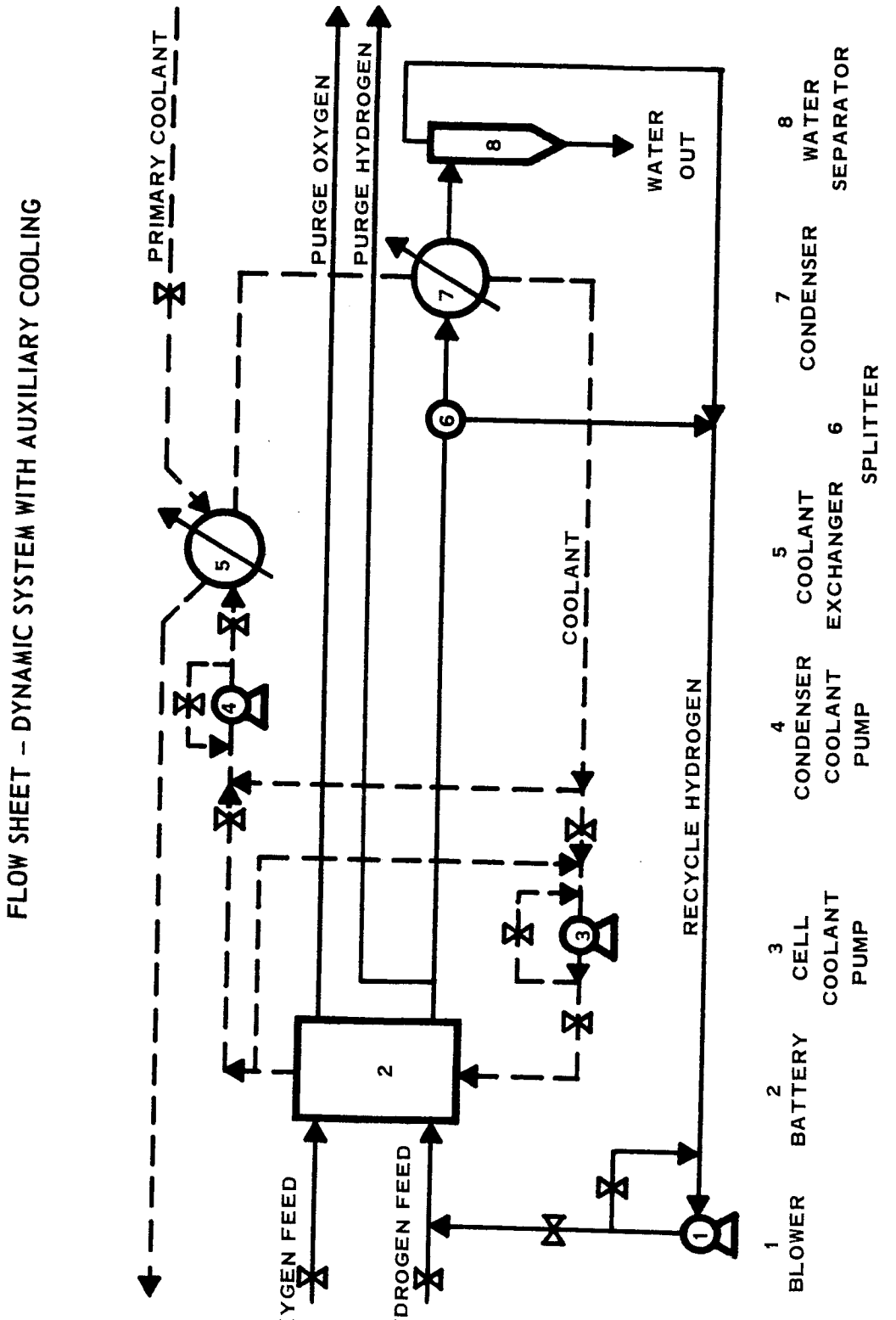
FLOW SHEET – DYNAMIC SYSTEM WITH AUXILIARY COOLING
PRIMARY COOLANT
PURGE OXYGEN
PURGE HYDROGEN
WATER OUT
OXYGEN FEED
HYDROGEN FEED
COOLANT
RECYCLE HYDROGEN
1 BLOWER
2 BATTERY
3 CELL COOLANT PUMP
4 CONDENSER COOLANT PUMP
5 COOLANT EXCHANGER
6 SPLITTER
7 CONDENSER
8 WATER SEPARATOR

FIGURE 7-1

2 KW BATTERY
BIPOLAR CELL PLATE
LIQUID & GAS COOLING DESIGN

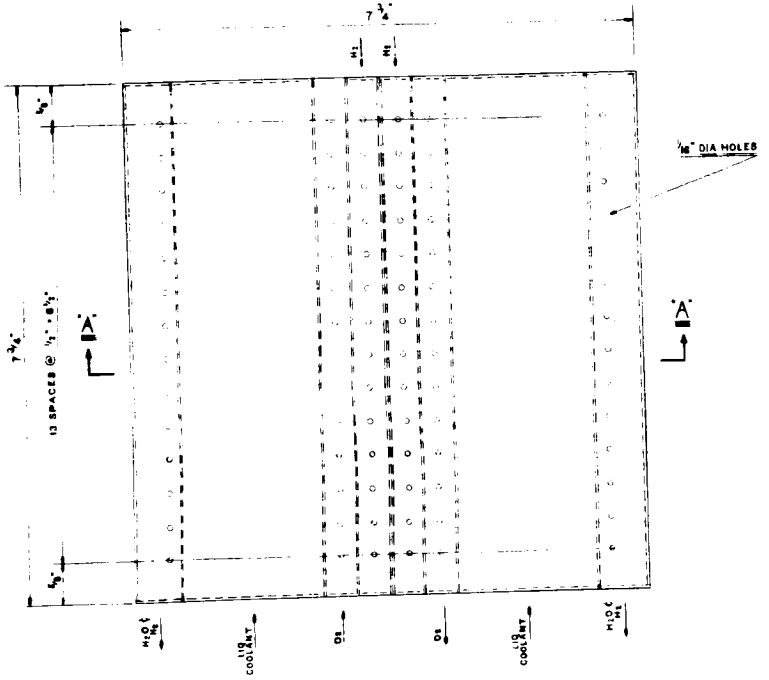

PLAN VIEW
FULL SIZE

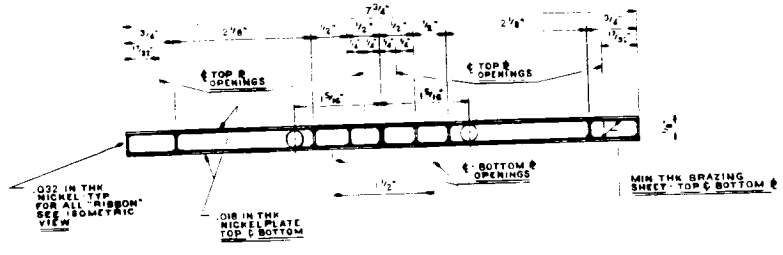

SECTION "A-A"
NOT TO SCALE VERTICALLY

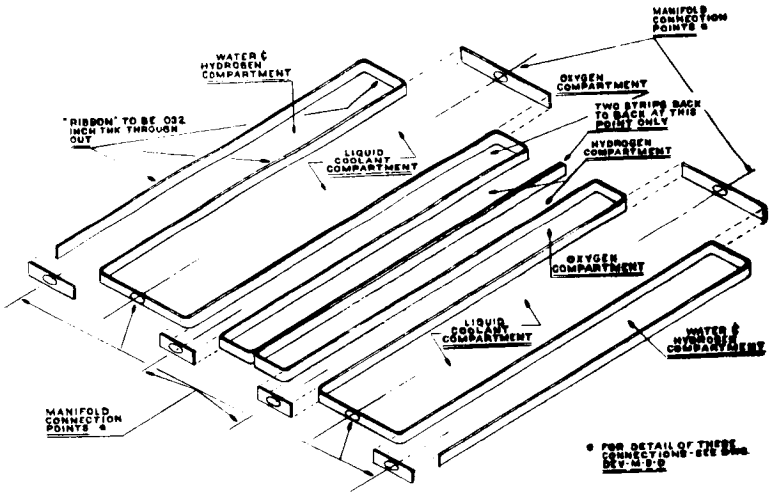

VIEW SHOWING SUGGESTED ARRANGEMENT OF "RIBBON" BETWEEN PLATES

NOTE:

BRAZING TO BE CONTINUOUS BETWEEN OXYGEN & HYDROGEN COMPARTMENTS

VENDOR TO SUPPLY DETAILED NOTES & DRAWINGS

FIGURE 7-2

2 KW BATTERY
BATTERY & PRESSURE CASING ASSEMBLY
LIQUID & GAS COOLING DESIGN

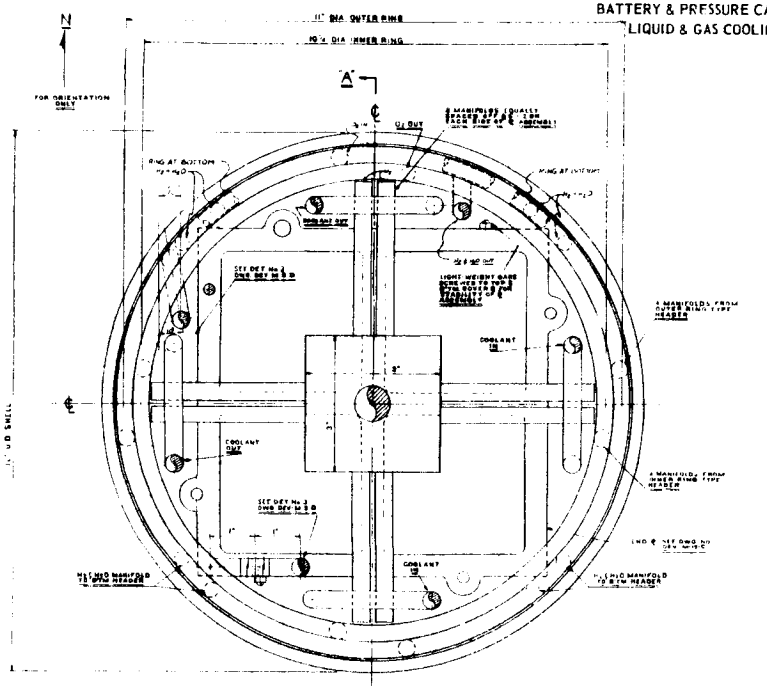

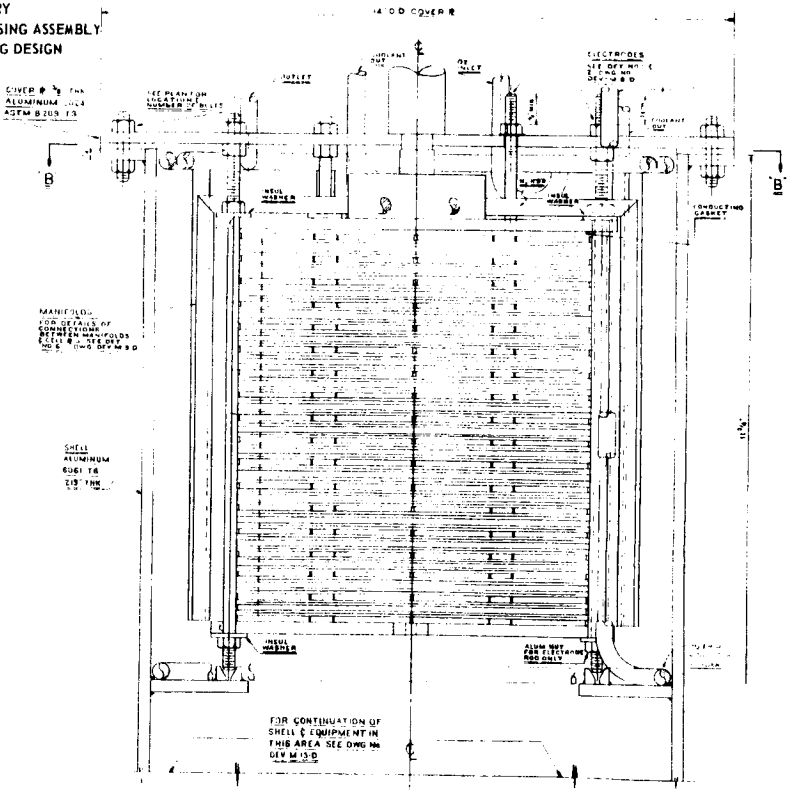

Reference Drawings

Bipolar Cells Plate & Details	Dev M 11-C
End Plate & Gasketing Details	Dev M 7-C
Assembly Details	Dev M 9-D
General Assembly Layout	Dev M 13-D

FIGURE 7-3

2 KW BATTERY
GENERAL ASSEMBLY
LIQUID & GAS COOLING DESIGN

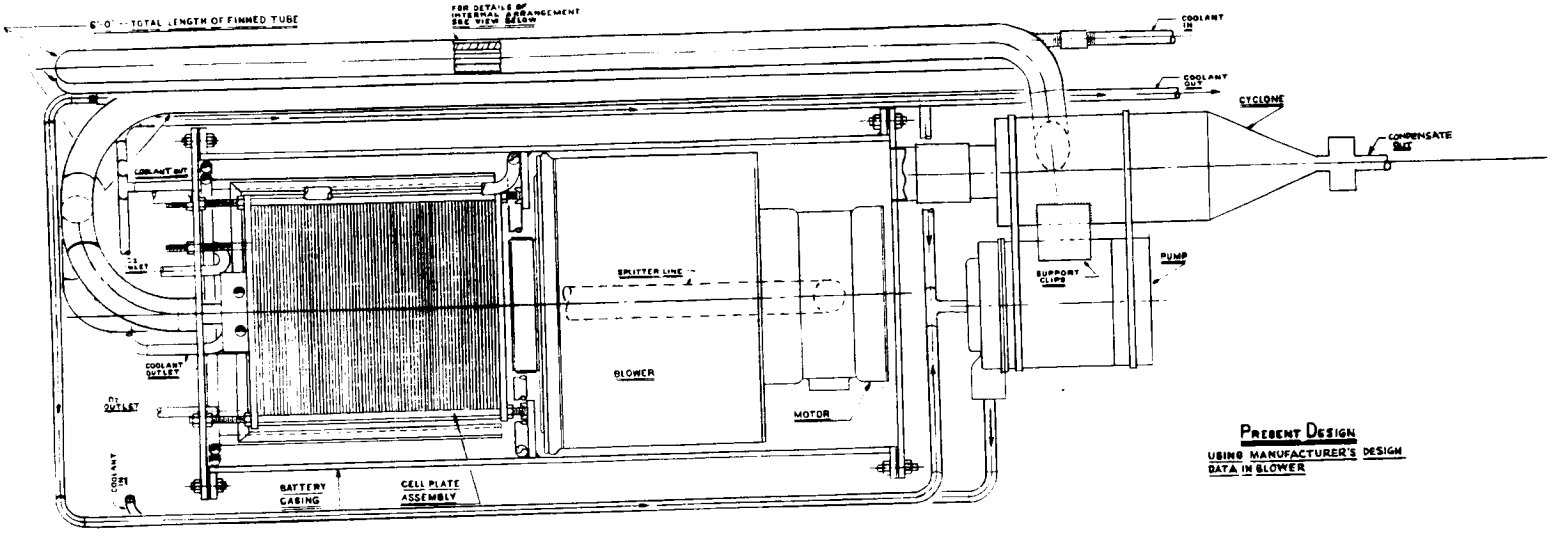

PRESENT DESIGN
USING MANUFACTURER'S DESIGN DATA IN BLOWER

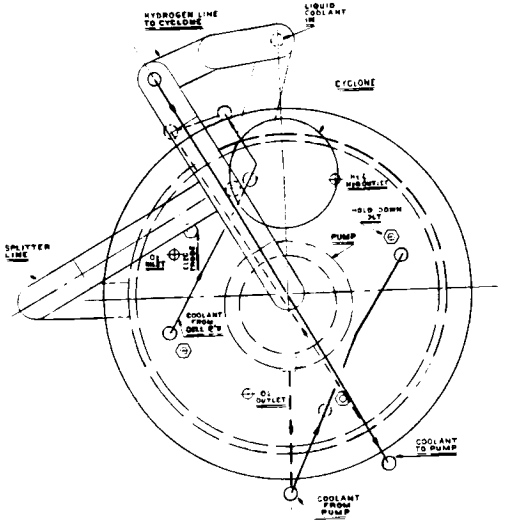

PLAN

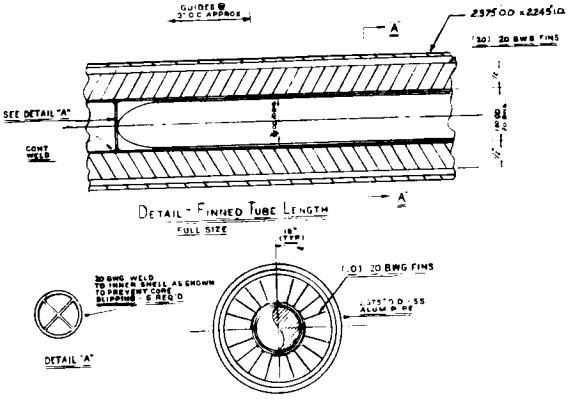

SECTION A-A

DETAIL - FINNED TUBE LENGTH
FULL SIZE

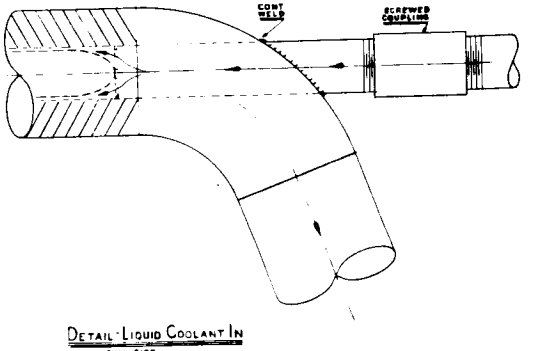

DETAIL - LIQUID COOLANT IN
FULL SIZE

FIGURE 7-4

2 KW BATTERY
END PLATE & GASKETING DETAILS

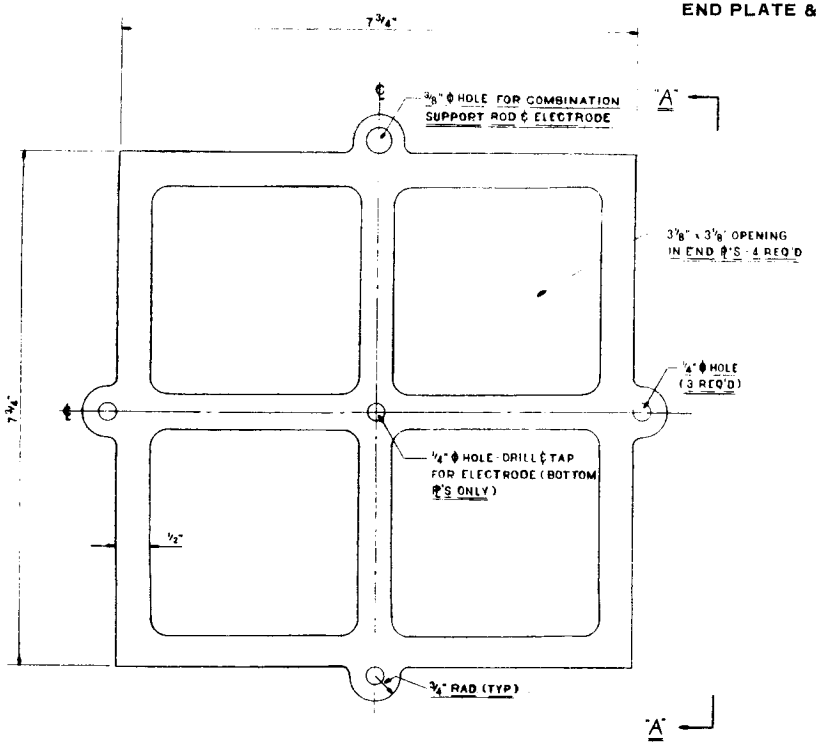

PLAN VIEW
FULL SIZE

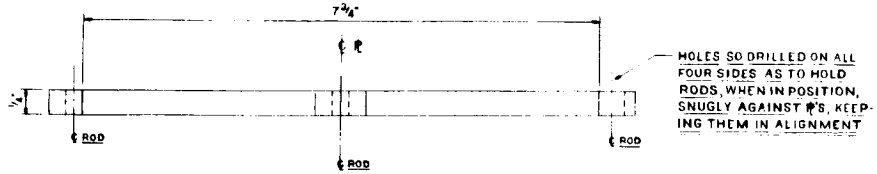

SECTION "A-A"
FULL SIZE

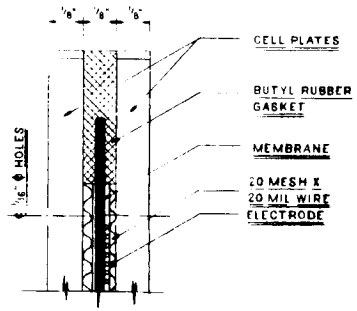

ENLARGED DETAIL OF GASKET & MEMBRANE

FIGURE 7-5

CELL CONFIGURATION FOR MATHEMATICAL MODEL

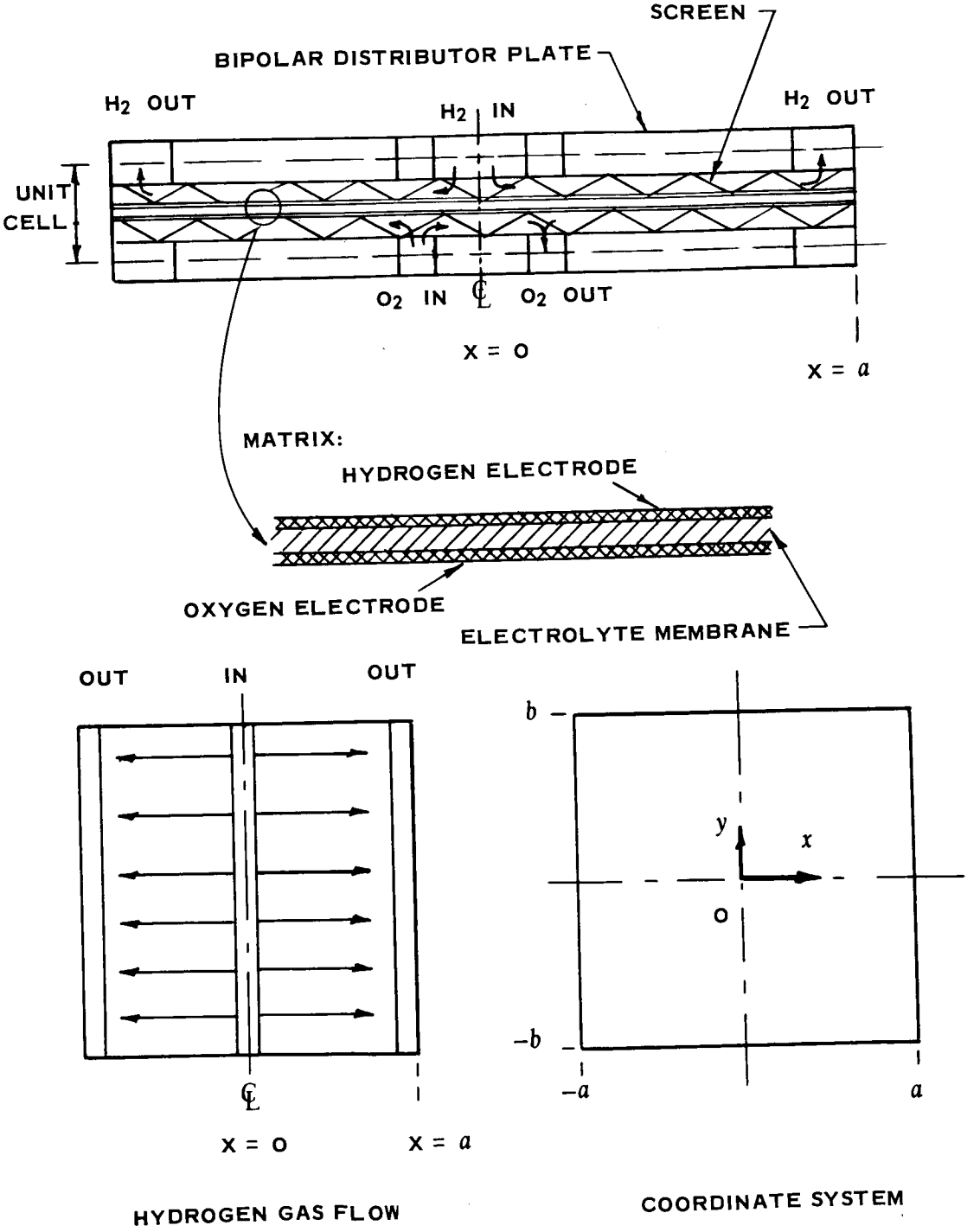

FIGURE 7-6

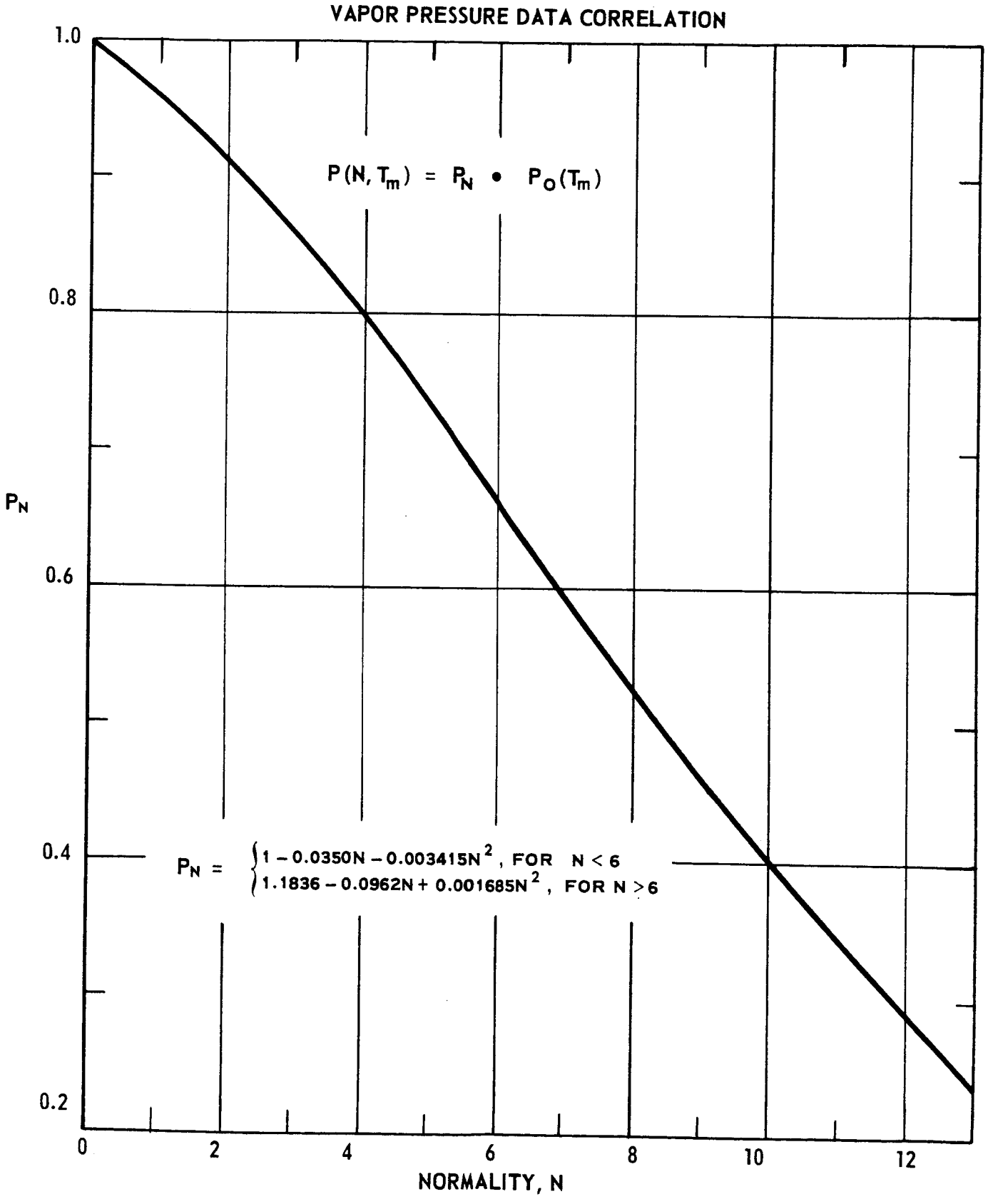
VAPOR PRESSURE DATA CORRELATION
$P(N, T_m) = P_N \bullet P_O(T_m)$
$P_N = \begin{cases} 1 - 0.0350N - 0.003415N^2, & \text{FOR } N < 6 \\ 1.1836 - 0.0962N + 0.001685N^2, & \text{FOR } N > 6 \end{cases}$
P_N
1.0
0.8
0.6
0.4
0.2
0
2
4
6
8
10
12
NORMALITY, N

FIGURE 7-7

CELL CONFIGURATION – AUXILIARY COOLING

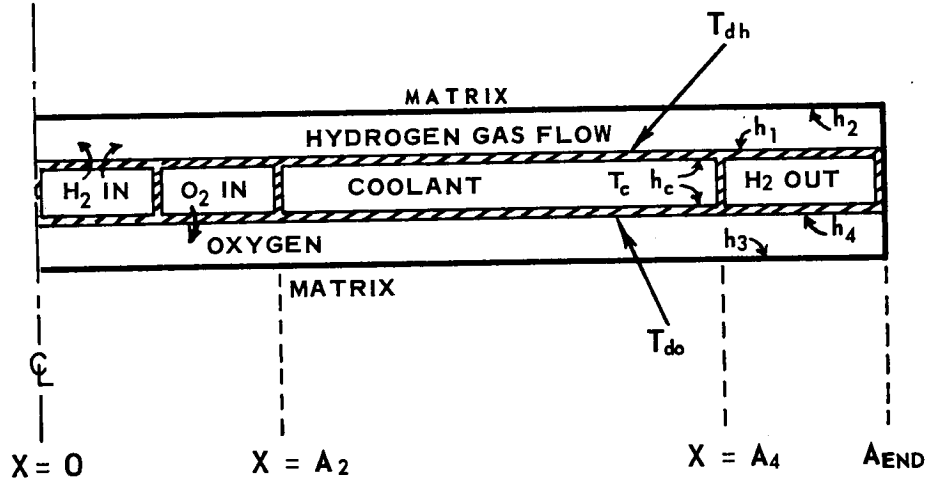

FIGURE 7–8

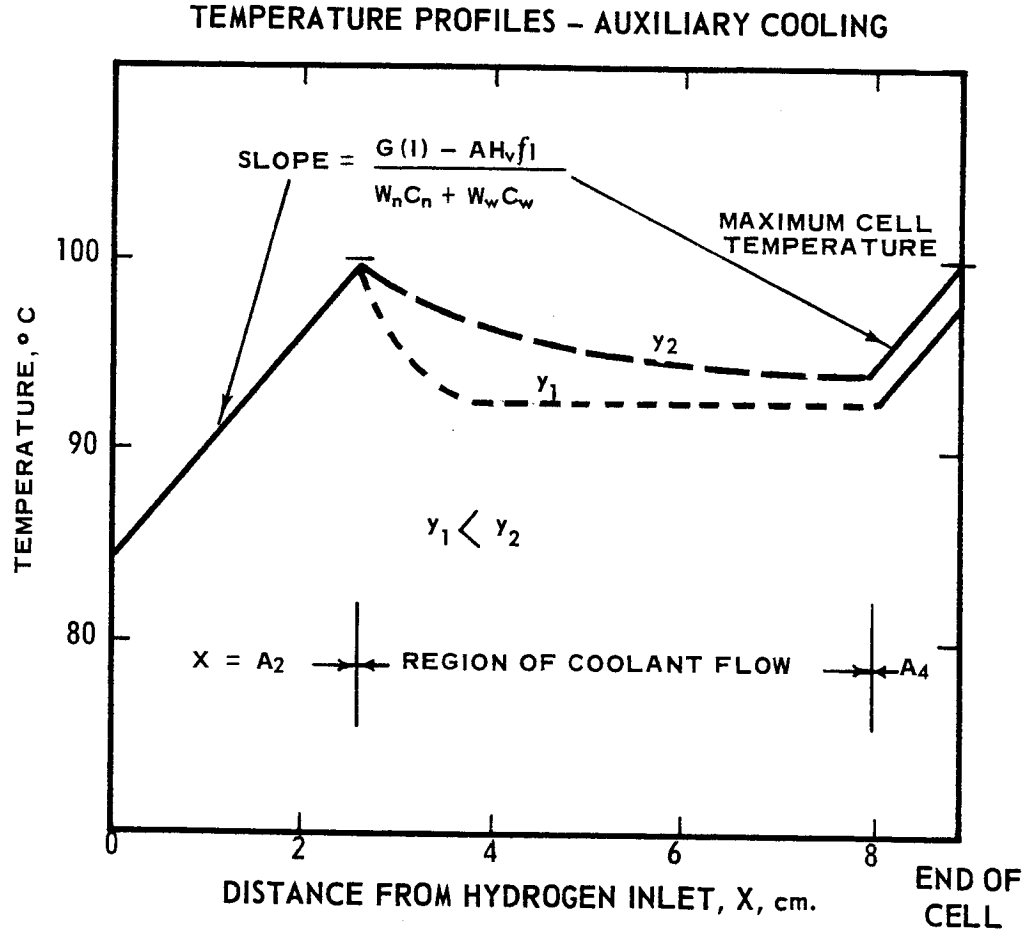
TEMPERATURE PROFILES – AUXILIARY COOLING
SLOPE = G(l) – AHvfl / WnCn + WwCw
MAXIMUM CELL TEMPERATURE
y2
y1
y1 < y2
X = A2
REGION OF COOLANT FLOW
A4
TEMPERATURE, °C
100
90
80
0
2
4
6
8
END OF CELL
DISTANCE FROM HYDROGEN INLET, X, cm.

FIGURE 7–9

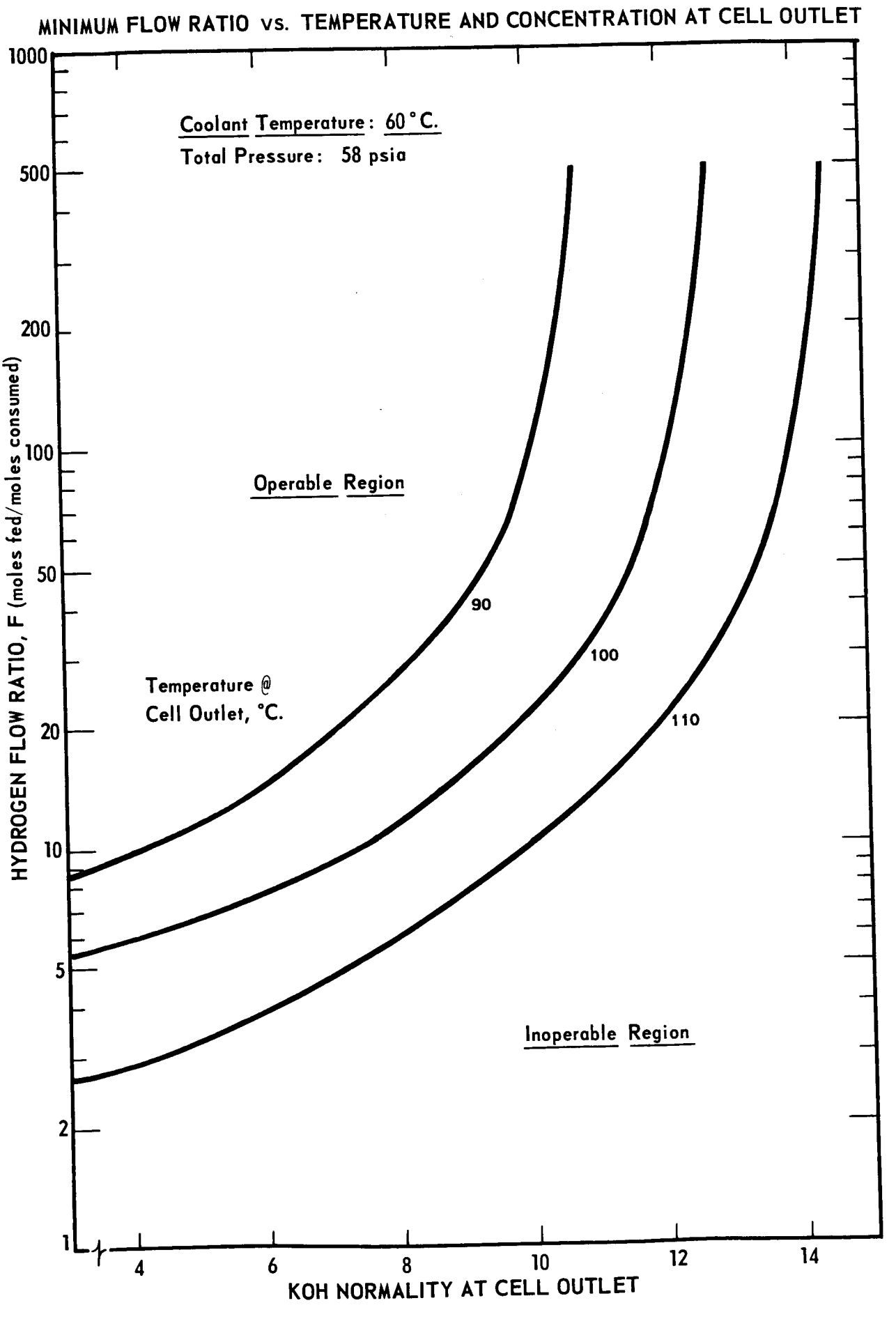
MINIMUM FLOW RATIO vs. TEMPERATURE AND CONCENTRATION AT CELL OUTLET
Coolant Temperature: 60°C.
Total Pressure: 58 psia
Operable Region
Inoperable Region
Temperature @
Cell Outlet, °C.
90
100
110
HYDROGEN FLOW RATIO, F (moles fed/moles consumed)
1000
500
200
100
50
20
10
5
2
1
4
6
8
10
12
14
KOH NORMALITY AT CELL OUTLET

FIGURE 7-10

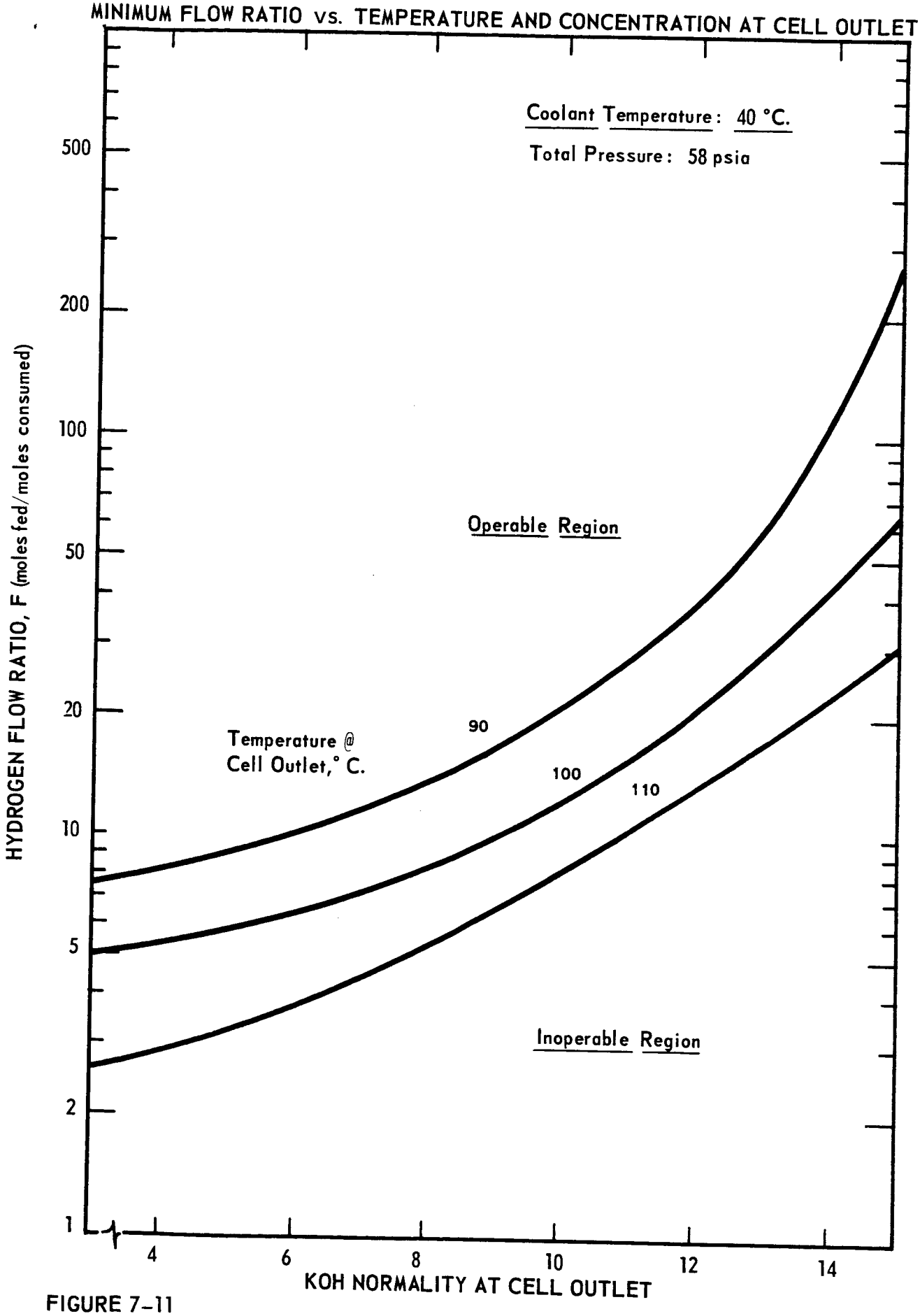
MINIMUM FLOW RATIO vs. TEMPERATURE AND CONCENTRATION AT CELL OUTLET
Coolant Temperature: 40 °C.
Total Pressure: 58 psia
Operable Region
Inoperable Region
Temperature @ Cell Outlet, ° C.
90
100
110
HYDROGEN FLOW RATIO, F (moles fed/moles consumed)
500
200
100
50
20
10
5
2
1
4
6
8
10
12
14
KOH NORMALITY AT CELL OUTLET

FIGURE 7-11

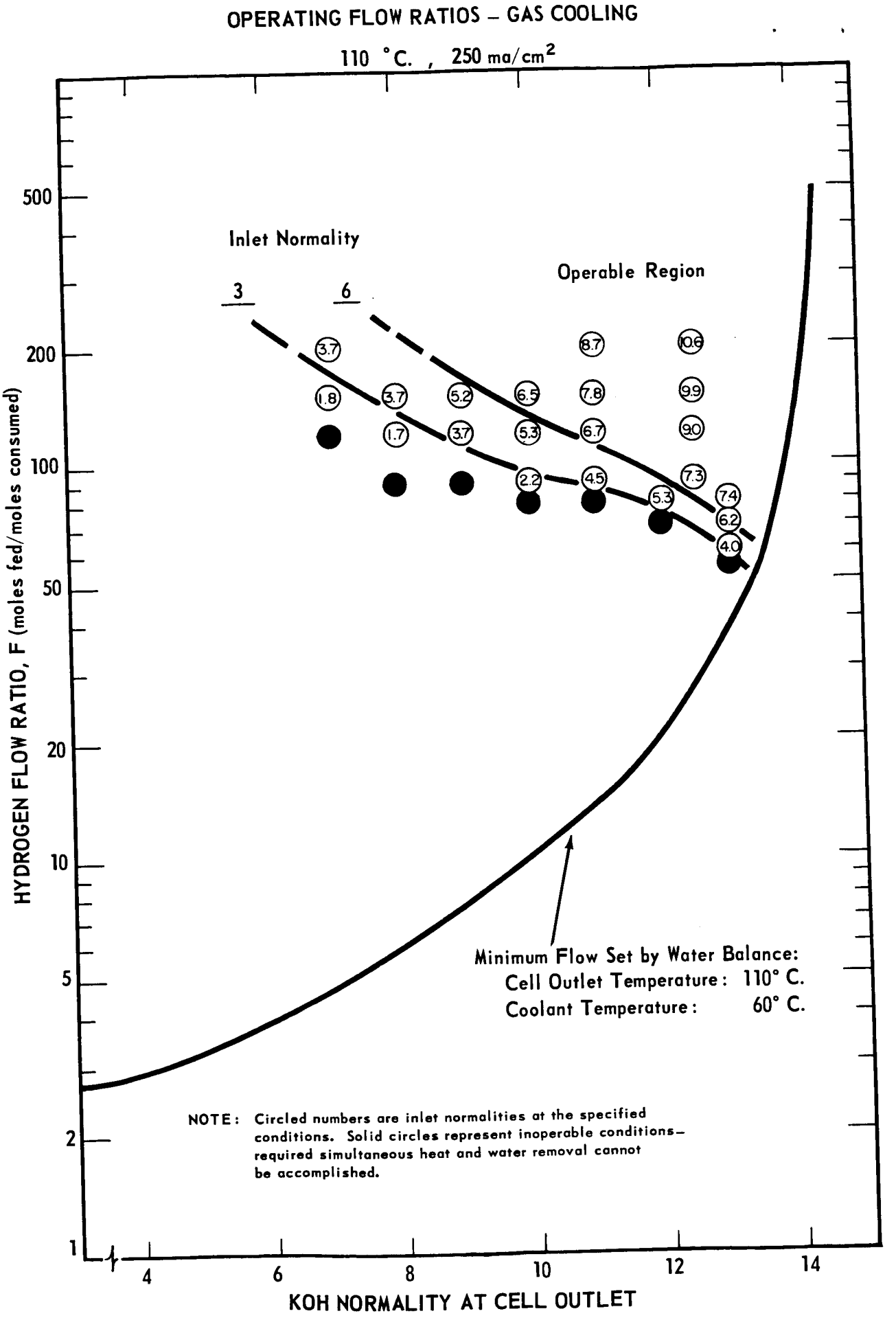
OPERATING FLOW RATIOS – GAS COOLING
110 °C. , 250 ma/cm²
Inlet Normality
3
6
Operable Region
3.7
1.8
3.7
1.7
5.2
3.7
6.5
5.3
8.7
6.7
7.8
10.6
9.9
9.0
7.3
2.2
4.5
5.3
7.4
6.2
4.0
Minimum Flow Set by Water Balance:
Cell Outlet Temperature: 110° C.
Coolant Temperature: 60° C.
NOTE: Circled numbers are inlet normalities at the specified conditions. Solid circles represent inoperable conditions– required simultaneous heat and water removal cannot be accomplished.
HYDROGEN FLOW RATIO, F (moles fed/moles consumed)
500
200
100
50
20
10
5
2
1
4
6
8
10
12
14
KOH NORMALITY AT CELL OUTLET

FIGURE 7–12

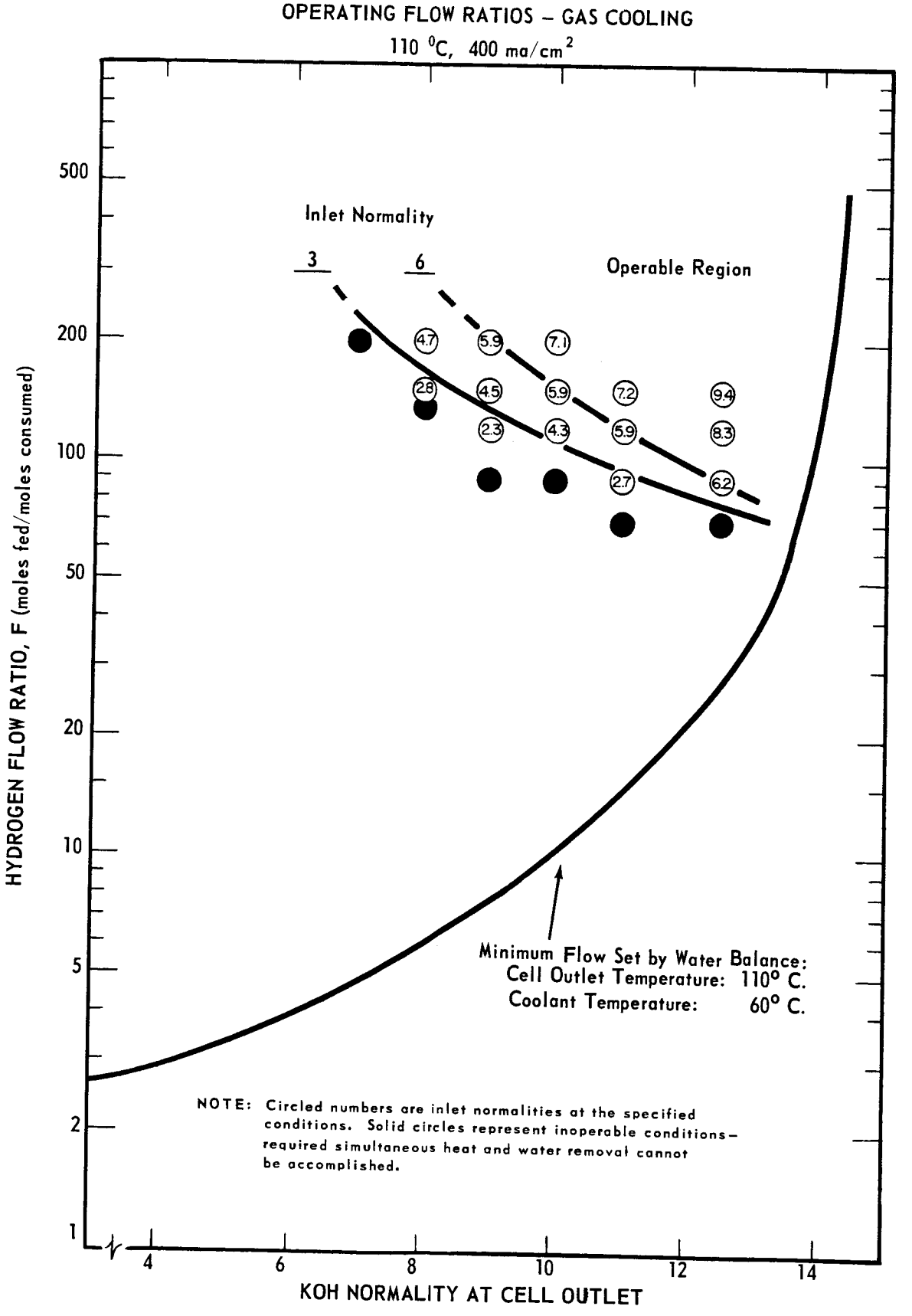
OPERATING FLOW RATIOS – GAS COOLING
110 °C, 400 ma/cm²
HYDROGEN FLOW RATIO, F (moles fed/moles consumed)
500
200
100
50
20
10
5
2
1
Inlet Normality
3
6
Operable Region
4.7
5.9
7.1
2.8
4.5
5.9
7.2
9.4
2.3
4.3
5.9
8.3
2.7
6.2
Minimum Flow Set by Water Balance:
Cell Outlet Temperature: 110° C.
Coolant Temperature: 60° C.
NOTE: Circled numbers are inlet normalities at the specified conditions. Solid circles represent inoperable conditions– required simultaneous heat and water removal cannot be accomplished.
4
6
8
10
12
14
KOH NORMALITY AT CELL OUTLET

FIGURE 7–13

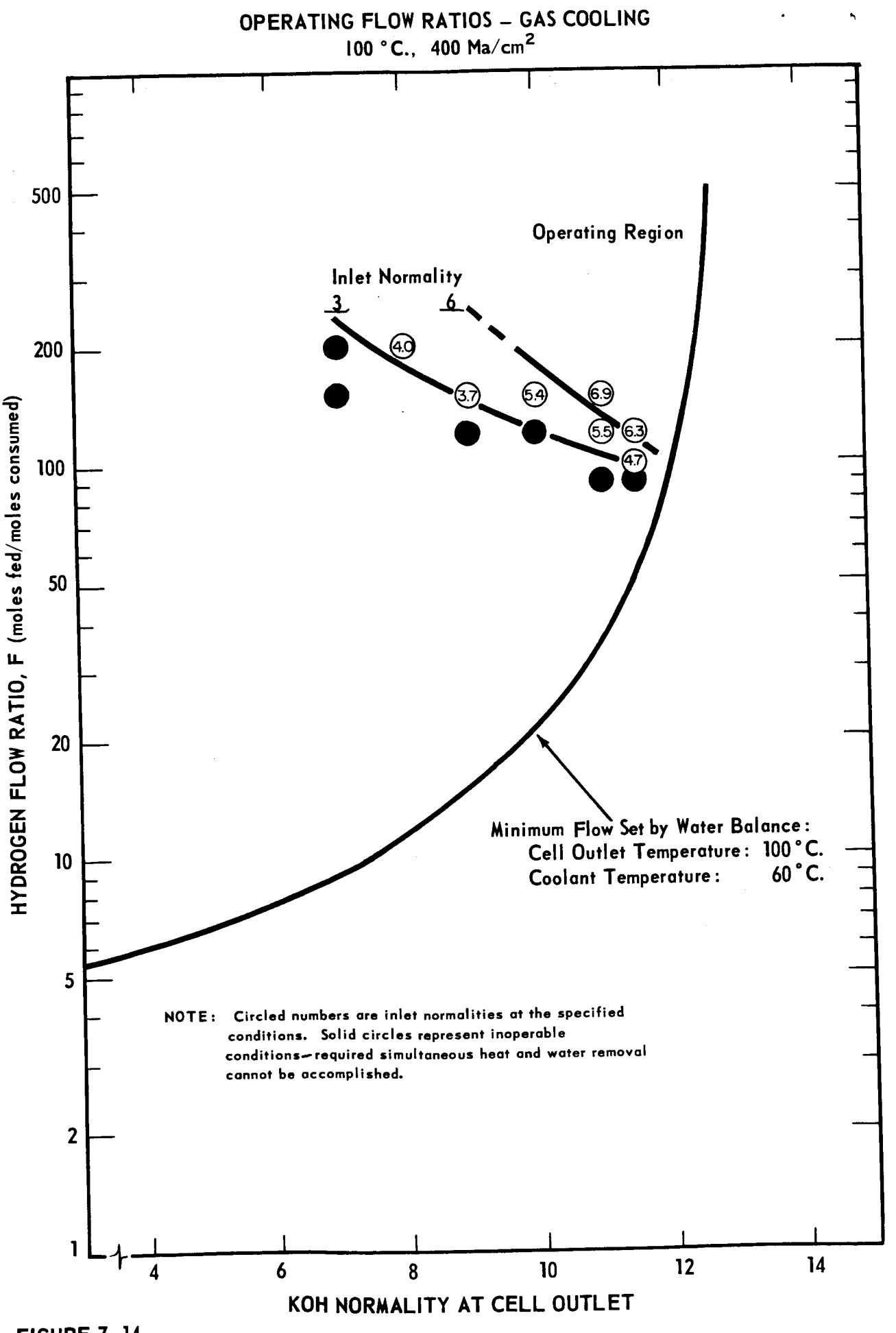
OPERATING FLOW RATIOS – GAS COOLING
100 °C., 400 Ma/cm²
HYDROGEN FLOW RATIO, F (moles fed/moles consumed)
500
200
100
50
20
10
5
2
1
Operating Region
Inlet Normality
3
6
4.0
3.7
5.4
6.9
5.5
6.3
4.7
Minimum Flow Set by Water Balance:
Cell Outlet Temperature: 100 °C.
Coolant Temperature: 60 °C.
NOTE: Circled numbers are inlet normalities at the specified conditions. Solid circles represent inoperable conditions—required simultaneous heat and water removal cannot be accomplished.
4
6
8
10
12
14
KOH NORMALITY AT CELL OUTLET

FIGURE 7-14

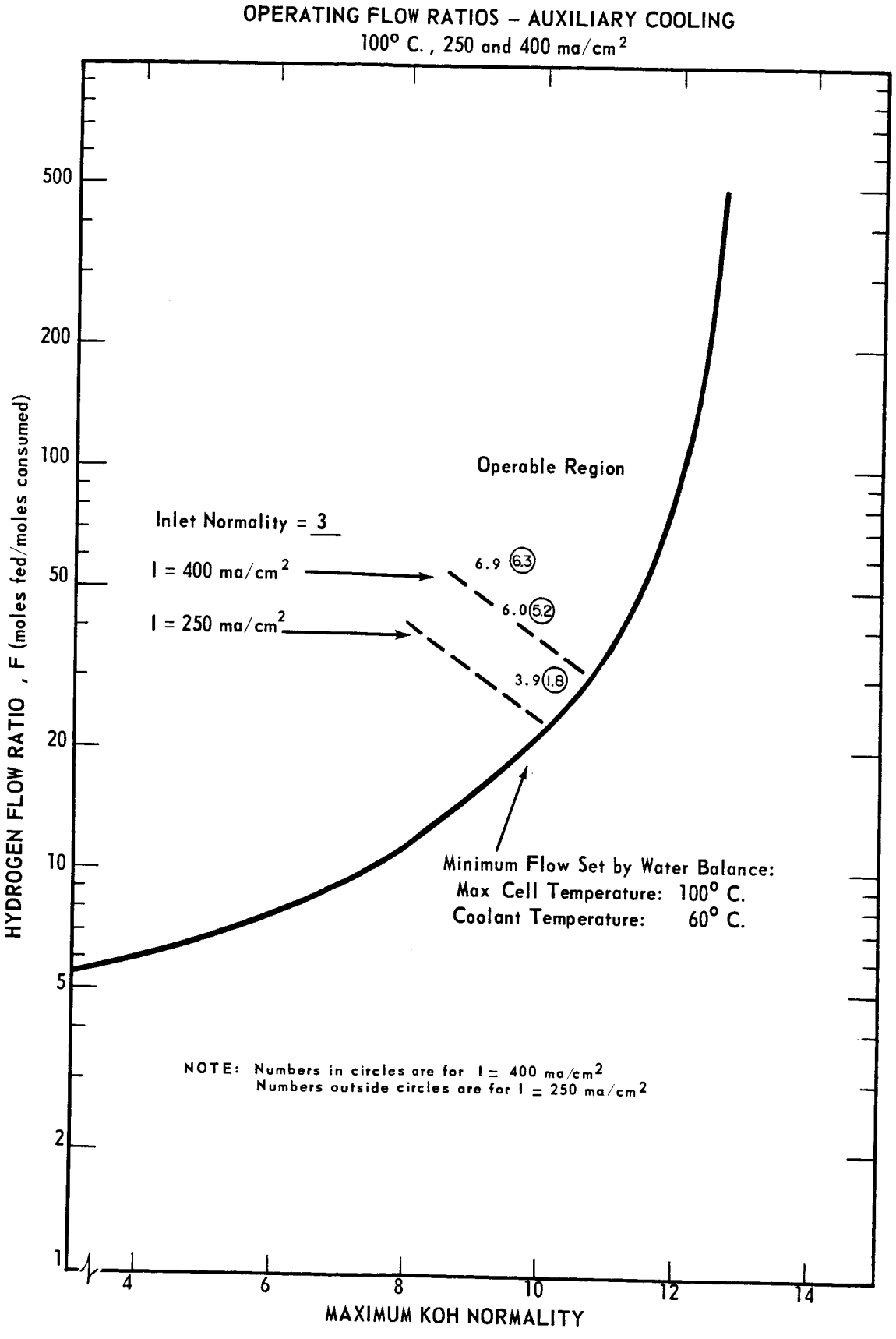
OPERATING FLOW RATIOS – AUXILIARY COOLING
100° C., 250 and 400 ma/cm²
HYDROGEN FLOW RATIO , F (moles fed/moles consumed)
500
200
100
50
20
10
5
2
1
Operable Region
Inlet Normality = 3
I = 400 ma/cm²
I = 250 ma/cm²
6.9 (6.3)
6.0 (5.2)
3.9 (1.8)
Minimum Flow Set by Water Balance:
Max Cell Temperature: 100° C.
Coolant Temperature: 60° C.
NOTE: Numbers in circles are for I = 400 ma/cm²
Numbers outside circles are for I = 250 ma/cm²
4
6
8
10
12
14
MAXIMUM KOH NORMALITY

FIGURE 7–15

ELECTROLYTE CONCENTRATION GRADIENTS
vs. FLOW RATIO
GAS COOLING AND AUXILIARY COOLING

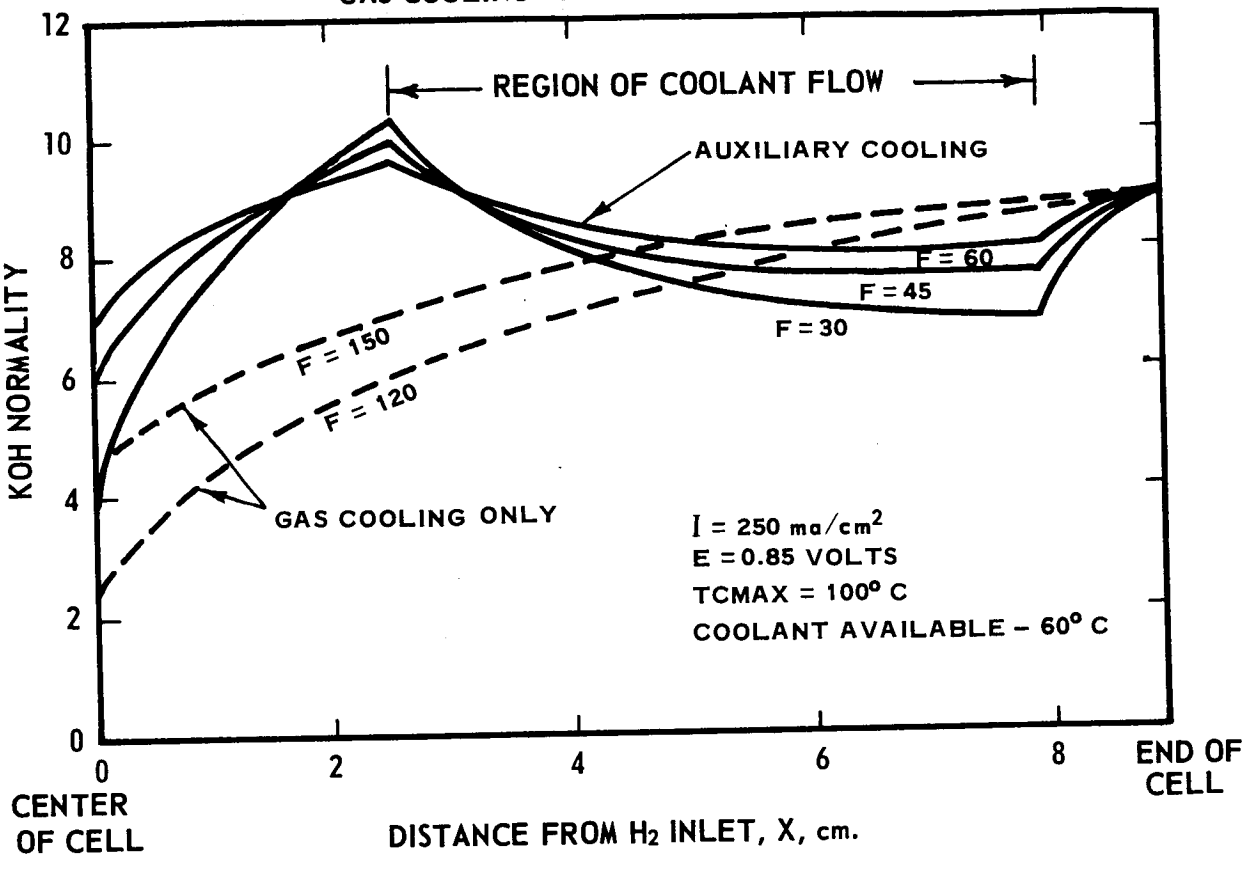

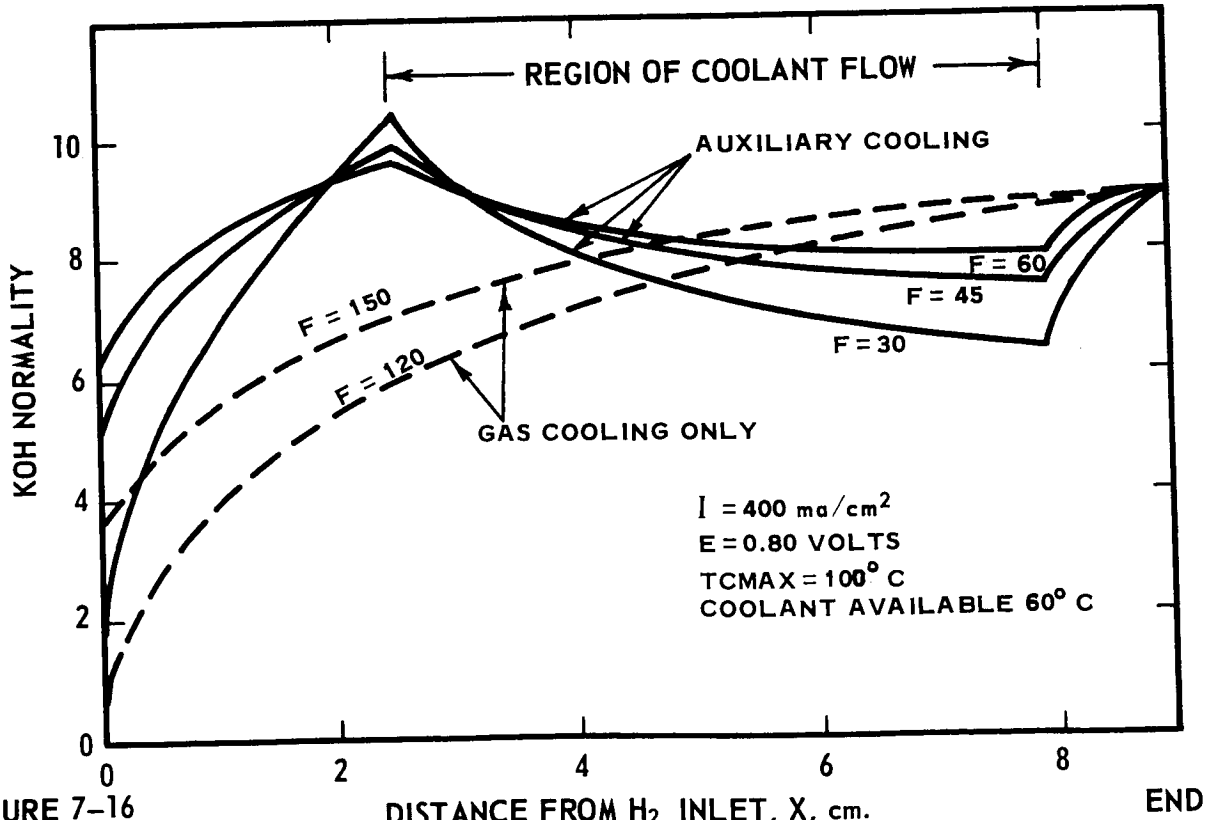

FIGURE 7–16

PRESSURE DROP *vs.* FLOW RATIO
FOR PROPOSED BATTERY DESIGN

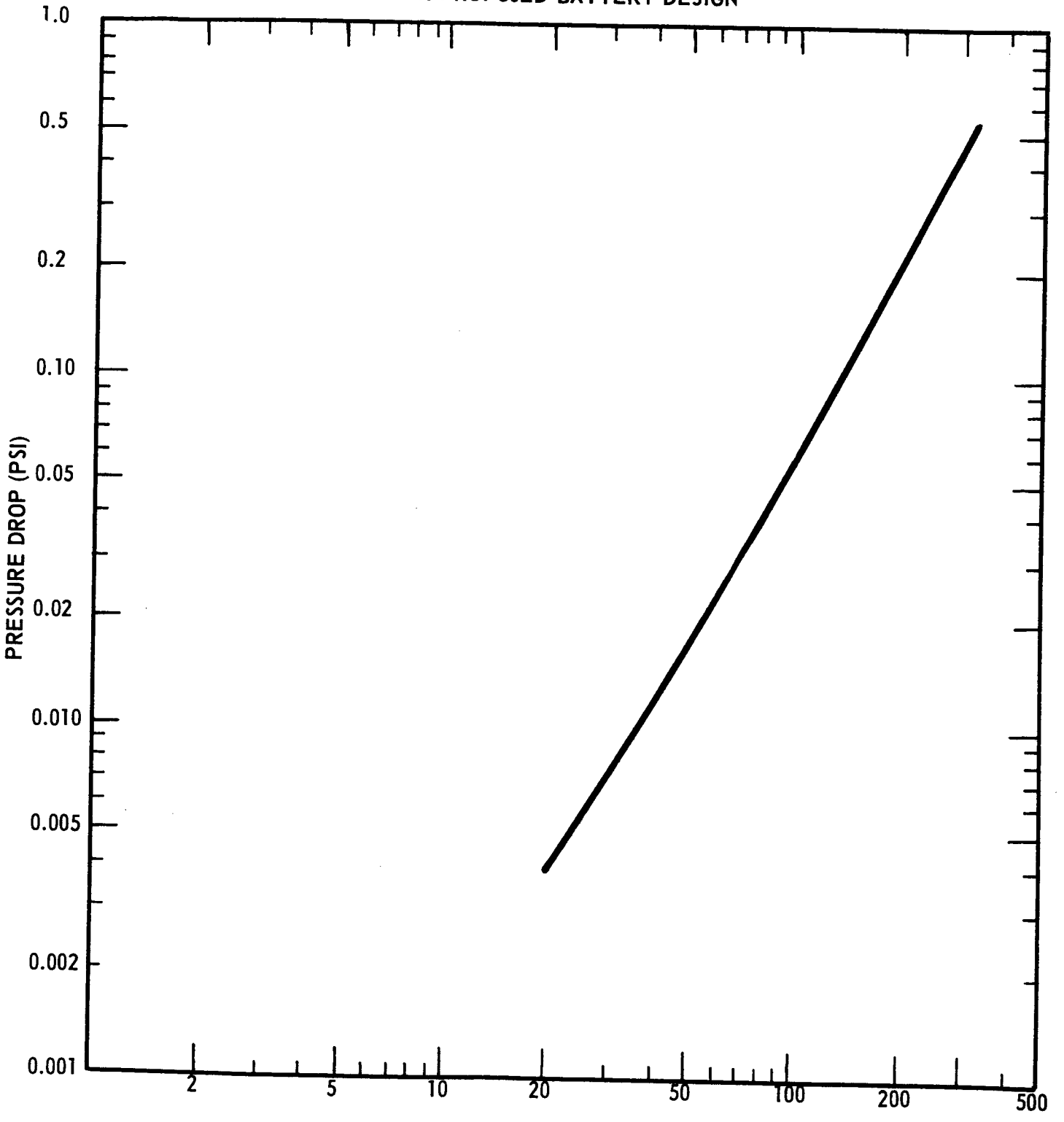

$$\text{FLOW RATIO} = \frac{\text{ACTUAL FLOW RATE}}{\text{STOICHIOMETRIC } H_2 + O_2 \text{ RATE FOR 34 CELLS (7" x 7") AT 250 MA/CM}^2}$$

FIGURE 7-17

8. REFERENCES

1. "Research and Development of High-Performance Light-Weight Fuel Cell Electrodes:, American Cyanamid Company, First Quarterly Report, November 1, 1963 to January 31, 1964, NASA-CR-54022.

   1A. ibid p. 8
   1B. ibid p. 21
   1C. ibid p. 24
   1D. ibid p. 28
   1E. ibid p. 41
   1F. ibid p. 60
   1G. ibid p. 74

2. "Research and Development of High-Performance Light-Weight Fuel Cell Electrodes", American Cyanamid Company, Second Quarterly Report, February 1, 1964 - April 30, 1964, NASA-CR-54084.

   2A. ibid p. 5
   2B. ibid p. 37
   2C. ibid p. 10
   2D. ibid p. 12
   2E. ibid p. 14
   2F. ibid p. 18
   2G. ibid p. 24
   2H. ibid p. 34
   2I. ibid p. 39
   2J. ibid p. 41
   2K. ibid p. 31

3. "Research and Development of High-Performance Light-Weight Fuel Cell Electrodes", American Cyanamid Company, Third Quarterly Report, May 1, 1964 - July 31, 1964. NASA-CR-54171

   3A. ibid p. 14
   3B. ibid p. 20
   3C. ibid p. 23
   3D. ibid p. 40
   3E. ibid p. 52
   3F. ibid p. 42
   3G. ibid p. 6
   3H. ibid p. 61
   3I. ibid p. 96-97

4. M. A. Klechdo and M. M. Godneva, Zhur. Neorg. Khim (Russian) 4, 2130 (1959).

5. A. M. Adams, F. T. Brown, and R. G. H. Watson (1963) in "Fuel Cells" (W. Mitchell, Jr. ed.) Chap. 4 (Interscience).

6. International Critical Tables 4, 239.

7. A. International Critical Tables 3, 373
   B. Handbook of Chemistry and Physics 44, 2421 (1962).

9. APPENDIX

Nomenclature for Mathematical Analysis

Symbol	Definition	Units
a	one-half electrode length in x-direction	cm
b	one-half electrode length in y-direction	cm
c_j	heat capacity of j	cal/g-mole°C
D_w	diffusivity of water in matrix	cm^2/hr
D_k	diffusivity of K^+ ions in matrix	cm^2/hr
f	moles H_2 consumed per hr. per ma of current	g-moles/hr. ma
F	moles H_2 fed/mole H_2 reacted	
$G_R(I)$	heat generated due to irreversibility with reactants entering at R°C and the product being liquid water at R°C.	cal/hr. cm^2
$H_j(T)$	enthalapy of component j at temperature T	cal/g-mole
ΔH_v	Latent heat of vaporization	cal/g-mole
h_1	heat transfer coefficient at hydrogen distributor plate	cal/hr. cm^2 °C
h_2	heat transfer coefficient at hydrogen electrode	cal/hr. cm^2 °C
h_3	heat transfer coefficient at oxygen electrode	cal/hr. cm^2 °C
h_4	heat transfer coefficient at oxygen distributor plate	cal/hr. cm^2 °C
I	current density	ma/cm^2
k_2	mass transfer coefficient at hydrogen electrode	g-moles/hr. cm^2 psig
k_1	conversion factor	cal/hr. watt
k_d	effective thermal conductivity of the distributor plate	cal/hr. cm^2 °C/cm
k_m	effective thermal conductivity of matrix composed of screen-electrode-solution and membrane-electrode-screen	cal/hr. cm^2 °C/cm

Symbol	Definition	Units
l	thickness of distributor plate	cm
N	normality of KOH solution in matrix	equiv/liter
N_w	mass flux of water	g-moles/cm^2 hr.
N_{KOH}	mass flux of KOH	g-moles/cm^2 hr.
$P(N,T)$	partial pressure of water over matrix at temperature T and normality N	psia
P_{wj}	partial pressure of water in j stream j=h=hydrogen	psia
Q	heat transferred to coolant	cal/hr.-cm^2
R	reference temperature	°C
t	thickness of membrane + electrodes	cm
T	temperature	°C
U	overall heat transfer coefficient	cal/hr. cm^2 °C
W_j	flow rate of j	g-moles/hr. cm of width
x	distance coordinate	cm
X	mole-fraction	cm
y	distance coordinate	cm
ϕ	total mole concentration of electrolyte	g-moles/cm^3
π	total pressure	psia

Subscripts

h	hydrogen
o	oxygen
w	water
m	matrix
d	distributor
c	coolant
wh	water in the H_2 stream

CONTRACT NAS3-2786

Report NASA CR-54436

Distribution List

Final Report

One copy is to be sent to each addressee, unless otherwise indicated. Note that more than one addressee may be shown for the same address.

National Aeronautics & Space Administration
Washington, D.C. 20546
Attention: Ernst M. Cohn, Code RNW
George F. Esenwein, Code MAT
J. R. Miles, Code SL
A. M. Andrus, Code ST

National Aeronautics & Space Administration
Scientific and Technical Information Facility
P.O. Box 5700
Bethesda, Maryland 20014 (2 copies + 1 reproducible)

National Aeronautics & Space Administration
Goddard Space Flight Center
Greenbelt, Maryland 20771
Attention: Thomas Hennigan, Code 632.2

National Aeronautics & Space Administration
Langley Research Center
Langley Station
Hampton, Virginia 23365
Attention: S. T. Peterson

National Aeronautics & Space Administration
Lewis Research Center
21000 Brookpark Road
Cleveland, Ohio 44135
Attention: Dr. B. Lubarsky, Mail Stop 500-201
R. L. Cummings, Mail Stop 500-201
H. J. Schwartz, Mail Stop 500-201
J. E. Dilley, Mail Stop 500-309
N. D. Sanders, Mail Stop 302-1
M. J. Saari, Mail Stop 500-202
R. R. Miller, Mail Stop 500-202
Technology Utilization Office, Mail Stop 3-16
W. A. Robertson, Mail Stop 500-201 (1 copy + 1 photo-ready)
Library, Mail Stop 3-7
Report Control, Mail Stop 5-5
V. Hlavin, Mail Stop 3-14

National Aeronautics & Space Administration
Marshall Space Flight Center
Huntsville, Alabama 35812
Attention: Philip Youngblood
R. Boehme

National Aeronautics & Space Administration
Ames Research Center
Moffett Field, California 94035
Attention: James R. Swain, Pioneer Project

National Aeronautics & Space Administration
Ames Research Center
Moffett Field, California 94035
Attention: Mr. T. Wydeven, Environmental Control Branch
John Rubenzer, Biosatellite Project

National Aeronautics & Space Administration
Manned Spacecraft Center
Houston, Texas 77058
Attention: Richard Ferguson (EP-5)
Robert Cohen, Gemini Project Office
F. E. Eastman (EE-4)

National Aeronautics & Space Administration
Western Operations Office
Santa Monica, California 90406
Attention: P. Pomerantz

Jet Propulsion Laboratory
4800 Oak Grove Drive
Pasadena, California 91103
Attention: Aiji Uchiyama

U.S. Army Engineer R & D Labs.
Fort Belvoir, Virginia 22060
Attention: Dr. Galen Frusinger (Code SMOFB-EP)
Electrical Power Branch

U.S. Army Electronics R & D Labs.
Fort Monmouth, New Jersey
Attention: Arthur F. Daniel (Code SELRA/SL-PS)
David Linden " " "
Dr. Adolph Fischbach " "
Dr. H. F. Hunger " "

Research Office
R & D Directorate
Army Weapons Command
Rock Island, Illinois
Attention: G. Riensmith, Chief

U.S. Army Research Office
Chief, Rand D.
Department of the Army
3D442, The Pentagon
Washington, D.C. 20546
Attention: Dr. Sidney J. Mangram

U.S. Army Research Office
Physical Sciences Division
3045 Columbia Pike
Arlington, Virginia

Harry Diamond Labs.
Room 300, Building 92
Connecticut Avenue & Van Ness St., N.W.
Washington, D.C.
Attention: Nathan Kaplan

Army Materiel Command
Research Division
AMCRD-RSCM T-7
Washington 25, D.C.
Attention: John W. Crellin

Natick Labs.
Clothing & Organic Materials Division
Natick, Massachusetts
Attention: Leo A. Spano

U.S. Army Research Office
Box CM, Duke Station
Durham, North Carolina
Attention: Dr. Wilhelm Jorgensen

U.S. Army Mobility Command
Research Division
Center Line, Michigan 48090
Attention: O. Renius (AMSMO-RR)

Hq., U.S. Army Materiel Command
Development Division
Washington 25, D.C.
Attention: Marshall D. Aiken (AMCRD-DE-MO-P)

Office of Naval Research
Department of the Navy
Washington 25, D.C.
Attention: Dr. Ralph Roberts, Code 429
Head, Power Branch

Bureau of Naval Weapons
Department of the Navy
Washington 25, D.C.
Attention: Whitwell T. Beatson, Code RAAE-52

U.S. Naval Research Laboratory
Washington, D.C. 20390
Attention: Dr. J. C. White, Code 6160

Bureau of Ships
Department of the Navy
Washington 25, D.C.
Attention: Bernard B. Rosenbaum, Code 340
C. F. Viglotti, Code 660

Naval Ordnance Laboratory
Department of the Navy
Corona, California
Attention: William C. Spindler (Code 441)

Naval Ordnance Laboratory
Department of the Navy
Silver Spring, Maryland
Attention: Philip B. Cole (Code WB)

Flight Vehicle Power Branch
Air Force Aero Propulsion Laboratory
Wright-Patterson Air Force Base, Ohio
Attention: J. E. Cooper (Code APIP)

AF Cambridge Research Lab.
Attention: CRZE
L. C. Hanscom Field
Bedford, Massachusetts
Attention: Francis X. Doherty

Rome Air Development Center, RSD
Griffiss AFB, New York 13442
Attention: Frank J. Mollura (RASSM)

Army Reactors, DRD
U.S. Atomic Energy Commission
Washington 25, D.C.
Attention: D. B. Hoatson

Office, DDR&E: USW & BSS
The Pentagon
Washington 25, D.C.
Attention: G. B. Wareham

Institute for Defense Analyses
Research and Engineering Support Division
400 Army-Navy Drive
Arlington, Virginia 22202
Attention: Dr. George C. Szego

Power Information Center
University of Pennsylvania
Moore School Building
200 South 33rd Street
Philadelphia 4, Pennsylvania

Office of Technical Services
Department of Commerce
Washington, D.C. 20009

Aeronutronic Division
Philco Corporation
Ford Road
Newport Beach, California 92663
Attention: Dr. S. W. Weller

Alfred University
Alfred, New York
Attention: Prof. T. J. Gray

Allis-Chalmers Manufacturing Company
1100 South 70th Street
Milwaukee, Wisconsin 53201
Attention: J. Plattner

Allison Division
General Motors Corporation
Indianapolis 6, Indiana
Attention: Dr. Robert B. Henderson

American Machine & Foundry
689 Hope Street
Springdale, Connecticut
Attention: Dr. L. H. Shaffer
Research & Development Division

Astropower, Incorporated
Douglas Aircraft Company, Inc.
2121 College Drive
Newport Beach, California
Attention: Dr. Carl Berger

Battelle Memorial Institute
505 King Avenue
Columbus, Ohio 43201
Attention: Dr. C. L. Faust

Bell Telephone Laboratories, Inc.
Murray Hill, New Jersey
Attention: Mr. U. B. Thomas

Clevite Corporation
Mechanical Research Division
540 East 105th Street
Cleveland, Ohio 44108
Attention: A. D. Schwope

Electrochimica Corporation
1140 O'Brien Drive
Menlo Park, California
Attention: Dr. Morris Eisenberg

Electro-Optical Systems, Inc.
300 North Halstead Street
Pasadena, California
Attention: E. Findl

Engelhard Industries, Inc.
497 DeLancy Street
Newark 5, New Jersey
Attention: Dr. J. G. Cohn

Esso Research & Engineering Company
Process Research Division
P.O. Box 121
Linden, New Jersey 07036
Attention: Dr. R. Epperly

The Franklin Institute
Benjamin Franklin Avenue at 20th St.
Philadelphia 3, Pennsylvania
Attention: Robert Goodman

General Electric Company
Direct Energy Conversion Operations
Lynn, Massachusetts
Attention: Dr. E. Oster

General Electric Company
Research Laboratory
Schenectady, New York
Attention: Dr. H. Liebhafsky

General Motors Corporation
Box T.
Santa Barbara, California
Attention: Dr. C. R. Russell

General Motors Corporation
Research Laboratories
Electrochemistry Department
12 Mile & Mound Roads
Warren, Michigan 48090
Attention: Mr. Seward Beacom

Globe-Union, Inc.
900 East Keefe Avenue
Milwaukee, Wisconsin 53201
Attention: Dr. W. Towle

Hughes Research Laboratories Corporation
Malibu, California
Attention: T. M. Hahn

Institute of Gas Technology
State & 34th Streets
Chicago, Illinois
Attention: Mr. Bernard Baker

Ionics, Incorporated
152 Sixth Street
Cambridge, Massachusetts 02142
Attention: Dr. Werner Glass

Leesona Moos Laboratories
Lake Success Park
Community Drive
Great Neck, New York
Attention: Dr. A. Moos

Monsanto Research Corporation
Everett, Massachusetts 02149
Attention: Dr. J. Smith

North American Aviation Inc.
S&ID Division
Downey, California
Attention: Dr. James Nash

Power Sources Division
Whittaker Corporation
9601 Canoga Avenue
Chatsworth, California 91311
Attention: Dr. M. Shaw

Pratt & Whitney Aircraft Division
United Aircraft Corporation
East Hartford 8, Connecticut
Attention: Librarian

Radio Corporation of America
Astro Division
Heightstown, New Jersey
Attention: Dr. Seymour Winkler

Rocketdyne
6633 Canoga Avenue
Canoga Park, California
Attention: Library, Department 586-306

Speer Carbon Company
Research & Development Laboratories
Packard Road at 47th Street
Niagara Falls, New York
Attention: Dr. L. M. Liggett

Thiokol Chemical Corporation
Reaction Motors Division
Denville, New Jersey
Attention: Dr. D. J. Mann

Thompson Ramo Wooldridge, Inc.
23555 Euclid Avenue
Cleveland, Ohio 44117
Attention: Librarian

University of Pennsylvania
Philadelphia, Pennsylvania 19104
Attention: Prof. John O'M. Bockris

Unified Science Associates, Inc.
826 South Arroyo Parkway
Pasadena, California
Attention: Dr. Sam Naiditch

Union Carbide Corporation
12900 Snow Road
Parma, Ohio
Attention: Dr. George E. Evans

University of California
Space Science Laboratory
Berkeley 4, California
Attention: Prof. Charles W. Tobias

Western Reserve University
Cleveland, Ohio
Attention: Prof. Ernest Yeager

Westinghouse Electric Corporation
Research and Development Center
Churchill Borough
Pittsburgh, Pennsylvania
Attention: Dr. A. Langer

Yardney Electric Corporation
40-50 Leonard Street
New York, New York
Attention: Dr. Paul Howard

Texas Instruments, Inc.
13500 North Central Expressway
Dallas, Texas
Attention: Dr. I. Trachtenberg

Tyco Laboratories Inc.
Bear Hill
Waltham 54, Massachusetts
Attention: W. W. Burnett

Arthur D. Little Inc.
Acorn Park
Cambridge, Massachusetts 02140
Attention: Dr. E. W. Stone